Film Formation of Aqueous Dispersions of Ionically Cross-Linked Pressure-Sensitive Adhesives Studied with Förster Resonance Energy Transfer (FRET)

Doctoral Thesis

(Dissertation)

to be awarded the degree

Doctor rerum naturalium (Dr. rer. nat.)

submitted by

M. Sc. Hares Wahdat

from Goslar, Germany

approved by the Faculty of Natural and Materials Sciences,

Clausthal University of Technology

Date of oral examination

April 26, 2019

Dean

Prof. Dr. Karl-Heinz Spitzer

Chairperson of the Board of Examiners

Prof. Dr. Arnold Adam

Supervising tutor

P.D. Dr. Jörg Adams

Reviewer

Prof. Dr. Diethelm Johannsmann

This thesis was written at the Institute of Physical Chemistry, Clausthal University of Technology, Clausthal-Zellerfeld, Germany, in the time between December 2016 and February 2019 under supervision of P.D. Dr. Jörg Adams.

Acknowledgements

I thank P.D. Dr. Jörg Adams for the interesting topic as well as the great supervision and support during my work. I thank Prof. Dr. Diethelm Johannsmann for being the reviewer of this thesis and for helpful discussions.

I thank Dr. Matthias Gerst and Dr. Markus Rückel from BASF SE for providing the polymer dispersions as well as many interesting and helpful discussions. I thank B. Sc. Stephan Möbius and Udo Spuhler from BASF SE for synthesis of the polymer dispersions.

Furthermore, I thank Andreas Böttcher (Institute of Physical Chemistry, IPC) for building the measurement chamber used for the film formation studies of the dispersions.

Regarding analysis of polymer dispersions, I thank Martina Heinz (Institute of Technical Chemistry, ITC) for performing GPC measurements, and Ulrike Koecher (ITC), Werner Bischof (ITC) and Martin Schwedes (ITC) for performing DSC measurements.

I thank all the employees of the Institute of Physical Chemistry, Clausthal University of Technology for the relaxed atmosphere. I acknowledge helpful discussions with Dr. Arne Langhoff, Dr. Heike Römermann, B. Sc. Christopher Hirth, M. Sc. Li Yang, B. Sc. André Eitzeroth, M. Sc. Phillip Sievers, M. Sc. Frederick Meyer and Kevin Hoffmann.

Lastly and mostly, I thank my parents and my family for the continuous support during my life.

Abstract

In this work, the film formation, focused on the stage of polymer interdiffusion, of aqueous dispersions of pressure-sensitive adhesives (PSAs) was investigated by employing *Förster Resonance Energy Transfer* (FRET). Mainly, interdiffusion in films from industrially relevant acrylic PSA dispersions provided by BASF SE was studied and the objective was to evaluate whether homogeneous films consisting of ionically cross-linked chains have been formed.

In the first part of the work, the film formation of dispersions containing uncross-linked (i.e. linear) chains was investigated with respect to the softness of the polymer particles. It was found that the formation of a skin at the top takes place immediately after film casting and that deformation of particles occurs before drying is finished. As a consequence of skin formation, interdiffusion at the bottom of the film can be faster than at the top.

In the second part, interdiffusion in films from dispersions of linear chains blended with aluminum acetylacetonate ($Al(acac)_3$), an ionic cross-linker, was investigated. Interdiffusion studies suggest that cross-linking by $Al(acac)_3$ occurs after interdiffusion has almost finished, indicating the formation of homogeneous films. Cross-linking in the final films was proven by gel content determinations and flat-punch tack tests. Further research concerned the influence of the serum pH on the kinetics of polymer interdiffusion and polymer cross-linking. Neutralizing the serum pH from 2 to 7 results in a slower interdiffusion and faster cross-linking reaction.

In the third part, interdiffusion in films from dispersions of ionically cross-linked polymers was studied with respect to the reversibility of the ionic bond between carboxylate groups in the chains and Zn^{2+} ions. The reversibility of the bond was found to slow down but not entirely hinder interdiffusion, which is of advantage for film formation.

Table of Contents

1 Introduction

1.1 Motivation

Pressure-sensitive adhesives (PSAs) are soft, viscoelastic, polymer films which stick to surfaces upon application of light mechanical pressure.[1] PSAs are employed as for instance labels, tapes or temporary protective films. Often, PSAs must be removable from the substrate, and thus it is necessary that they can be peeled off without leaving residues. Depending on the final application, the (non-linear) rheology of a PSA must be balanced, making the manufacture of a PSA a complicated and challenging task.[2,3] One type of base polymers commonly employed as PSAs are acrylates (i.e. acrylics) with a glass transition temperature, T_g, much below 0 °C. Acrylics have good adhesive properties. However, they lack cohesive strength, and therefore the chains must be partially cross-linked.[4]

Acrylic PSA films can be prepared from both solutions in organic solvents and aqueous polymer dispersions.[4] Polymer dispersions (i.e. polymer latexes) are colloidal nanoparticles of polymers dispersed in water.[5] Preparing polymer films from aqueous dispersions is environmentally friendly because no or only small amounts of volatile organic compounds are released during drying.[5] However, the performance of films from dispersions is slightly inferior to the performance of films from solutions. This is because the film formation of polymer dispersions is much more complicated than that of solutions, resulting in structural heterogeneities.[6] Film formation of polymer dispersions encompasses three stages which are water evaporation (stage I), particle deformation (stage II) and polymer interdiffusion (stage III).[5] Polymer interdiffusion is crucial for the formation of a homogeneous, mechanically stable film.[5] During this stage, chains from adjacent particles interdiffuse into each other and form entanglements with other chains. As a result of the formation of chain entanglements, cohesion inside the film is developed.[5] Due to the low T_g of the polymers,

particle deformation and polymer interdiffusion are fast, even at room temperature,[7] thus a homogeneous film is formed if the chains are uncross-linked (i.e. linear) (Figure 1 a)). However, as stated above, chains in acrylic PSAs must be cross-linked to achieve the desired cohesion necessary for the final application. Irreversible, covalent cross-linking of chains before film formation can limit interdiffusion to the extent that a fragile film is obtained in which deformed particles are still separated by boundaries (Figure 1 b)).[8–10] To circumvent problems resulting from cross-linking in terms of interdiffusion, it is attractive either to cross-link polymer chains after interdiffusion has finished (Figure 1 c)) or to reversibly cross-link the polymer chains in the wet dispersion (Figure 1 d)).[11] Here, ionic cross-linking (Figure 1 c) and d)), which can be reversible,[12] is relevant.

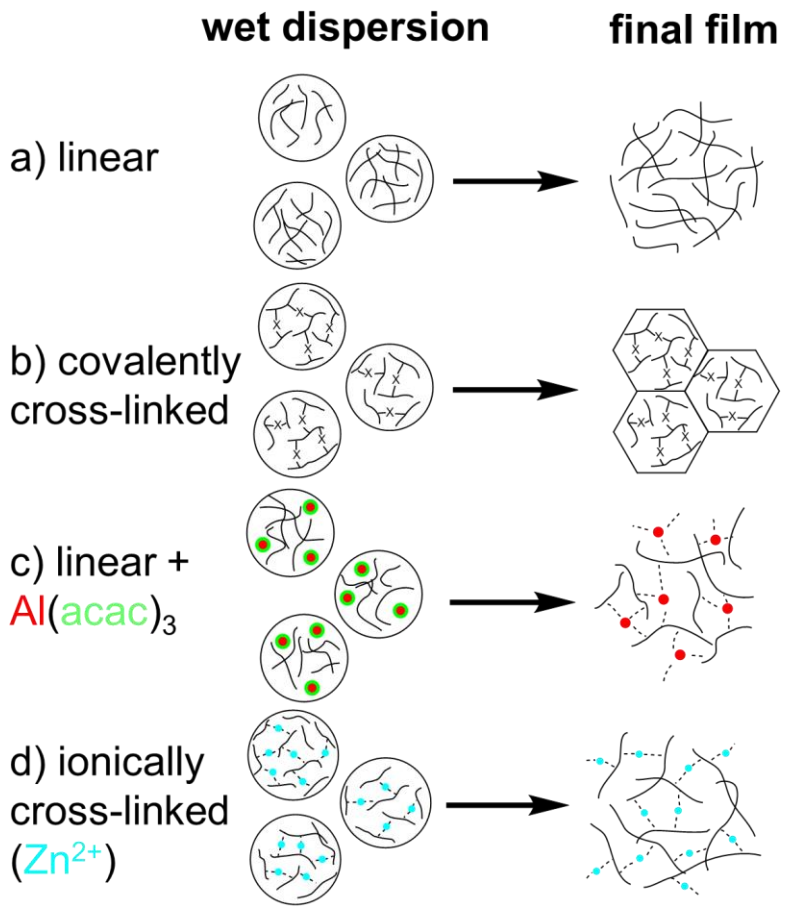

Figure 1: Expected influence of polymer cross-linking in the wet dispersion on the final film.

In this work, the stage of polymer interdiffusion during film formation of industrially relevant acrylic PSA dispersions provided by BASF SE is investigated. The motivation is to prepare homogeneous films consisting of ionically cross-linked chains from aqueous dispersions. Ionic cross-linking can be reversible which principally allows for the preparation of self-healing polymer films.[12]

One possibility to prepare homogeneous PSA films consisting of ionically cross-linked chains from polymer latexes is to blend acrylic PSA dispersions containing linear chains with metal chelates such as aluminum acetylacetonate, $Al(acac)_3$ (Figure 1 c)).[13,14] Cross-linking of polymers by metal acetylacetonates is based on a reaction between carboxylate groups in the chains and acetylacetonate groups bond to the metal cation. As a result of the reaction, a cross-linked polymer network in which chains are interconnected by ionic bonds between carboxylate groups and metal cations is formed. As a by-product, acetylacetone is formed.[15] It is known that films prepared from acrylic PSAs dispersions blended with $Al(acac)_3$ have an improved cohesion compared to films consisting of linear chains.[13–15] However, less is known about the degree of cross-linking prior to film casting in these dispersions. An equilibrium is expected to be present because acetylacetone, formed after the cross-linking reaction, remains in the latex. If the degree of cross-linking before film formation is small and if the cross-linking reaction is slower than polymer interdiffusion, a homogeneous film with a high degree of ionic cross-linking can be prepared. The desired progress of film formation of a PSA dispersion blended with $Al(acac)_3$ is sketched in Figure 2.

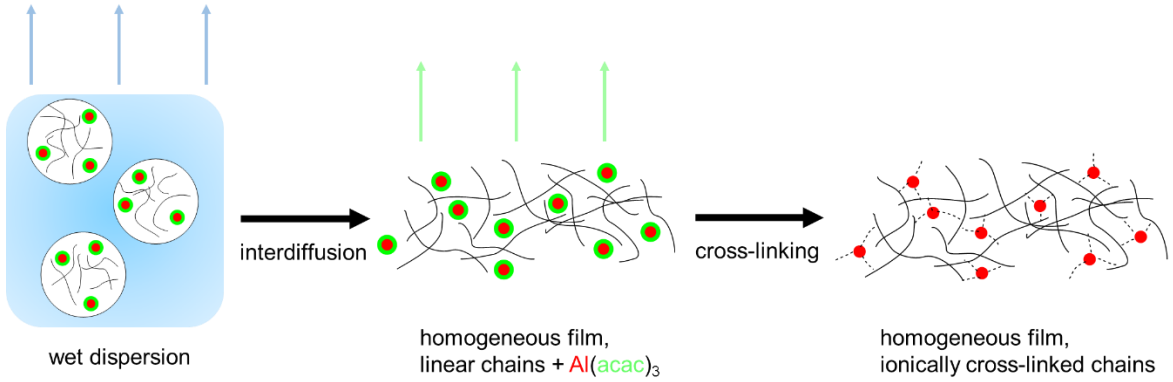

Figure 2: Desired progress of film formation of a PSA dispersion blended with Al(acac)$_3$. Blue arrows: Water evaporation, green arrows: evaporation of acetylacetone.

The formation of a homogeneous film can be evaluated by studying interdiffusion in a film from a latex blended with Al(acac)$_3$.

An alternative possibility to obtain homogeneous, ionically cross-linked films from polymer latexes can be based on reversible, ionic cross-linking of polymer chains in the particles by Zn^{2+} before film casting (Figure 1 d)). This can be achieved by using zinc dimethacrylate, ZnDMA, as a co-monomer during the synthesis of the dispersions. According to rheological measurements performed in the literature, the ionic bond between carboxylate groups in polymer chains and Zn^{2+} ions is reversible.[12] Chains can reversibly detach from the metal cations at elevated temperatures.[12] Reversible cross-linking is advantageous for interdiffusion because chains are not forever fixed within their initial particles but can intermix with chains from neighboring particles.

In this work, polymer interdiffusion in film forming acrylic PSA dispersions is studied. The progress of polymer interdiffusion can be followed by making use of *Förster Resonance Energy Transfer* (FRET). FRET describes a process in which a fluorescent dye (donor) non-radiatively transfers its excitation energy to a dye (acceptor) in its immediate vicinity instead of fluorescing, thereby increasing the curvature in the donor's fluorescence decay curve.[16]

FRET can only occur if the distance between donors and acceptors is within a few nanometers, thus it can be used as a proximity probe ("spectroscopic ruler").[16] In order to study polymer interdiffusion in film forming latexes, dispersions with identical properties must be prepared twice, once with donor-dyes covalently attached to the polymer chains and once with acceptor-dyes attached to the chains.[17] By continuously recording donor fluorescence decays on a film forming blend of donor- and acceptor-labeled dispersions and analyzing how the curvature of the donor decays changes in a kinetic experiment, information about the progress of polymer interdiffusion can be extracted.[17]

1.2 Objective of Thesis

The objective of this thesis is to investigate the film formation, focused on the stage of polymer interdiffusion, of industrially relevant acrylic PSA dispersions provided by BASF SE. To track polymer interdiffusion, *Förster Resonance Energy Transfer* (FRET) is employed. In addition to FRET measurements, scattered excitation light from the same spot of the film is detected simultaneously to follow the state of particle deformation shortly after film casting. Regarding material development, it is to evaluate whether homogeneous films from polymer dispersions with a high degree of ionic cross-linking can be prepared. To corroborate the results of film formation studies of the dispersions by BASF SE, supporting experiments on model dispersions prepared by miniemulsion polymerization are performed.

In the first part of this thesis, the film formation of dispersions containing linear chains only is studied with respect to the softness of the polymer particles. The kinetics of particle deformation and the consequence of skin formation on long-time interdiffusion is investigated. Furthermore, hydroplasticization and the influence of a tackifier, an additive commonly formulated with PSAs,[1] on interdiffusion is studied.

In the second part, the influence of $Al(acac)_3$, an ionic cross-linker which has been blended with latexes of linear chains, on interdiffusion is studied. By comparing interdiffusion in film forming latexes with linear chains only and with linear chains blended with $Al(acac)_3$, it is discussed whether a homogeneous film has been formed. Cross-linking in the final film is evaluated by flat-punch tack tests. For comparative studies, interdiffusion in a film with covalently cross-linked chains is investigated as well. Furthermore, the influence of the serum pH on interdiffusion kinetics and the kinetics of polymer cross-linking by $Al(acac)_3$ is studied.

In the third part, the influence of the reversibility of the ionic bond between carboxylate groups in the chains and Zn^{2+}, which was proven in Ref. [12], on interdiffusion is studied. In

this thesis, the discussion focuses on data from studies of model dispersions prepared by miniemulsion polymerization. The motivation for these studies originates from results of interdiffusion studies of industrially relevant PSA dispersions by BASF SE which are not shown in this thesis, but in Ref. [18]. In Ref. [18], it was found that interdiffusion in films from dispersions with ionically cross-linked chains is slowed down but not entirely hindered, which can be advantageous for film formation.

Most of these results, especially from the first (Ref. [19]) and second part (Ref. [18]) of this thesis have already been published. In some instances, a more sophisticated interpretation of the data is provided in these publications.

2 Theory

2.1 Pressure-Sensitive Adhesives (PSAs)

Pressure-sensitive adhesives (PSAs) are soft, viscoelastic polymer films adhering to substrates after applying weak mechanical pressure.[1,2] They do not undergo a physical transition or chemical reaction while forming molecular contact to the substrate, contrary to structural adhesives.[1,2] Typical applications of PSAs are for instance tapes, note papers, labels on clothes or temporary protective films for automobiles.[1,2] For temporary applications, it is necessary for the PSA to be easily removable from the substrate without leaving residues whereas for permanent applications, a strong tack is necessary.[1] Since PSAs must provide for both adhesion and cohesion, their rheology is of prime importance. During the bonding process, the PSA must be viscous and flow while during the debonding process, the PSA must be elastic and resist flow. This makes it complicated to manufacture PSAs because increasing the cohesion might result in a decreased adhesion, and vice versa.[1–3]

The three most common base materials used in PSAs are natural rubbers, isoprene-styrene-isoprene triblock copolymers and acrylates (i.e. acrylics). Their chemical structures are shown in Figure 3.[3,4] Other base materials employed as PSAs, which are not shown in Figure 3, are polyvinyl ethers, polybutadienes or polydimethylsiloxanes.[4]

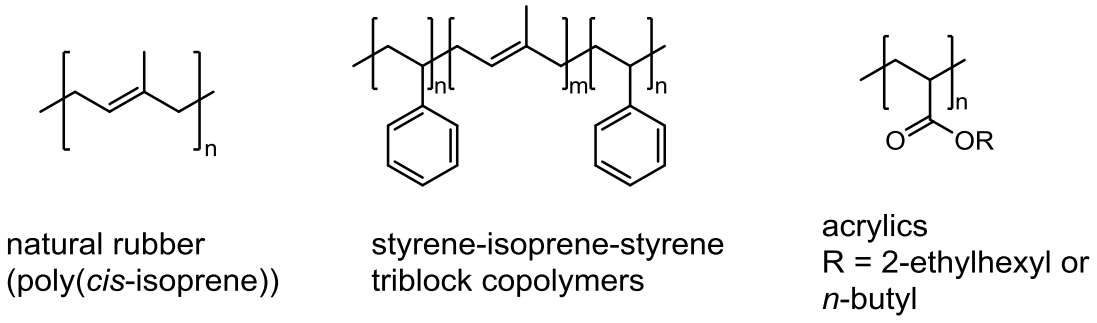

Figure 3: Base polymers used as PSAs.

Usually, the base materials are formulated with additives such as tackifiers or are chemically modified for example by cross-linking the polymer chains. Properties of natural rubber, isoprene-styrene-isoprene triblock copolymers and acrylics are summarized in Table 1.[1–4,20]

Table 1: Properties of common base materials used as PSAs.[1–4,20]

Base polymer	Properties	Preparation method
Natural rubber	• Cheapest • High peel-strength • Prone to oxidation • Must be cross-linked and tackified	• Organic solutions
Isoprene-styrene-isoprene triblock copolymers	• Good heat resistance • Must be tackified	• Hot melts
Acrylics	• Most expensive • Tacky • Good weathering characteristics • Must be cross-linked	• Organic solutions • Water-borne polymer dispersions

Natural rubber is the cheapest among the three PSA types presented in Table 1.[3] It has a high peel-strength by itself but is prone to oxidation due to the unsaturated double bonds along the chains (see Figure 3).[20] For this reason, it is necessary to add antioxidants for stabilization. Natural rubber PSAs usually are cross-linked to increase their cohesive strength and resistance

against organic solvents. To increase their adhesive properties, they are blended with tackifiers ("tackified").[3,20] PSA films of natural rubber are prepared from organic solutions.[3] PSAs based on styrene-isoprene-styrene triblock copolymers are more expensive than natural rubber based PSAs. In general, they have a good heat resistance. Cohesion in these films results from a phase separation between the polystyrene and polyisoprene blocks in the triblock copolymer. The separated polystyrene phases act as physical cross-links, thereby providing for cohesive strength. Styrene-isoprene triblock polymers are usually formulated with tackifiers to improve their adhesive properties.[3] PSA films of styrene-isoprene block copolymers are prepared from hot melts. Acrylics are the most expensive PSAs. They have good weathering characteristics and therefore are suitable for outdoor applications. Acrylics used as PSAs have a glass transition temperature, T_g, much below 0 °C. They have good adhesive properties, but lack cohesive strength. To improve cohesion in acrylic PSAs, chains are partially cross-linked. Acrylic PSA films can be prepared from organic solutions or water-borne polymer dispersions, the latter procedure being environmentally friendly and discussed in Section 2.5.[1–4,5] More physicochemical properties of acrylic PSAs are discussed in Sections 2.3 and 2.4.

Common additives for PSAs are tackifiers, which can be blended with acrylic PSA dispersions. In this thesis, the influence of tackifiers on polymer interdiffusion has been investigated, therefore they are shortly introduced. Tackifiers are low molecular weight oligomers which are formulated with PSAs to increase their tack and peel-adhesion upon dissolving in the base polymer (see Section 2.2 for more information on these properties).[1] They have a higher T_g (antiplasticizer) and a lower elastic modulus compared to the base polymer. The increased T_g impedes bond rupture while the decreased modulus enhances bond formation to the substrate.[1,20] Different types of tackifiers, depending on the base polymer's composition are employed.[1,20] Chemical structures of typical monomers used to prepare tackifiers are shown in Figure 4.[1]

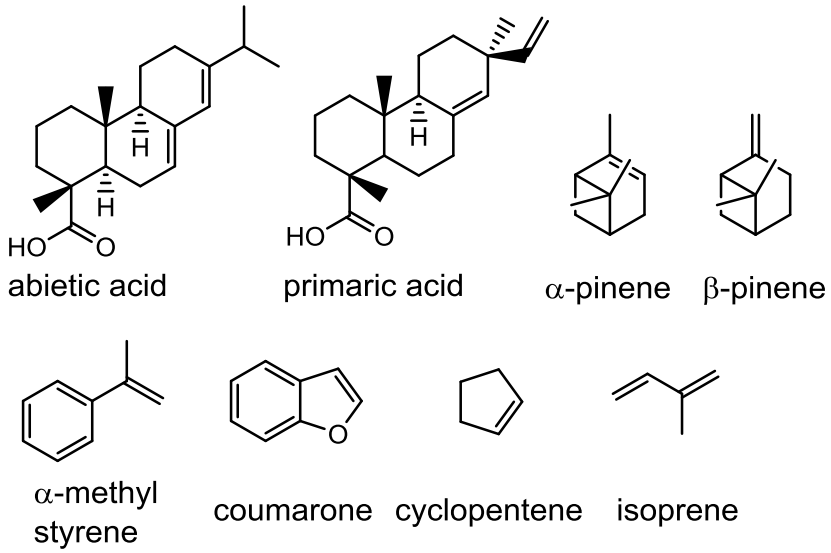

Figure 4: Monomeric form of base materials typically used as tackifiers.[1]

It can be distinguished between natural based tackifiers and petroleum based tackifiers. As the former, rosin esters such as hydrogenated derivatives of primaric or abietic acid, or cationically polymerized terpenes such as α- or β-pinene are used. Petroleum based tackifiers are polymerized aromatics such as α-methyl styrene or coumarone, or polymerized aliphatics consisting of 5 carbon atoms such as cyclopentene or isoprene.[1]

2.2 Performance Tests for PSAs

Common performance tests evaluating the adhesion and cohesion of PSAs are the flat-punch tack test, the shear-holding power test and the peel-off test, which are all sketched in Figure 5 a), b) and c), respectively.[1] Flat-punch tack test on PSA films were also performed within this thesis, and therefore this technique is introduced in more detail, whereas the other techniques are shortly outlined. Flat-punch tack tests (Figure 5 a)) are carried out to quantify the tackiness (i.e. tack) of a PSA.[1,2]

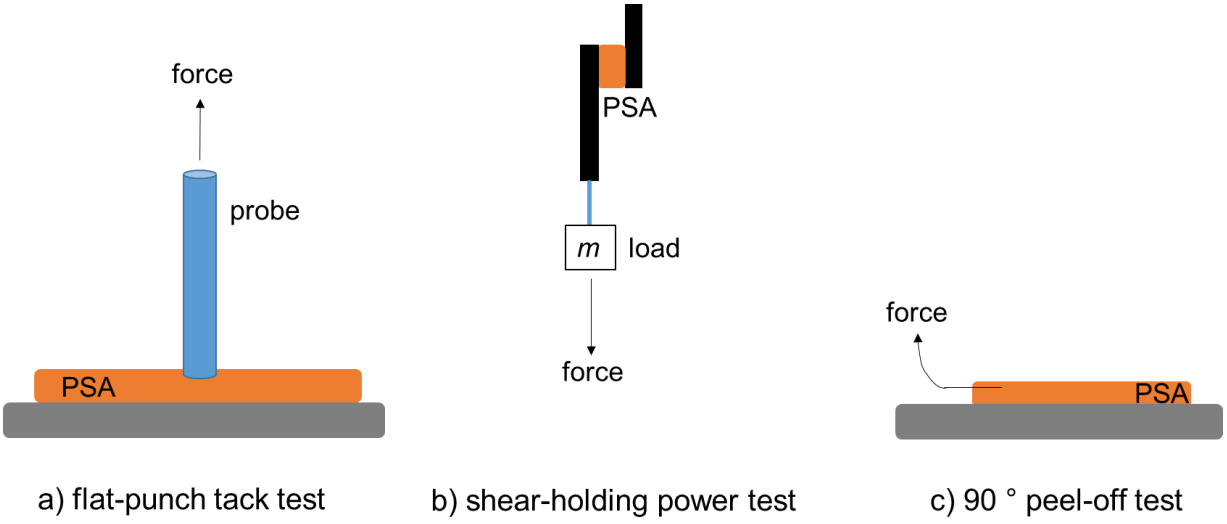

Figure 5: Common performance tests for PSAs.

In the flat-punch tack test, a probe (for example a cylindrical metal stamp) approaches the PSA film and penetrates into its surface. It remains in the film for a specific time, which is in the order of seconds, to establish molecular contact. Afterwards, the probe is removed from the sample at a constant debonding speed between 1 – 10^4 mm/s. During the debonding process, the tensile force as a function of the distance between probe and sample is measured.[2] The force is normalized to the stress σ, while the distance is normalized to the strain ε. An exemplary stress-strain curve recorded on a PSA film with uncross-linked (i.e. linear) chains within this thesis is shown in Figure 6.

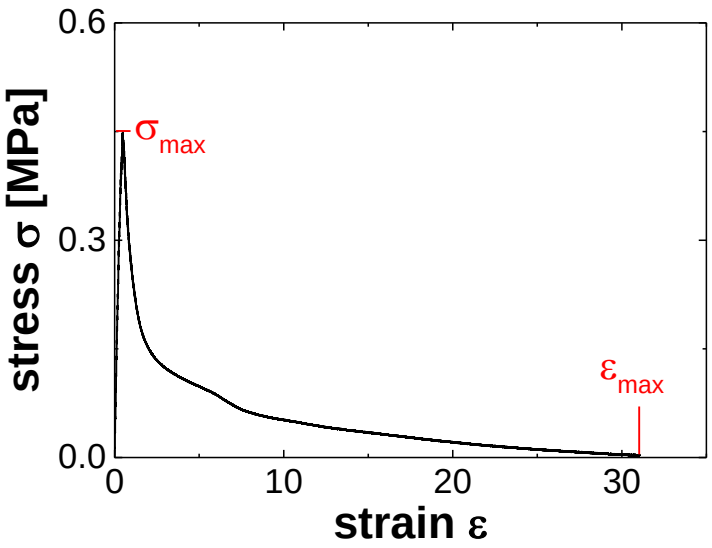

Figure 6: Exemplary stress-strain curve.

The shape of the stress-strain curve depends on many parameters such as the PSA's surface chemistry, the roughness of its surface, its degree of cross-linking, etc.[2] Typical quantities extracted from tack tests are the peak stress, σ_{max}, the maximum strain ε_{max}, when the stress levels off to zero and the adhesion energy, W_{adhes}, which is the area under the curve multiplied by the film thickness.[2] To extract more information about the debonding mechanism such as the growth of cavities and fibrillation, a video recording from the bottom of the film can be carried out simultaneously to the tack measurement.[2,21] In general, the occurrence of fibrils during the debonding process and a high adhesion energy are desired for PSAs.[2] In this thesis, tack measurements are mainly carried out to examine whether or not a cross-linked polymer film with a high gel content has been obtained from the respective dispersion. High cross-linking degrees significantly reduce the mobility of chains and their adhesive properties. Compared to films consisting of linear polymer chains, ε_{max} is decreased for highly cross-linked polymers.[2,22]

The shear-holding power test (Figure 5 b)) evaluates the creep of a PSA under a constant shear stress, which is important if the PSA must for example hold a picture on a wall.[1] A load of typically 0.5 – 1 kg is attached to the PSA film (~100 μm thickness) sticking to a substrate and the time when the film ruptures is measured.[1,2]

The peel-off test (Figure 5 c)) evaluates the peel-strength of a PSA.[1] The peel-strength is important for temporary applications because the film must be removed without leaving residues on the substrate. The PSA film is applied on a stiff substrate such as steel or glass and peeled-off at angles of either 90° or 180°.[1]

2.3 Acrylate-Based PSAs

Acrylate-based (i.e. acrylics) PSAs are copolymers in which the main component is a monomer whose corresponding homopolymer has a T_g much below 0 °C (low-T_g). Typical monomers are *n*-butyl acrylate, *iso*-octyl acrylate or 2-ethylhexyl acrylate. Chemical structures of their homopolymers are provided in Figure 7.[4,23]

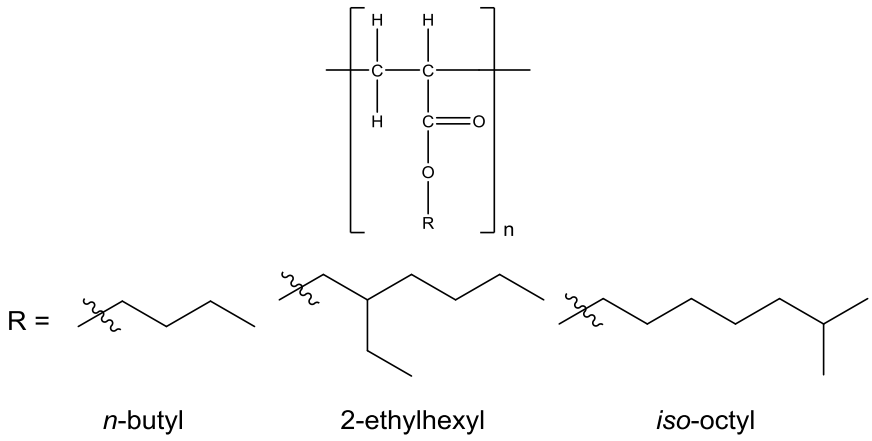

Figure 7: Base polymers used in acrylic PSAs. R is the alkyl group.

The flexible side groups along the main chain of the polymers increase the free volume, and thus decrease the T_g. Usually, acrylics having a broad molecular weight distribution are employed, with small, mobile chains providing for adhesion and large, entangled chains providing for cohesion.[3] To adjust the polymer's viscoelasticity, the T_g is usually slightly increased by copolymerization with small amounts of monomers whose corresponding homopolymers have a high T_g, such as styrene or methyl methacrylate.[4] In order improve adhesion towards polar substrates, methacrylic acid or acrylic acid are employed as co-monomers.[2] Improving the cohesion of acrylic PSAs is mainly achieved by partially cross-linking the polymer chains,[4,20] which is discussed in more detail in Section 2.4.

2.4 Cross-Linking of Acrylic PSAs

Cross-linking of polymer chains can significantly change their viscoelastic properties. In case of acrylic PSAs, chains are partially cross-linked in order to balance adhesive and cohesive properties.[2] A small cross-linking degree enables fibrillation during debonding and increases the adhesion energy,[22] whereas a high cross-linking degree decreases the adhesion energy.[18] The shear strength is increased by cross-linking. The peel-strength increases at small cross-linking degrees and decreases at high cross-linking degrees.[4] Regarding the stage of polymer interdiffusion, which is relevant when preparing acrylic PSA films from polymer dispersions (see Section 2.5 and 2.6), irreversible cross-linking of chains in the particles can limit interdiffusion to the extent that a heterogeneous, fragile film is obtained.[5]

Cross-linking of polymer chains can be based on covalent or non-covalent bonds and results in the formation of a polymer gel.[24] Polymer gels are three-dimensionally interconnected networks of chains which do not dissolve, but swell in a solvent for the corresponding linear chains.[24] The fraction of a polymer film which does not dissolve is referred to as the gel fraction and the fraction which dissolves is referred to as the sol fraction. Typical types of interactions for network formation are sketched in Figure 8.[24] In general, all types of polymer cross-linking sketched in Figure 8 can be reversible.[12,25] Making use of reversible cross-linking is frequently done to prepare self-healing polymer films.[24–26]

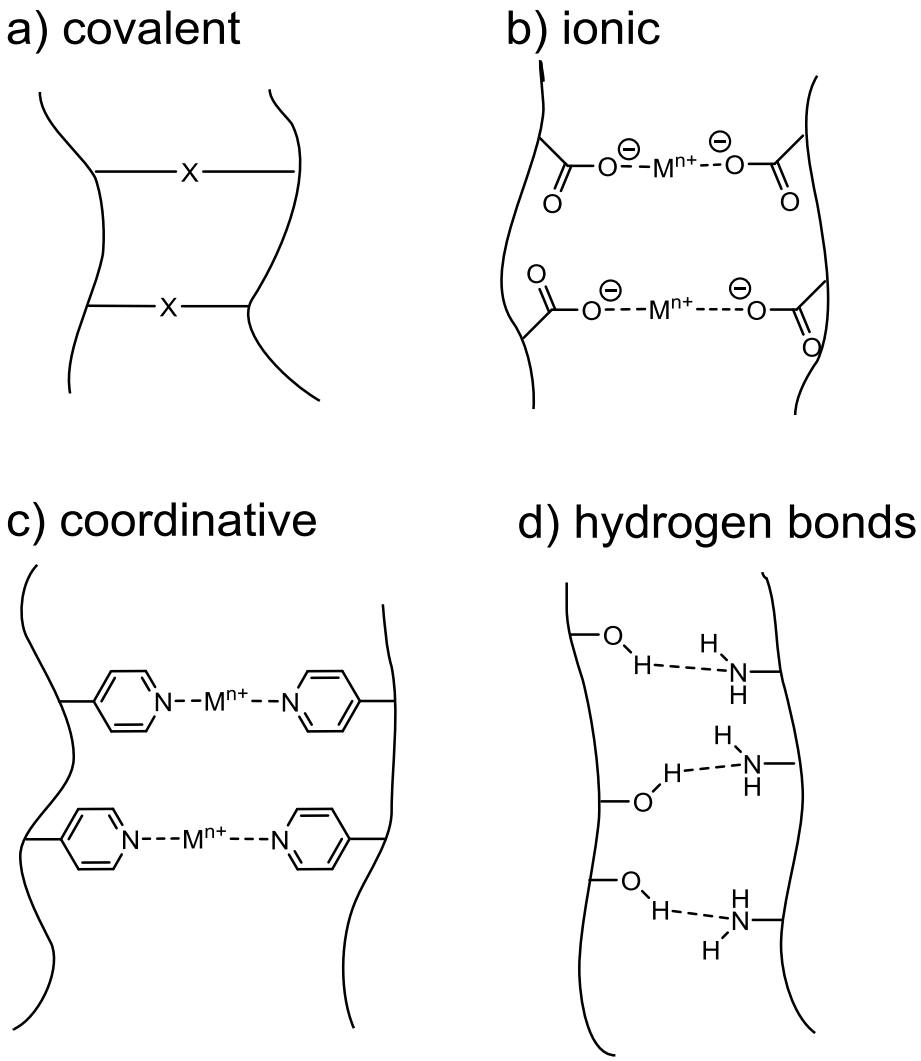

Figure 8: Types of possible interactions for polymer cross-links. Adapted from Ref. [24].

The first type of cross-linking shown in Figure 8 a) is covalent cross-linking, with X the bridging moiety. In case of acrylic PSAs, covalent cross-linking can be achieved by employing small amounts of bi-functional monomers such as ethylene glycol dimethacrylate or 1,4-butanediol diacrylate during the synthesis.[4,27] Reversible covalent cross-linking can be achieved making use of the retro Diels-Alder reaction.[25]

Ionic cross-linking, which was investigated in this thesis, is shown in Figure 8 b). Ionic cross-linking is often based on electrostatic interactions between anionic groups along the polymer chains (usually carboxylate groups) and metal cations. Ionic bonds between

carboxylate groups and metal cations can be reversible.[12] By thermal energy, the attractive interactions can be overcome and the chains can reversibly detach from the metal cations.[12,30–34] To achieve ionic cross-linking in acrylic PSAs, their solutions or dispersions can be blended with metal salts reacting with carboxylate groups in the polymer chains during drying.[13,14,28] Usually, metal chelates such as zirconium acetylacetonate or aluminum acetylacetonate, $Al(acac)_3$, are employed.[13,28] Cross-linking by metal acetylacetonates is discussed below in more detail. Alternatively, ionic cross-linking of chains in acrylic PSA dispersions can be achieved by employing salts of methacrylic acid such as zinc dimethacrylate, ZnDMA, as co-monomers during the synthesis. More details about cross-linking by ZnDMA are given below.

Cross-linking based on coordinative interactions is shown in Figure 8 c). Usually, chains containing ligands (such as nitrogen atoms in pyridine groups) are cross-linked by metal cations. Coordinative bonds are known to be reversible, allowing to prepare molecular velcros consisting of soft polymers.[35]

Hydrogen bonds between intermolecular amine and hydroxyl groups in polymer chains are shown in Figure 8 d). Acrylic PSAs consisting of chains bearing groups that can undergo hydrogen bonds show an increased cohesion.[27,36] Polymer cross-linking via hydrogen bonds is generally reversible.[27]

One objective of this work is to study the film formation of acrylic PSA dispersions blended with the ionic cross-linker aluminum acetylacetonate, $Al(acac)_3$. $Al(acac)_3$ is frequently added into solutions or dispersions of acrylic PSAs with linear chains. The cross-linking reaction according to Czech[15] is

$$3\ P\text{–}COO\text{–}H\ +\ Al(acac)_3 \leftrightharpoons Al^{3+}(\ ^{-}OOC\text{–}P)_3\ +\ 3\ acac\text{–}H \qquad (I)$$

P is the polymer chain. Carboxylate groups in the chains react with $Al(acac)_3$ to form an ionically cross-linked polymer, $Al^{3+}(\ ^{-}OOC\text{–}P)_3$, and acetylacetone (acac–H) as a by-product, the formation of the latter proven by Czech using gas chromatography.[15] Films from blends of acrylic PSAs (solutions and dispersions) and metal chelates have an increased shear strength and a decreased tack.[13–15] For solutions of PSAs in organic solvents blended with $Al(acac)_3$, stabilization by ethanol or isopropyl alcohol is necessary to prevent gelation.[15] For water-borne PSA dispersions blended with $Al(acac)_3$, less is known about the degree of cross-linking in the wet dispersion prior to film casting. An equilibrium is expected to be present because acetylacetone (acac–H), formed after cross-linking reaction remains in either the polymer particles or the aqueous phase. If the degree of cross-linking in the wet dispersion is small and if the cross-linking reaction is slower than polymer interdiffusion, a homogeneous film with a high gel content can be prepared.

Based on his studies reported in Ref. 15, Czech proposed a mechanism for the polymer cross-linking reaction by zirconium acetylacetonate. In Figure 9, this mechanism is applied for $Al(acac)_3$.

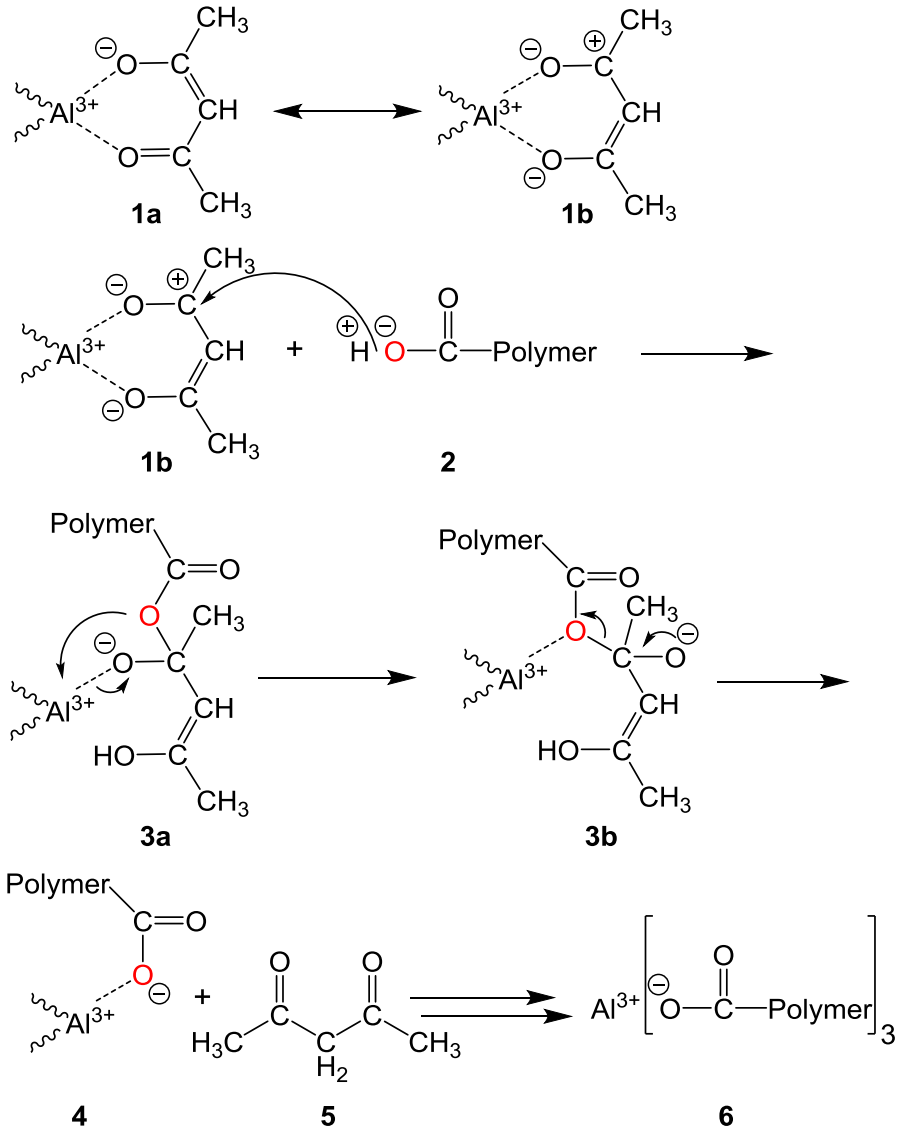

Figure 9: Proposed mechanism according to Ref. [15] for the cross-linking reaction between carboxylate groups attached to polymer chains and aluminum acetylacetonate. Dashed lines: electrostatic interactions, wavy lines: remaining acetylacetonate groups coordinating to Al^{3+}.

Acetylacetonate groups coordinating to Al^{3+} (**1a**) can form a zwitterion (**1b**). A carboxylate group attached to a polymer attacks the carbocation of **1b**. Rearrangement of the bonds (red oxygen in **3a** and **3b**) leads to the formation of a bond between a carboxylate group attached to the polymer and Al^{3+} (**4**). Acetylacetone (**5**) is formed as a by-product. After the other acetylacetonate groups have been substituted, an ionically cross-linked polymer (**6**) is obtained.

An alternative possibility to obtain homogeneous films with cross-linked chains from polymer dispersions can be based on making use of reversible, here, ionic cross-linking of chains in the particles before drying. In this work, zinc dimethacrylate, ZnDMA, the zinc salt of methacrylic acid, was used as a co-monomer to prepare dispersions containing ionically cross-linked chains. In contrast to aluminum trimethacrylate, the aluminum salt of methacrylic acid, which is neither soluble in organic solvents or water, ZnDMA is partially water-soluble and can therefore be used as a co-monomer in emulsion polymerization. The monomeric structure is given in Figure 10.[I]

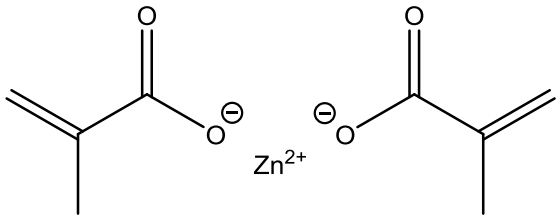

Figure 10: Chemical structure of zinc dimethacrylate, ZnDMA.[I]

In general, ZnDMA is used to reinforce elastomeric rubbers. The reinforcement is assumed to originate from ionic interactions.[29] In this thesis, the influence of the reversibility of the ionic bond between carboxylate groups in the chains and Zn^{2+} ions on interdiffusion is studied. The carboxylate-Zn^{2+} bond has been found to be reversible according to rheological measurements performed by Bose *et al.* in Ref. [12]. The reversibility of the bond can be advantageous for film formation because polymer interdiffusion is generally possible as chains are not forever fixed within their particles.

[I] Zinc carboxylates usually form clusters.[37] In Figure 10, a probably simplified structure is shown.

2.5 Film Formation of Aqueous Polymer Dispersions

Polymer films can be prepared form aqueous polymer dispersions (i.e. polymer latexes). Polymer dispersions are colloidal polymer nanoparticles dispersed in water which are stabilized against aggregation, the latter usually achieved by using surfactants.[5] Compared to the film formation of polymer solutions, the film formation of polymer dispersions is more complicated and can lead to structural heterogeneities in the final film.[6] The film formation of a drying polymer dispersion is divided into three steps as proposed by Voyutski[38] and is sketched in Figure 11.[5]

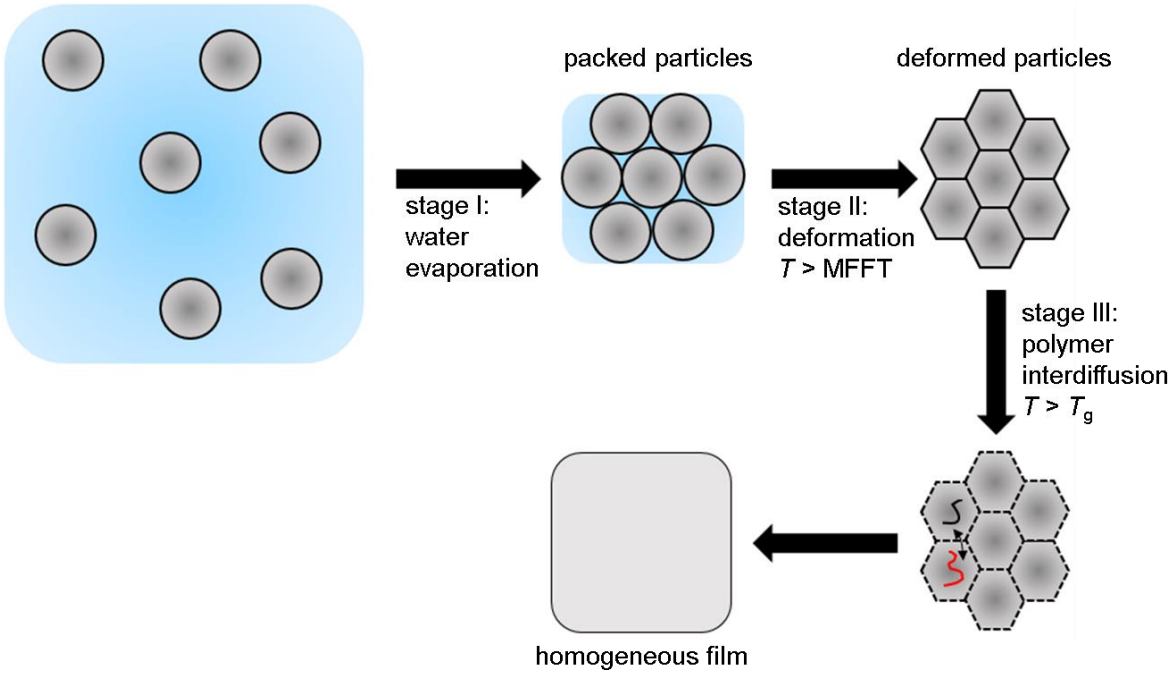

Figure 11: Film formation of aqueous polymer dispersions. Adapted from Ref. [5].

Latex film formation consists in three stages which are water evaporation (stage I), particle deformation (stage II) and polymer interdiffusion (stage III).[5]

In stage I, water evaporates, leading to an increase of the concentration of the polymer particles. After reaching a certain concentration, the particles overcome their repulsive

interactions and form a packing of spheres. In this stage, the film still appears turbid because light is scattered by the water remaining in the interstices.[5]

In stage II, the water in the interstices dries out and the particles deform into polyhedra if the temperature is above the minimum film formation temperature, MFFT. The film has turned clear but the particles are still separated by boundaries. As a result of particle deformation, stress in the film is developed.[5]

In stage III, polymer interdiffusion takes place if the ambient temperature is above the polymer's T_g. Polymer chains from adjacent particles diffuse into each other, leading to relaxation of stress in the film created by the preceding particle deformation. During interdiffusion, the particle boundaries disappear and cohesion inside the film is developed due to the formation of entanglements between chains from neighboring particles. When interdiffusion has finished, a homogeneous film is obtained.[5] Since this work focuses on polymer interdiffusion, it is discussed in more detail in Section 2.6.

Polymer dispersions usually are stabilized by surfactants which remain in the final film. In case of ionic surfactants, which have been used as emulsifiers in the dispersions investigated within this thesis, they can form hydrophilic pockets within the film and/or accumulate at the film–air and film–substrate interface.[5]

This work mainly concerns the stage of polymer interdiffusion which was investigated by employing *Förster Resonance Energy Transfer* (FRET). Light scattered by the dispersion was detected simultaneously which allows to extract information on the state of drying and particle deformation.[5] Details about drying and particle deformation are shortly outlined. The drying of a polymer dispersion is usually non-uniform along the film depending on the geometry and drying conditions. Both, heterogeneous vertical and horizontal drying can influence the final film morphology. In this work, vertical drying is of relevance because the polymer particles

are soft and phenomena such as skin formation (as discussed below) can be of relevance. Particle deformation is fast for acrylic PSA dispersions ($T_{ambient}$ > MFFT) but can occur following different mechanisms which might affect the morphology of the final film. Deformation mechanisms are wet sintering, dry sintering, capillary deformation, formation of capillary rings and the Sheetz deformation.[5] The mechanism of particle deformation depends on the drying conditions and the softness of the polymer particles.[5] In the following, first, consequences of heterogeneous vertical drying and second, the mechanisms of particle deformation relevant for soft polymer dispersions are discussed.

In case of vertical drying, the relation between the characteristic time for diffusion of the polymer particles, τ_{diff}, and the characteristic time for film drying, τ_{dry}, is important.[5] Their ratio is expressed by the dimensionless Péclet number, *Pe*, in eq. 1.

$$Pe = \frac{\tau_{diff}}{\tau_{dry}} = \frac{HE}{D} \qquad \text{eq. 1}$$

H is the film thickness, *E* the water evaporation rate and *D* the diffusion coefficient of the polymer particles. If *Pe* is smaller or equal to 1, homogeneous drying from the top to the bottom of the film takes place and the particle concentration remains equal along the depth profile of the film. If *Pe* is larger than 1, which is usually the case if the dispersion is dried very fast, particles accumulate at the surface of the film.[5]

The deformation mechanism depends on the quotient between the characteristic time for deformation, τ_{def}, and the characteristic time for drying, τ_{dry}, which is expressed by the dimensionless number λ (eq. 2).[5]

$$\lambda = \frac{\tau_{def}}{\tau_{dry}} = \frac{\eta RE}{\gamma H} \qquad \text{eq. 2}$$

γ is the surface tension at the interface and R the particle radius. η is the viscosity of the polymer. Its temperature dependence is described by the Williams-Landel-Ferry (WLF) equation (eq. 3).[5]

$$\eta = \eta_g \exp\left[\frac{-34(T - T_g)}{80 + T - T_g}\right] \qquad \text{eq. 3}$$

η_g is the viscosity of the polymer at its T_g. By combining results from different experiments, Routh and Russel have developed a deformation map in which λ is plotted against *Pe* which can be used to predict the deformation mechanism (see Ref. [5] or [40]). In the following, the mechanisms relevant for soft particles, which are wet sintering, capillary deformation and the Sheetz deformation, are outlined. In case of wet sintering, the particles deform before water evaporation has finished. It occurs if $\lambda << 1$, the driving force is the reduction of the water–polymer interface.[5] Capillary deformation is a process in which the particles deform as a result of the negative pressure of water at the water–air interface (see Figure 12). The negative pressure results from a concave meniscus of the water between two particles. In case of soft particles, the (higher) ambient pressure can lead to deformation.[5]

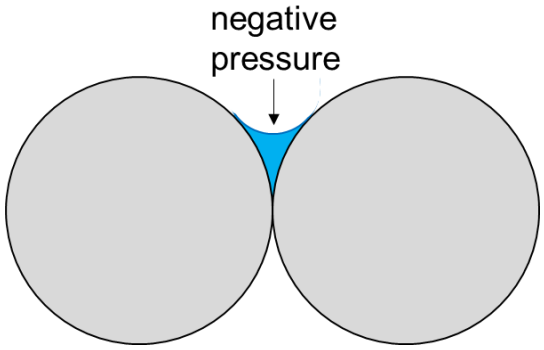

Figure 12: Concave meniscus of water between two particles at the top of the film. Adapted from Ref. [5].

The Sheetz deformation describes skin formation.[5] In case of fast drying (*Pe* >> 1) and soft polymer particles (λ << 1), particles accumulated at the film–air interface can deform, thereby forming a layer which slows down further water evaporation (Figure 13).[5]

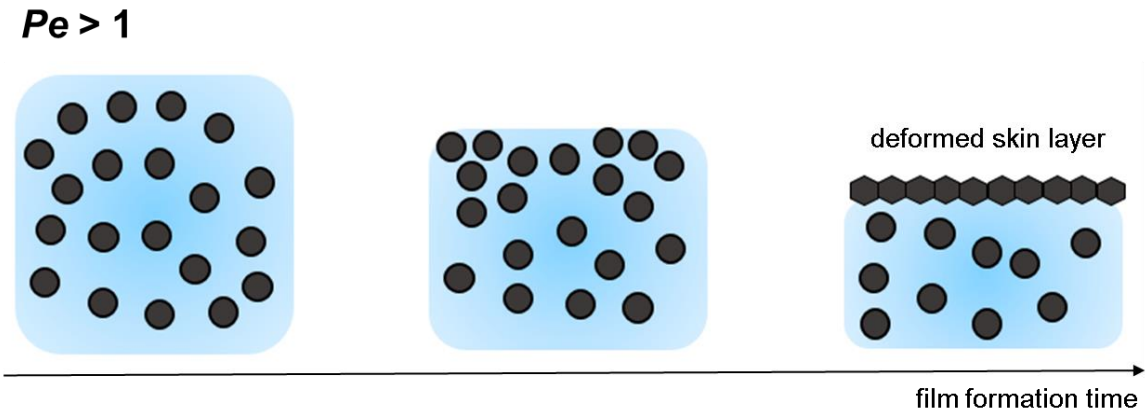

Figure 13: Scheme for skin formation in film forming dispersions. Adapted from Ref. [5].

Gravimetric and NMR studies on drying dispersions performed in literature,[39] have revealed that skin formation is the reason that softer latexes take longer to dry than harder latexes. A consequence of skin formation regarding the final application can be corrosion of the substrate by the entrapped water.[5]

2.6 Polymer Interdiffusion

Polymer interdiffusion in film forming latexes is crucial to obtain a homogeneous film.[5] Chains from neighboring particles interdiffuse into each other, particle boundaries disappear and cohesive strength inside the film is developed.[5] In Section 2.6.1, the diffusion of polymer chains in melts (which include polymer films from dispersions above the polymer's T_g) in general is discussed and in Section 2.6.2, the polymer interdiffusion in film forming latexes.

2.6.1 General Polymer Diffusion

The diffusion of polymer chains in melts or concentrated solutions differ from that of smaller particles (gases, ions or small organic molecules in solutions) in that it is not necessarily described by Fick's law.[41] This is attributed to the large size of polymer chains compared to small molecules. If the molecular weight of polymer chains surpasses a critical value M_c, chains in polymer melts form entanglements with neighboring ones. The situation is sketched in Figure 14 and is known as the tube model by Doi and Edward.[42] The black chains entangling with the turquoise, test chain in Figure 14 form a tube. The test chain can only move along this tube. Due to these geometric constraints, the motion of the test chain inside the tube is not described by Fick's law, which predicts a linear relationship between the mean squared displacement, *msd*, and the time *t* in the log-log plot, but by the reptation model.[41]

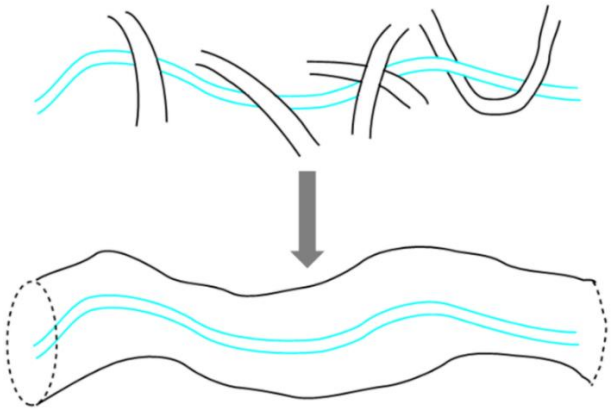

Figure 14: Tube model for polymer chains in melts according to Ref. [42].

The description of a polymer chain in the reptation model follows the Rouse model.[41] According to the Rouse model, a polymer chain is built by *N* segments interconnected by springs. In the reptation model, the displacement of the entire chain is deduced from the displacement of a single segment within the chain. A sketch for the displacement of a segment in a chain is shown in Figure 15.[41]

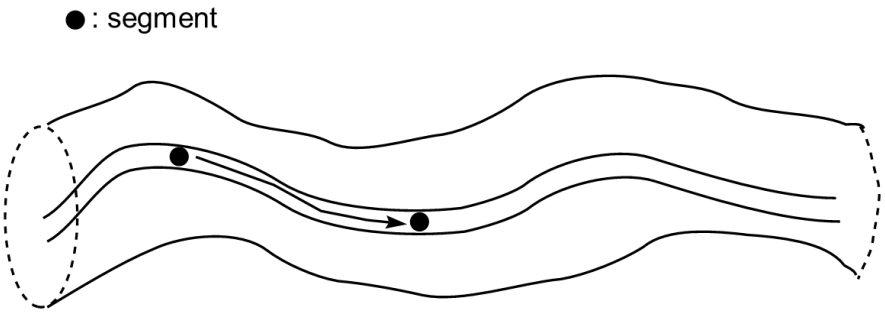

Figure 15: Displacement of a segment inside a polymer chain. Adapted from Ref. [41].

There are four different regimes of time scaling for the mean-squared displacement, *msd*, of a segment in the log-log plot as shown in Figure 16.[41]

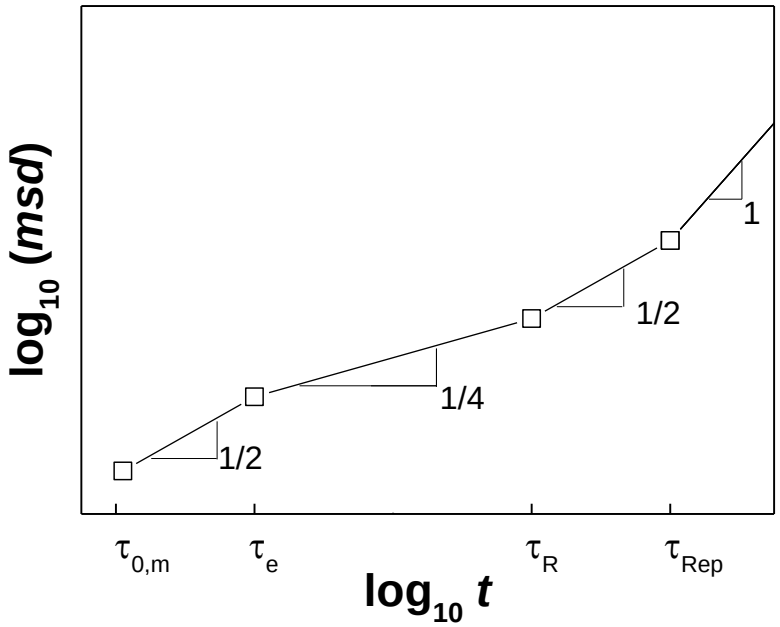

Figure 16: Regimes of time scaling for the mean-squared displacement of a segment in a polymer chain. Adapted from Ref. [41]

$\tau_{0,m}$ is the relaxation time for a single segment.[41] In case of short diffusion distances taking place between $\tau_{0,m}$ and the relaxation time of an entanglement strand, τ_e, the constraints do not interfere with the motion of the segment and *msd* scales with $t^{0.5}$ in the log-log plot. At times between τ_e and the Rouse time τ_R, topological constraints hinder movements tangential to the axis and *msd* scales with $t^{0.25}$ in the log-log plot. After τ_R, each segment of the chain participates in a coherent motion and *msd* scales with $t^{0.5}$ in the log-log plot up to the reptation time, τ_{Rep}. τ_{Rep} is the time when the chain has diffused out of its initial tube. At times later than τ_{Rep}, *msd* scales linearly with *t* in the log-log plot, following Fick's law.[41] A magnitude of order for these characteristic times is provided for polystyrene. From neutron reflection studies performed in literature, it was found for polystyrene with a molar mass of 233 kg/mol at 120 °C (20 °C above the T_g) that τ_e is ~ 6 s, τ_R is ~ 10 min and τ_{Rep} is ~ 17 h.[43]

τ_{Rep} can be estimated via eq. 4.[41]

$$\tau_{Rep} \approx \frac{\langle L \rangle^2}{D_c} \qquad \text{eq. 4}$$

$$D_c = \frac{kT}{N\xi} \qquad \text{eq. 5}$$

$\langle L \rangle$ is the average length of the tube and D_c is the curvilinear diffusion coefficient (eq. 5). In eq. 5, k is the Boltzmann's constant, T is the temperature and $N\xi$ is the Rouse friction coefficient.[41] As a result of theoretical calculations, it was found that τ_{Rep} is proportional to the third power of the polymer chain's molecular weight, M^3.[41] However, in experiments,[41] it was found that

$$\tau_{Rep} \sim M^{3.4} \qquad \text{eq. 6}$$

This deviation is attributed to tube length fluctuations caused by the displacement of the segments at the end of the tube.[41] For the curvilinear diffusion coefficient, D_c, following relation was found by experiment:[44]

$$D_c \sim M^{-2.3} \qquad \text{eq. 7}$$

2.6.2 Polymer Interdiffusion in Film Forming Latexes

This section concerns polymer interdiffusion in film forming latexes. Polymer interdiffusion (earlier also termed "further coalescence") is the last stage of latex film formation as assumed in 1958 by Voyutski[38] and indicated by experiments by Vanderhoff in 1968.[45] A sketch of polymer interdiffusion across two interfaces is given in Figure 17.

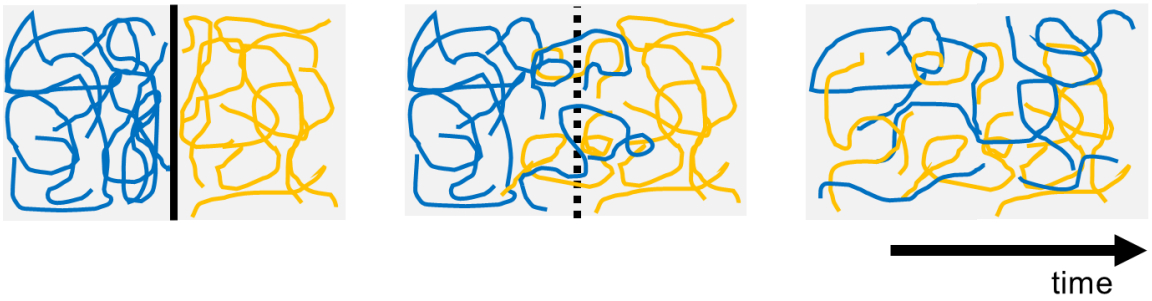

Figure 17: Polymer interdiffusion at interfaces. Different colors for the otherwise identical chains were chosen for the sake of clarity. Solid line (left): particle boundary before interdiffusion, dashed line (middle): disappearance of particle boundary during interdiffusion. Adapted from Ref. [5].

During interdiffusion, chains from adjacent particles intermix and form entanglements with each other, which provides for cohesion in the final film. The particle boundaries disappear and eventually a homogeneous film is obtained.[5] Mainly depending on the difference between $T_{ambient}$ and polymer's T_g, the time needed to reach the maximum degree of interdiffusion can be in orders of minutes, hours or even days.[5],II

In the following, experimental evidences and proofs for interdiffusion are outlined, and then the parameters affecting interdiffusion are discussed.

II Disappearance of particle boundaries at polymer-polymer interfaces is not only possible by chain interdiffusion but also by chain relaxation. If the radius of gyration of the chains, R_g, located at the boundaries is larger than the particle radius, their conformation differs from the conformation of the chains in the bulk of the particle. Upon contact of the polymer particles, the chains can relax along the boundaries into their Gaussian conformation. The time needed for the relaxation can be in the same magnitude of order as the reptation time[17,41,46,47] However, for polymer dispersions prepared by emulsion polymerization, which were investigated in this thesis, it can be assumed that the shorter chains are located at the particle boundaries.

The disappearance of particle boundaries during interdiffusion has been proven by electron microscopy.[45,48] The development of cohesion in the final film as a result of interdiffusion was proven by tensile tests, as it was found that the stress and strain at fracture increase with increasing time for interdiffusion.[48–50] It has been concluded that cohesion in films from dispersions is mainly provided by entanglements of polymer chains from initially neighboring particles.[5,50] In literature,[5] it is stated that the maximum cohesion in the film is achieved when the diffusion distance of a chain becomes comparable to its radius of gyration, R_g.[49] This was experimentally found for films from miniemulsified latexes of pre-synthesized polystyrene with a narrow molecular weight distribution.[49]

Polymer interdiffusion on a molecular scale was first studied by small angle neutron scattering.[51,52] Later, *Förster Resonance Energy Transfer* (FRET) was employed to track polymer interdiffusion (more details on studying polymer interdiffusion with FRET are given in Section 2.8).[53] Most of the studies of polymer interdiffusion in film forming latexes are based on FRET experiments. Recently, an experiment in which interdiffusion was followed by analyzing the excimer formation of pyrene has been reported.[54]

The main parameter influencing polymer interdiffusion is the difference between the ambient temperature and the polymer's T_g.[5] Other parameters affecting interdiffusion are for example the polymer architecture (i.e. cross-linking), the molar mass of the chains, the drying conditions and the presence of additives (plasticizers, organic solvents, or in this thesis tackifiers). The effects are shortly commented, polymer cross-linking is discussed in a following paragraph. Increasing the ambient temperature results in faster polymer interdiffusion due to the enhanced mobility of the chains.[5,17,53] The molar mass in polymer dispersions prepared by emulsion polymerization is usually broad. The diffusivity of a chain is inversely related to its molar mass (see Section 2.6.1), and thus smaller chains interdiffuse faster than larger chains.[53] The drying conditions affect polymer interdiffusion in that at high

ambient humidity, water vapor can condense into the film as it is absorbed by hydrophilic pockets formed by ionic surfactants.[55] Water in the film is known to plasticize the polymer chains (hydroplasticization), thereby decreasing their T_g and accelerating interdiffusion.[55–58] Tackifiers are known to loosen chain entanglements, which is expected to accelerate polymer interdiffusion.[59,60]

Cross-linking is of prime importance for acrylic PSAs.[1] Despite the fact that interdiffusion in PSA latexes is fast due to the polymer's low T_g, irreversible cross-linking of chains in the particles can limit interdiffusion to the extent that a fragile film is formed.[8–10] If the degree of cross-linking is too large, the final film lacks cohesive strength because it is composed of deformed particles separated by boundaries.[10] Therefore, cross-linking is usually performed after interdiffusion has finished (post cross-linking).[11] Post cross-linking can be achieved either by employing latexes with polymer chains bearing groups reacting during interdiffusion or by blending latexes with cross-linking reagents interconnecting the chains during interdiffusion.[11] In both cases, it is crucial that polymer cross-linking is slower than polymer interdiffusion.[61,62]

In this thesis, interdiffusion in ionically cross-linked acrylic PSA dispersions is investigated. For reasons discussed in Section 2.4, ionic cross-linking can be reversible.[12] Reversible cross-linking is advantageous for polymer interdiffusion because chains are not fixed forever within their particles but can diffuse out of them. In the first place, interdiffusion in films from latexes with linear chains blended with aluminum acetylacetonate, $Al(acac)_3$, an ionic cross-linker, is studied (see Section 2.4). In addition, interdiffusion in films from dispersions with chains ionically cross-linked prior to film casting, the latter achieved by employing ZnDMA as a co-monomer, is investigated.

2.7 Förster Resonance Energy Transfer (FRET)

Förster Resonance Energy Transfer (FRET) is a non-radiative energy transfer process between an excited fluorophore (i.e. donor) and a dye (i.e. acceptor) in the ground state, which can occur if their distance is within a few nanometers.[16] The FRET process was firstly described by Theodor Förster in 1948.[63] Nowadays, FRET is widely employed as a proximity probe to study processes occurring on a nanoscopic scale ("spectroscopic ruler") such as change of conformation in proteins[16] or polymer interdiffusion in dispersions.[17] A scheme for the FRET process between a donor, D, and an acceptor, A, is given in Figure 18.

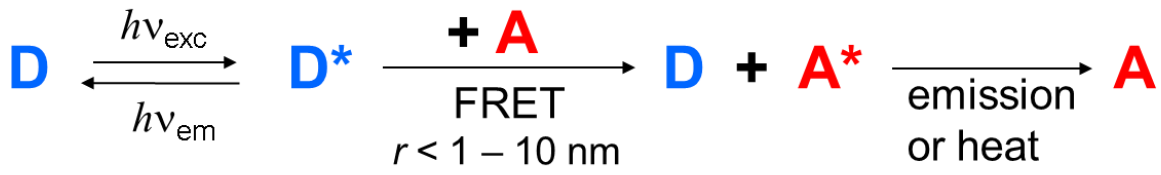

Figure 18: Reaction scheme for FRET. D and A denote donor and acceptor, respectively. Asterisks denote excited states, *r* is the distance between the dyes.

In the FRET process, the excited donor, D*, transfers its excitation energy to an acceptor, A, in the ground state instead of fluorescing. This direct, non-radiative energy transfer is based on dipole-dipole interactions between the two dyes and can only take place if their distance r is equal or smaller than the so called Förster radius, R_F, which is in the range of 1–10 nanometers. After the excited donor has transferred its excitation energy to the acceptor, the latter becomes excited, A*. Depending on the acceptor-dye, it can be either a fluorophore which relaxes by emission of light or a non-fluorescent dye which relaxes by release of heat.[16]

To describe the FRET process in more detail, a Jablonski diagram is provided in Figure 19.[16]

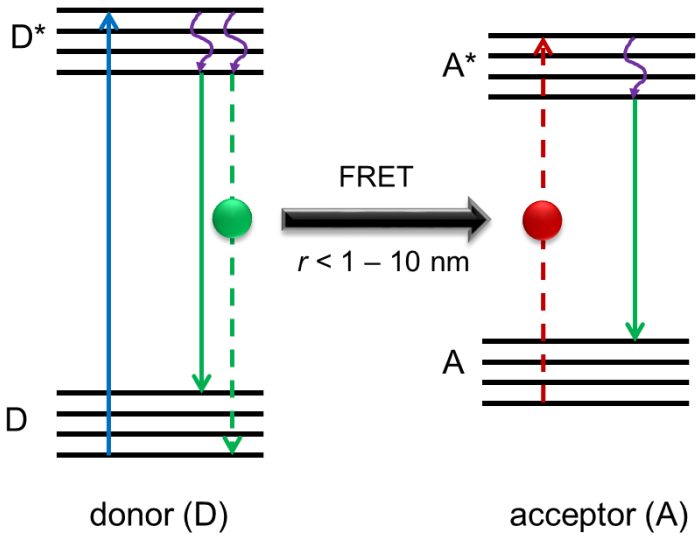

Figure 19: Jablonski scheme for FRET according to Ref. [16]. D and A denote donor and acceptor, respectively. Asterisk denotes excited states, *r* is the distance between the dyes. Dashed arrows are relaxation and excitation via FRET.

Molecules can be described as oscillating electric dipoles. Non-radiative energy transfer between an excited donor and an acceptor in the ground state can take place if the frequencies of their transition dipoles are similar, or in other words if the emission spectrum of the donor overlaps with the absorption spectrum of the acceptor. The FRET efficiency depends on the distance between donor and acceptor. The rate constant of FRET, k_{FRET}, is defined as

$$k_{FRET} = \frac{1}{\tau_D}\left(\frac{R_F}{r}\right)^6 \qquad \text{eq. 8}$$

τ_D is the lifetime of the excited state of the donor (i.e. donor's lifetime) which is typically in orders of nanoseconds. If the distance between donor and acceptor, *r*, is smaller than the Förster radius, R_F (1 – 10 nm), FRET is more likely to occur than donor fluorescence.[16]

The Förster radius R_F depends on many parameters and is defined as

$$R_F^6 = \frac{9000 \ln(10)\kappa^2 Q_D}{128\pi^5 N_A n^4} \cdot J(\lambda) \qquad \text{eq. 9}$$

$J(\lambda)$ is the overlap integral of the donor's emission spectrum and acceptor's absorption spectrum. Q_D is the quantum yield of the donor, n is the refractive index of the medium and N_A is Avogadro's number. κ is the orientation factor of the transition dipoles of D* and A, which is 0.476 for random orientation of immobile molecules.[16]

This work here relies on time-resolved fluorescence to quantify FRET which is suited to obtain quantitative fluorescence data from systems changing their optical properties like film forming polymer dispersions. The donor's fluorescence decay becomes curved when it performs FRET.[16] Decays of a dry polymer film from a donor-labeled dispersion (no FRET) and that of a homogeneous film from a blend of donor- and acceptor-labeled dispersions (FRET) are shown in Figure 20.

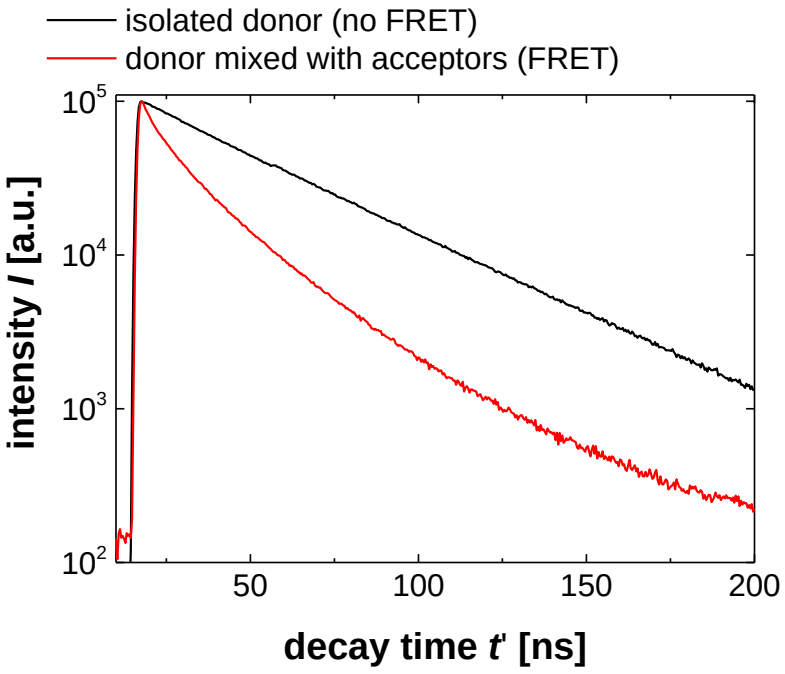

Figure 20: Fluorescence decays of an isolated donor (no FRET) and a donor intermixed with acceptors (FRET).

An isolated donor has a mono-exponential fluorescence decay $I(t')$ (eq. 10), with τ_D being the decay constant, t' the decay time, both usually in orders of nanoseconds, and I_0 the intensity after the excitation pulse. A donor intermixed with acceptor-dyes performs FRET and has a curved decay that can be fitted according to the Förster equation (eq. 11).[16]

$$I(t') = I_0 \exp(-t'/\tau_D) \qquad \text{eq. 10}$$

$$I(t') = I_0 \exp\left((-t'/\tau_D) - 2\gamma\sqrt{(t'/\tau_D)}\right) \qquad \text{eq. 11}$$

2γ is defined as

$$2\gamma = \frac{4}{3}\pi^{3/2} N_A R_F^3 c_A \qquad \text{eq. 12}$$

c_A is the molar concentration of acceptor-dyes surrounding the donor in a sphere with a radius R_F.[16] The principle of the study of polymer interdiffusion with FRET and the dyes used as labels are presented in Section 2.8.

2.8 Study of Polymer Interdiffusion with FRET

FRET is the most applied technique to follow the progress of polymer interdiffusion in film forming latexes.[17,53] To track interdiffusion, a set of two dispersion with identical properties except for the labeling must be prepared. In one dispersion, donor-dyes are covalently attached to the chains and in the other one, acceptor-dyes are attached to the chains. Donor fluorescence decays of a film forming blend of donor- and acceptor-labeled latexes are recorded continuously in a kinetic experiment. As interdiffusion progresses, donors intermix with acceptors and perform FRET, leading to an increase of curvature in the donor decays. A sketch for such an experiment is given in Figure 21.[17]

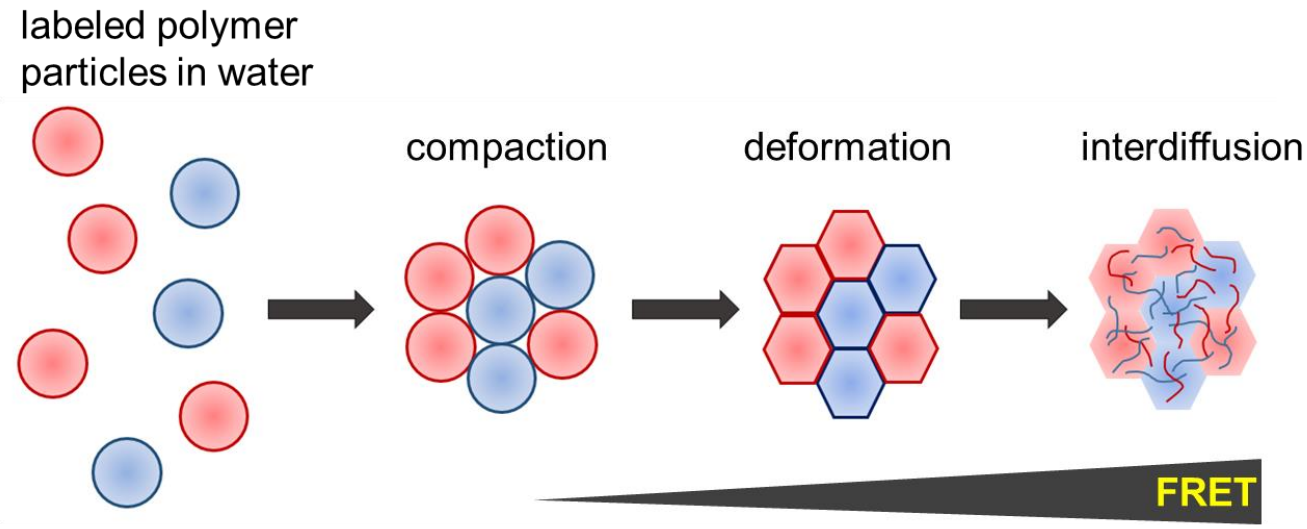

Figure 21: Principle of tracking interdiffusion in film forming polymer dispersions with FRET.

As the labeled chains intermix, FRET becomes more pronounced in the donor decays. The evolution of the curvature of donor decays obtained in a kinetic experiment is given in Figure 22.

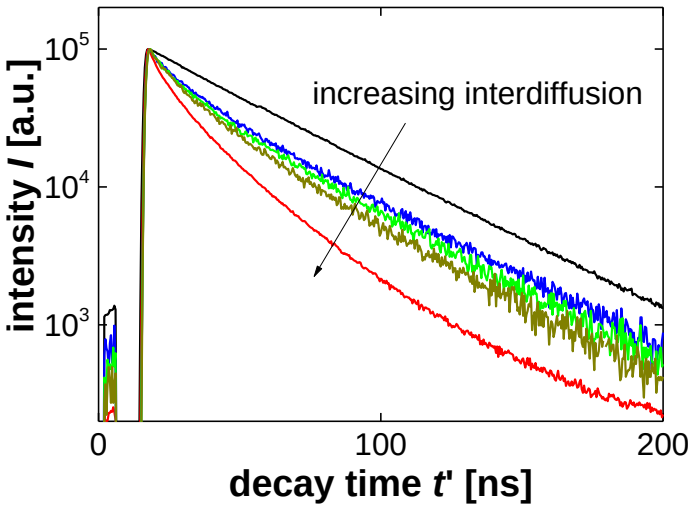

Figure 22: Increase of curvature in donor fluorescence decays during interdiffusion of labeled chains.

In the beginning, the donor decay is mono-exponential (eq. 10) because no interdiffusion has occurred and donors are isolated from acceptors. In the homogeneous film, where labeled chains have fully intermixed and FRET occurs at the maximum rate possible for the given system, a curved decay that can be fitted to the Förster equation (eq. 11) is obtained. To describe the intermediate state quantifying the progress of interdiffusion, decays are fitted according to the two-state model developed by the Winnik group (eq. 13).[53]

$$I(t') = I_0 \left[A_2 \cdot \exp\left(\left(-\frac{t'}{\tau_D} \right) - 2\gamma \sqrt{\frac{t'}{\tau_D}} \right) + (1 - A_2) \cdot \exp\left(-\frac{t'}{\tau_D} \right) \right] \qquad \text{eq. 13}$$

A_2 is the central fit parameter and increases as labeled chains intermix due to interdiffusion. τ_D and 2γ are set constant during the fitting procedure after being determined in separate experiments. τ_D is the fluorescence lifetime of the donor and obtained from a dry, donor-labeled film ($A_2 = 0$, eq. 10). 2γ is related to the acceptor concentration in the vicinity of the donor at maximum interdiffusion (eq. 12) and is obtained from a homogeneous film where chains are expected to be fully intermixed ($A_2 = 1$, eq. 11). The state of full intermixing can be achieved

by thoroughly intermixing a film consisting of linear chains with a solvent such as THF and letting it dry afterwards. Keeping 2γ constant during fitting results in simplifications because the local acceptor concentration changes during interdiffusion. In literature,[64] there are alternative models accounting for the change of the acceptor concentration but in this thesis the two-state model is employed because it suffices to point out the structure-property relationships, mainly cross-linking, in the investigated dispersions.

Usually, A_2 is converted to a normalized quantity, the fraction of intermixing, f_m (eq. 14).[53]

$$f_m(t) = \frac{A_2(t) - A_{2,min}}{1 - A_{2,min}} \qquad \text{eq. 14}$$

$A_{2,min}$ is the A_2 value obtained on a wet, non-drying blend of donor- and acceptor-labeled latexes. In general, a value close to zero is expected for $A_{2,min}$ because no interdiffusion should have occurred prior to drying. However, in case of the herein investigated dispersions, $A_{2,min}$ was found to be larger than zero. More on this issue is discussed in Section 4.1.

Sometimes in this thesis, f_m is plotted against the corrected film formation time t'' (eq. 15) for reasons discussed in Section 4.2 and Ref. [19].

$$t'' = t - t_0 \qquad \text{eq. 15}$$

t_0 is the time after the film becomes transparent, i.e. when the intensity of scattered excitation light becomes zero (as discussed in Sections 3.5 and 4.2).

To estimate a polymer diffusion coefficient, *D*, Winnik has proposed to apply the spherical diffusion model (eq. 16)[65] to fit f_m data (eq. 17).[53] As a simplification, Fickian diffusion is assumed, which is not necessarily valid for polymer chains as discussed in Section 2.6. However, it allows for a qualitative estimation of the magnitude of order of polymer diffusion coefficients. *D* can be interpreted as a cumulative, apparent diffusion coefficient of all chains that have diffused up to the time *t*''.[53]

$$C(r,t'') = \frac{C_0}{2}\left[\operatorname{erf}\left(\frac{R+r}{2\sqrt{Dt''}}\right) + \operatorname{erf}\left(\frac{R-r}{2\sqrt{Dt''}}\right)\right] - \frac{C_0}{R}\sqrt{\frac{Dt''}{\pi}} \times \left\{\exp\left[-\frac{(R+r)^2}{4Dt''}\right] - \exp\left[-\frac{(R-r)^2}{4Dt''}\right]\right\} \quad \text{eq. 16}$$

$$f_m(t'') \approx 1 - \frac{3}{4\pi R^3 C_0}\int_0^R C(r,t'')4\pi r^2 \mathrm{d}r \quad \text{eq. 17}$$

C_0 is an initial concentration, *R* the size of the spherical polymer particles and *r* the diffusion distance in nanometers. Chains having diffused out of their particles ($r > R$) contribute to an increase of f_m.[53]

Structures of the monomeric dyes used to label the polymer chains in the herein investigated dispersions are given in Figure 23. (9-Phenanthryl)methyl methacrylate (Phen-MMA) has been used as the donor (a) and 1-(4-nitrophenyl)-2-pyrrolidinemethyl acrylate (NPP-A) as the non-fluorescent acceptor (b).[66] Since both dyes are esters of methacrylic acid and acrylic acid, they can be copolymerized with acrylic monomers.

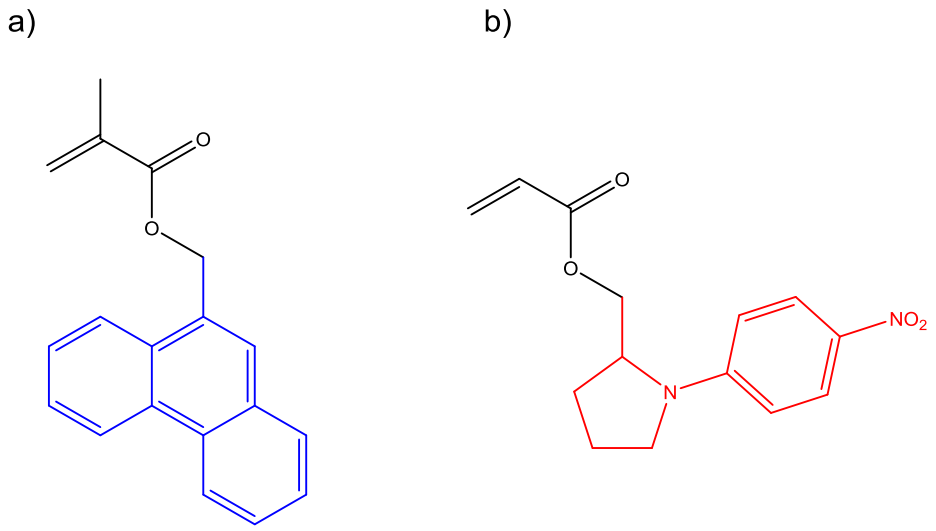

Figure 23: Chemical structures of (9-phenanthryl)methyl methacrylate (donor) and 1-(4-nitrophenyl)-2-pyrrolidinemethyl acrylate (acceptor).

Employing a non-fluorescent acceptor is advantageous for the signal-to-noise ratio in time-resolved fluorescence measurements because a cutoff filter only eliminating excitation light can be employed in the setup.

The emission spectrum of a donor-labeled dispersion and the absorption spectrum of an acceptor-labeled dispersion, both dissolved in THF, are shown Figure 24.

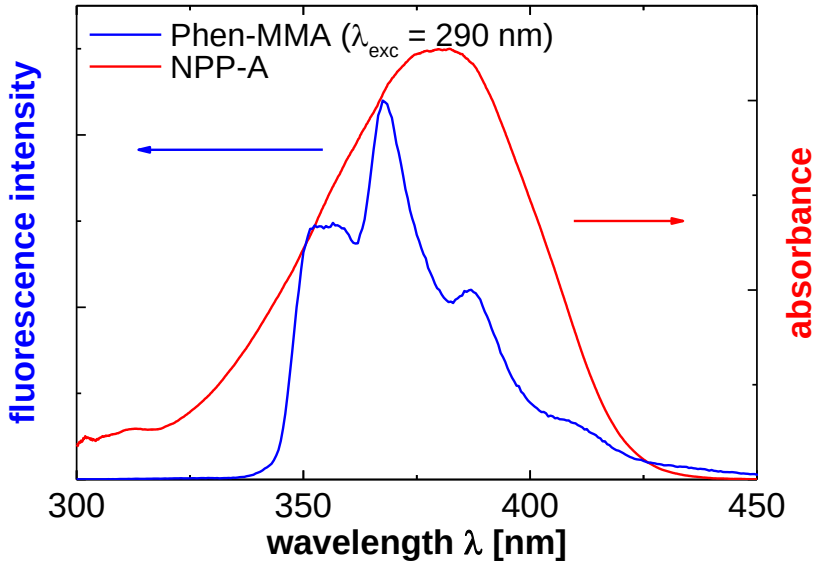

Figure 24: Fluorescence and absorption spectra of donor- and acceptor-labeled dispersions dissolved in THF, respectively.

Clearly, there is a spectral overlap between the fluorescence spectrum of the donor and the absorption spectrum of the acceptor. For copolymers of *n*-butyl acrylate and methyl methacrylate, R_F for the Phen-NPP pair was found to be around 2.5 nm.[66]

3 Experimental Section

3.1 Chemicals

Most of the polymer dispersions were prepared and provided by BASF SE. Details about their synthesis are given in Ref. [19]. The used tackifier was Snowtack FH94G which was supplied by Lawter Europe. It is an aqueous dispersion of a fully hydrogenated rosin ester (properties according to the data sheet: softening point = 93 °C, d_{90} = 0.927 μm, d_{50} = 0.454 μm). It was diluted to 28% to match the solids content of the dispersions with which it was blended. Water was purified using an Arium 611 VF system by Sartorius.

In the following, chemicals used for synthesis (miniemulsion polymerization) and analysis of polymer dispersions are listed. If not mentioned otherwise, their purity is at least 99%. *n*-butyl acrylate (BA), methacrylic acid (MAA), methyl methacrylate (MMA), 2-ethylhexyl acrylate (EHA), 1-dodecyl mercaptan (DDM), ethylene glycol dimethacrylate (EGDMA, 98%), 1-(4-nitrophenyl)-2-pyrrolidonemethyl acrylate (NPP-A, 97%), zinc dimethacrylate (ZnDMA), zinc acetylacetonate hydrate ($Zn(acac)_2$), dimethyl sulfoxide, methyl ethyl ketone (MEK), acetylacetone and tetrahydrofuran (THF, inhibitor-free, analytical grade) were purchased from Sigma Aldrich. Calcium chloride ($CaCl_2$, anhydrous), sodium persulfate (NaPS) and hexadecane (HD) were purchased from Merck. (9-Phenanthryl)methyl methacrylate (Phen-MMA) was purchased from TRC. Silica gel, sodium dodecyl sulfate (SDS) and sodium bromide (NaBr) were purchased from Carl Roth. Cyclohexane (spectroscopic grade) was purchased from Acros Organics. Inhibitors were removed from BA, MAA, MMA and EHA using inhibitor remover resin (Sigma Aldrich). All other chemicals were used as received.

3.2 Characterization of Polymer Dispersions

Solids contents were determined gravimetrically.

Particle sizes were determined using dynamic light scattering (DLS, ALV/CGS-3 equipped with a multi-τ digital correlator). Temperature was 25 °C, scattered light was detected at 90°. In this thesis, the values for the hydrodynamic diameter, d_h, correspond to the value from the mass weighted fit, d_w. The size dispersity (d_w/d_n) was never higher than 1.2 in all cases.

Molecular weight distributions, M_w, M_w/M_n, were determined using gel permeation chromatography (GPC, Agilent 1200, SDV columns (PSS)). Freshly distilled THF was used as eluent, polystyrene standards were used for calibration and temperature was 25 °C. All GPC measurements were carried out by Martina Heinz at the Institute of Technical Chemistry, Clausthal University of Technology.

Glass transition temperatures, T_g, of the polymers were determined using differential scanning calorimetry (DSC, Mettler Toledo) on polymer films prepared by drying the dispersions first at room temperature and then under vacuum overnight. The heating rate was 10 K/min. The T_g obtained from the second heating curve was used for analysis. DSC measurements were carried out by Ulrike Koecher, Werner Bischof and Martin Schwedes at the Institute of Technical Chemistry, Clausthal University of Technology.

Gel contents of the polymers were determined as follows: Dispersions were dried for at least 4 days at room temperature and then at 50 °C overnight. The film was swollen in MEK (with $m_{MEK} = 100 \cdot m_{film}$, m_{MEK} is the mass of MEK and m_{film} the mass of the film) for 3 – 4 days without stirring. Afterwards, the mixture was filtered using nylon filters (Sefar Nitex, 120 μm pore diameter) and the gel content determined as $100\% \cdot m_{gel}/m_{film}$, with m_{gel} the mass of the gel collected by the filter. Gel content determinations of films from dispersions provided by BASF SE were carried out by Stephan Möbius at BASF SE, Ludwigshafen.

3.3 Preparation of Polymer Dispersions

This section covers the preparation of polymer dispersions. The properties of the investigated dispersions are provided in Section 3.4.

Mainly, industrially relevant PSA dispersions synthesized and provided by BASF SE were investigated. The details about their synthesis are given in Ref. [19] and are only shortly outlined here. The dispersions were prepared by seeded emulsion polymerization under starve-fed conditions.[67] The polymers in the dispersions were statistical copolymers of 2-ethylhexyl acrylate/styrene/*n*-butyl acrylate/methyl acrylate/methacrylic acid in a weight ratio of 59/20/15/5/1. A mixture of the ionic surfactants Dowfax 2A1 and Disponil FES 77 was used as stabilizers, sodium persulfate, NaPS, was used as the initiator. Sets consisting of two dispersions with identical properties except for the labeling were prepared. Donor-labeling was achieved with 1.6 pphm Phen-MMA (pphm: "parts per hundred monomer", weight percentage with respect to the monomer) and acceptor-labelling was achieved with 1 pphm NPP-A. Polymer architectures were varied, labeled dispersions with uncross-linked (here synonymous to linear ("L")) chains, linear chains blended with 1 pphm aluminum acetylacetonate, $Al(acac)_3$, ("L+$Al(acac)_3$") and covalently cross-linked chains ("cov-X") were provided. In case of L and L+$Al(acac)_3$, dispersions where the serum was neutralized from a pH of 2 (due to decomposition of the persulfate initiator during the synthesis)[68] to a pH of 7 using aqueous ammonia solution (10 wt-%) were provided as well. Neutralization of the serum was done to improve colloidal stability.[5] An unlabeled reference dispersion with linear chains with a serum pH of 2 was provided in addition.

Labeled dispersions for additional reference studies were prepared by miniemulsion polymerization (MEP)[69] in order to corroborate the results from studies on the dispersions provided by BASF SE. MEP is a suitable technique to prepare small amounts of stable dispersions.

A sketch of MEP initiated in the aqueous phase is given in Figure 25.

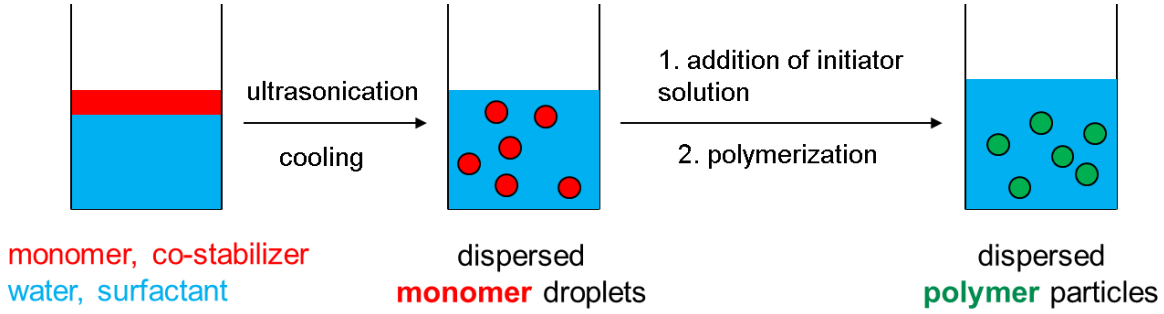

Figure 25: Sketch of MEP initiated in the aqueous phase.

The organic phase containing monomer and co-stabilizer and the aqueous phase containing water and surfactant are mixed and sonicated under cooling to obtain dispersed monomer droplets with a uniform size. Afterwards, the aqueous solution of the initiator is added and polymerization is started. Usually, in MEP, initiation occurs in the organic phase. MEP initiated using a water-soluble initiator is closer to emulsion polymerization with respect to the formation of water-soluble oligomers,[69,70] which do not form if the polymerization is initiated in the organic phase.

Monomer compositions were varied (see below), other reagents were added at a constant amount. Sodium dodecyl sulfate (SDS) was used as the surfactant, hexadecane (HD) as the co-stabilizer to prevent Ostwald ripening, 1-dodecyl mercaptan (DDM) as the chain transfer agent and sodium persulfate (NaPS) as the initiator. The general procedure consisted in mixing the aqueous and organic phase, ultrasonication for 2 min (Branson Sonifier, Output 7, Duty Cycle 70%) while cooling the mixture with an ice/ethanol mixture, adding the initiator solution, purging the mixture with argon for 5 min and starting the polymerization. Polymerization was carried out for 8 h at 60 °C.

First, a series of labeled polymer dispersions with different T_g and polymer hydrophilicity was prepared to evaluate the processes occurring before and shortly after film casting. These

dispersions have a maximum, theoretical solids content of 25%. The compositions of the phases and the mass of reagents added at a constant amount are provided in Table 2. "pphm" stands for parts per hundred monomer and refers to the weight percentage with respect to the total mass of the monomers.

Table 2: Composition of phases during the synthesis of dispersions by MEP with different T_g.

Phase	Chemicals
Aqueous phase	water (5.5 g), SDS (2 pphm, 0.046 g)
Organic phase	monomers (total mass: 2.32 g), HD (4 pphm, 0.093 g), DDM (0.1 pphm, 0.003 g)
Initiator solution	water (2 g), NaPS (2 pphm, 0.046 g)

The total mass of monomers was always 2.32 g, independent of dye-labeling. However, in case of donor-labeling, 0.036 g (1.6 pphm) Phen-MMA were used while in case of acceptor-labeling, 0.023 g (1 pphm) NPP-A were used. Monomer compositions for donor-labeled dispersions are provided in Table 3, methacrylic acid (MAA) was always added at a constant amount of 0.023 g. Subscripted numbers are the weight percentage of the monomer. For acceptor-labeled dispersions, monomer masses can be calculated accordingly from the weight percentages. The T_g was varied by employing different amounts of *n*-butyl acrylate (BA) and methyl methacrylate (MMA). To investigate the effect of the polymer's hydrophilicity, a dispersion in which 2-ethylhexyl acrylate (EHA), instead of BA, was used as a monomer (EHA is more hydrophobic than BA)[55] was prepared.

Table 3: Composition of monomer mixtures used to prepare donor-labeled dispersions by MEP with different T_g. Number in subscripts are weight fractions. Mass of MAA was always 0.023 g.

Monomer composition	Calc. T_g [°C]	Mass
BA_{99}-MAA_1	–52	BA: 2.267 g
BA_{78}-MMA_{21}-MAA_1	–30	BA: 1.769 g, MMA: 0.450 g
BA_{41}-MMA_{58}-MAA_1	+20	BA: 0.973 g, MMA: 1.326 g
EHA_{99}-MAA_1	–49	EHA: 2.254 g

Glass transition temperatures, T_g, of dispersions prepared by MEP could not be determined properly by differential scanning calorimetry (DSC) because hexadecane smeared out the inflection points in the DSC curves. Therefore, T_g values calculated from the Fox equation (eq. 18) are provided.[72]

$$\frac{1}{T_g} = \sum_i \frac{w_i}{T_{g,i}} \qquad \text{eq. 18}$$

w_i is the weight fraction of the monomer i and $T_{g,i}$ the glass transition temperature of the corresponding homopolymer. T_g values of the homopolymers taken from Ref. [23] are provided in Table 4.

Table 4: T_g values of homopolymers used to calculate the T_g of the copolymers. Data were taken from Ref. [23].

Polymer	T_g [°C]
PBA	–54
PMAA	+228
PMMA	+105
PEHA	–50

A second series of labeled dispersions was prepared to investigate effects of ionic cross-linking by Zn^{2+} on interdiffusion. Ionic cross-linking was achieved employing ZnDMA as a co-monomer. Composition of the phases are given in Table 5. Note, that ZnDMA was added into the aqueous phase because it is not soluble in the organic phase. Due to the limited solubility of ZnDMA in water, only dispersions with a maximum, theoretical solids content of 20% could be prepared.

Table 5: Composition of phases during the synthesis of dispersions by MEP with different degrees of ionic cross-linking.

Phase	Chemicals
Aqueous phase	water (6 g), SDS (2 pphm, 0.037 g), ZnDMA (varied)
Organic phase	BA (varied), MAA (varied), HD (4 pphm, 0.074 g), DDM (0.1 pphm, 0.002 g)
Initiator solution	water (2 g), NaPS (2 pphm, 0.037 g)

To achieve different degrees of ionic cross-linking, the composition of the monomer mixture consisting of BA, ZnDMA and MAA, was varied. It was adjusted such that the weight percentages of w_{BA} and w_{COOH} in the final dispersions were always 98 and 2, respectively (II). MAA contributes one carboxylate group, while ZnDMA contributes two carboxylate groups. Total monomer mass was around 1.83 g. For donor-labeling, 0.029 g (1.6 pphm) Phen-MMA were added into the organic phase and for acceptor-labeling 0.018 g (1 pphm) NPP-A. Again, monomer masses are only provided for donor-labeled dispersions in Table 6, for acceptor-labeled dispersions they can be calculated from the weight percentages given in the parentheses. "Zn-X" denotes cross-linking by Zn^{2+}, "1" denotes a molar ratio of $n_{COOH}/n_{Zn(II)} = 2/1$ (stoichiometric), while "0.5" denotes a molar ratio of $n_{COOH}/n_{Zn(II)} = 4/1$ (half-stoichiometric). Labeled dispersions with linear chains (MEP-L-II) were prepared as well. In addition, labeled dispersions with $w_{BA}/w_{MAA} = 95/5$ were synthesized. These dispersions were blended with $Zn(acac)_2$ for reference measurements (as discussed below). For comparative studies between ionic and covalent cross-linking, labeled dispersions with covalently cross-linked chains (MEP-cov-X) were prepared as well. The ratio of weight percentages was $w_{BA}/w_{EGDMA}/w_{MAA} = 94/4/2$, otherwise the protocol remained unchanged.

Table 6: Composition of monomer mixtures used to prepare donor-labeled dispersions by MEP having different degrees of ionic cross-linking. Numbers in parentheses are weight percentages.

Dispersion	m_{BA} [g]	m_{MAA} [g]	m_{ZnDMA} [g]
MEP-L-II	1.787 (98)	0.035 (2)	0
MEP-Zn-X-0.5	1.778 (97.5)	0.018 (1)	0.029 (1.5)
MEP-Zn-X-1	1.765 (97)	0	0.058 (3)
MEP-L-V	1.734 (95)	0.087 (5)	0

Blending of MEP-L-II and MEP-L-V with $Zn(acac)_2$ was done by intermixing 3 – 4 g of the respective dispersion with varying amounts of $Zn(acac)_2$ (ranging from 3.7 – 9.2 pphm). The amount of $Zn(acac)_2$ was such that either a molar ratio of "1" ($n_{MAA}/n_{Zn(II)}$ = 2/1, stoichiometric) or "0.5" ($n_{MAA}/n_{Zn(II)}$ = 4/1, half-stoichiometric) was present in the latex. Dispersions were used one week after the addition of $Zn(acac)_2$. The dispersions must not be stirred, more on this issue is discussed in Section 3.4.

3.4 Properties of Investigated Dispersions

Properties of dispersions prepared by BASF SE are given in Table 7. “D” denotes donor-labeling, “A” denotes acceptor-labeling, “L” denotes linear, “cov-X” denotes covalent cross-linking, and “2” and “7” are the serum pH. $Al(acac)_3$ was added at a constant amount of 1 pphm. T_g of polymers are between –40 to –30 °C (see Ref. [18]) and size dispersities are never larger than 1.2. Clearly, labeled dispersions within a set have nearly similar properties. Incorporation of labels into the chains, independent of their molecular weight, has been proven by GPC measurements where detectors sensitive to the respective labels were used. Data are provided in Ref. [19].

Table 7: Properties of dispersions provided by BASF SE.

Dispersion	Solids content [%]	d_h [nm]	M_w (M_w/M_n) [kg/mol]	Gel content [%]
D-L-2	28	154	379 (4.5)	0
A-L-2	27	140	184 (3.8)	0
D-L-2+$Al(acac)_3$	28	151	–	79
A-L-2+$Al(acac)_3$	27	142	–	70
D-L-7	29	154	309 (4.5)	0
A-L-7	25	194	223 (4.9)	0
D-L-7+$Al(acac)_3$	26	152	–	76
A-L-7+$Al(acac)_3$	28	194	–	74
D-cov-X-2	28	134	–	84
A-cov-X-2	27	164	–	90

Properties of dispersions prepared by miniemulsion polymerization (MEP, Table 2 and Table 3) for studies concerning the polymer's T_g and hydrophilicity are provided in Table 8. GPC measurements sensitive to the dye suggest equal distribution of the labels along all chains (see Section 6.2 and Refs. [53, 66]).

Table 8: Properties of dispersions prepared by MEP to study effects of the polymer's T_g and hydrophilicity on the processes occurring before or shortly after drying.

Dispersion	Calc. T_g [°C]	Solids content [%]	d_h [nm]	M_w (M_w/M_n) [kg/mol]
D-P(BA_{99}-MAA_1)	–52	24	156	527 (3.5)
A-P(BA_{99}-MAA_1)		23	168	345 (2.9)
D-P(BA_{78}-MMA_{21}-MAA_1)	–30	24	120	392 (3.2)
A-P(BA_{78}-MMA_{21}-MAA_1)		23	156	318 (2.9)
D-P(BA_{41}-MMA_{58}-MAA_1)	+20	22	109	289 (2.5)
A-P(BA_{41}-MMA_{58}-MAA_1)		23	135	153 (2.1)
D-P(EHA_{99}-MAA_1)	–49	25	170	330 (4.1)
A-P(EHA_{99}-MAA_1)		25	240	266 (2.9)

Properties of dispersions prepared by MEP (Table 5 and Table 6) for studies concerning the influence of ionic cross-linking by Zn^{2+} on interdiffusion are provided in Table 9. "MEP" stands for miniemulsion polymerization, "Zn-X" denotes cross-linking by Zn^{2+}, "1" denotes a molar ratio of $n_{COOH}/n_{Zn(II)} = 2/1$ (stoichiometric), "0.5" denotes a molar ratio of $n_{COOH}/n_{Zn(II)} = 4/1$ (half-stoichiometric). "II" and "V" denote the weight percentages of MAA employed in the synthesis (compared to BA), which are 2 and 5, respectively. It is evident that

increasing the amount of ZnDMA increases the particle size. Probably, this is attributed to a decreased colloidal stability in these dispersions. In films from dispersions provided by BASF SE (see Ref. [18]), the T_g was not affected by cross-linking through Zn^{2+}. For further evaluation of this finding, T_g determinations were performed on films from dispersions prepared by *batch* emulsion polymerization where the use of hexadecane was not necessary. The absence of hexadecane allowed for DSC measurements which were performed on films from L-II and Zn-X-1 (analogous, unlabeled dispersions of MEP-L-II and MEP-Zn-X-1, respectively). The T_g were measured to be at around –50 °C for both, L-II and Zn-X-1. Dye-sensitive GPC measurements for D-MEP-L-II and A-MEP-L-II are provided in the Appendix, Section 6.2.

Table 9: Properties of dispersions prepared by MEP to study ionic cross-linking on interdiffusion.

Dispersion	Solids content [%]	d_h [nm]	M_w (M_w/M_n) [kg/mol]	Gel content [%]
D-MEP-L-II	19	151	504 (2.9)	0
A-MEP-L-II	19	134	298 (2.1)	0
D-MEP-Zn-X-0.5	18	182	–	38
A-MEP-Zn-X-0.5	19	180	–	40
D-MEP-Zn-X-1	17	212	–	80
A-MEP-Zn-X-1	19	246	–	79
D-MEP-L-V	19	129	317 (2.8)	0
A-MEP-L-V	18	120	295 (2.9)	0
D-MEP-cov-X	19	127	–	71
A-MEP-cov-X	20	149	–	79

Dispersions D-MEP-L-II, A-MEP-L-II, D-MEP-L-V and A-MEP-L-V were blended with varying amounts of $Zn(acac)_2$ (3.7 – 9.2 pphm) for reference studies in which the influence of the cross-linking reaction between carboxylate groups and $Zn(acac)_2$ on interdiffusion was studied. Properties of the dispersions are given in Table 10.

Table 10: Properties of dispersions prepared by MEP blended with different amounts of $Zn(acac)_2$.

Dispersion	Amount of $Zn(acac)_2$ [pphm]	d_h [nm]	Gel content [%]
D-MEP-L-II+$Zn(acac)_2$-1	3.7	185	45
A-MEP-L-II+$Zn(acac)_2$-1		165	15
D-MEP-L-V+$Zn(acac)_2$-1	9.2	could not be determined	73
A-MEP-L-V+$Zn(acac)_2$-1		could not be determined	82
D-MEP-L-V+$Zn(acac)_2$-0.5	4.6	172	39
A-MEP-L-V+$Zn(acac)_2$-0.5		162	47

In all these dispersions, the cross-linking reaction between polymer chains and $Zn(acac)_2$ (Reaction (I)) before drying occurred to the extent that evaporating acetylacetone could be smelled upon opening the vial containing the respective dispersion. Particle sizes increased with increasing amount of $Zn(acac)_2$. The colloidal stability of the dispersions seems to decrease upon blending with $Zn(acac)_2$. For D-MEP-L-V+$Zn(acac)_2$-1 and A-MEP-L-V+$Zn(acac)_2$-1, the latexes into which the largest amount of $Zn(acac)_2$ was added (9 pphm), particle sizes could not be determined by DLS because large entities (probably particle

aggregates) were present. Upon stirring, the polymer particles have aggregated to a polymer film which was found to be insoluble in MEK in case of all dispersions blended with $Zn(acac)_2$. Note, that such a particle aggregation was *not* observed for dispersions prepared by BASF SE when stirred after addition of either $Zn(acac)_2$ or $Al(acac)_3$ (see Table 7 and Ref. [18]).

Another aspect to discuss is the difference between the gel contents of D-MEP-L-II+$Zn(acac)_2$-1 and A-MEP-L-II+$Zn(acac)_2$-1. For both films, it was observed that the gel does not remain a large, single polymer film upon swelling in MEK, but slowly decomposes and sediments. In contrast, the gels of all other films with ionically cross-linked chains (also including those cross-linked by $Al(acac)_3$ (Table 7)), remained a single film even after swelling for 3 – 4 days in MEK. In case of A-MEP-L-II+$Zn(acac)_2$-1, the decomposition seems to be more pronounced than in case of D-MEP-L-II+$Zn(acac)_2$-1, which might be attributed to the smaller molecular weight of corresponding base polymer with linear chains (see Table 9). The smaller gel content and the decreased solvent-stability of the gels of D-MEP-L-II+$Zn(acac)_2$-1 and A-MEP-L-II+$Zn(acac)_2$-1, compared to D-MEP-L-V+$Zn(acac)_2$-1 and A-MEP-L-V+$Zn(acac)_2$-1, might result from the fact that less cross-linkable COOH groups are incorporated along the chains in the former cases.

3.5 Study of Film Formation with FRET and Light Scattering

Time-resolved fluorescence and light scattering measurements were carried out in a home-built chamber which was built by Andreas Böttcher (Institute of Physical Chemistry, Clausthal University of Technology). It is sketched in Figure 26.

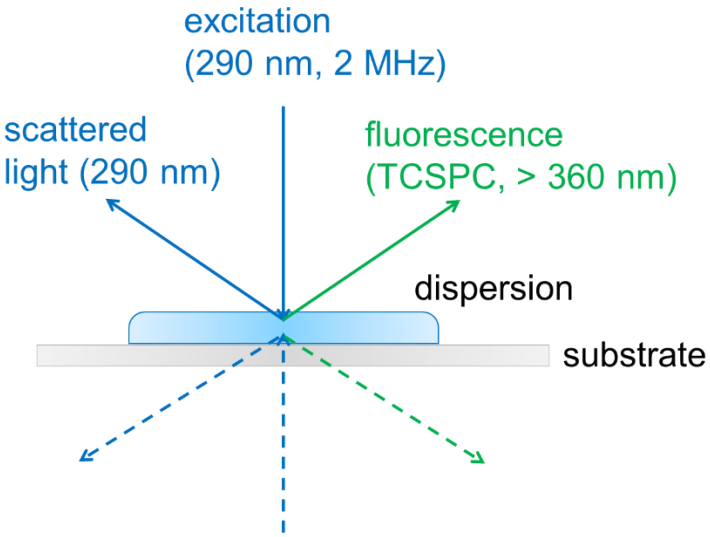

Figure 26: Sketch of measurement chamber for time-resolved fluorescence and scattered excitation light. Adapted from Ref. [19].

In all measurements, the substrate with the film was positioned exactly under the flash LED (λ = 290 nm, 2 MHz pulse rate, 1.4 ns full width at half maximum, Picoquant). The center of the sample was studied. The width of the focal point of the pulsed LED was 1 mm. Liquid light guides (Oriel, type 77556) were used to transmit fluorescence and scattered photons to the respective photomultiplier tubes (Hamamatsu) for time-correlated single-photon counting (TCSPC, 500 channels, 0.4 ns channel width, EG&G) and scattered excitation light. Fluorescence photons were passed through a long pass filter (>360 nm, Schott), scattered excitation photons through an interference filter (290 nm, Schott) before being detected by the photomultiplier tube.

The temperature and relative humidity, rH, were measured by a sensor during the experiments. In all cases, temperature was between 21–22 °C. The relative humidity was kept constant either by purging the chamber with a stream of dry air (leading to rH ~ 3%) or by using humidity control agents, which were silica gel (10% rH), saturated aqueous solutions of $CaCl_2$ (33% rH) and NaBr (56% rH) or pure water (96% rH).

The measurement chamber (Figure 26) allows to measure the film either from above or from below. In the latter case, UV-transparent fused silica was used as a substrate while in the former case microscope slides were used. In general, 3 μL of a blend of donor- and acceptor labeled dispersions (DA, 1/1 = *m*/*m*, intermixed for ~20 s) were cast on the substrate (ellipsoidal spot with an area of 16 cm^2). The thickness of the wet dispersion was ~190 μm, the calculated thickness of the final, dry film was between 40 – 50 μm, depending on the solids content of the dispersion. The observation depth in the final film was calculated to be around 5.5 μm (see Ref. [19] or the Appendix, Section 6.1).

In case of kinetic measurements, performed to follow the progress of polymer interdiffusion (A_2, eq. 13), the substrate carrying the film was immediately placed into the measurement chamber and the measurement was started. In case of drying with an air stream, the latter was turned on after the first 10 s of measurement. Accumulation time per decay was 10 s for the first 300 s and 30 s afterwards. The number of counts at the decay's maximum was always at least $1.5 \cdot 10^4$, indicating a good signal-to-noise ratio.

In order to obtain the state of intermixing of labeled chains before drying ($A_{2,min}$, (eq. 13) to calculate f_m from A_2 (eq. 14)), 1/1 = *m*/*m* blends of labeled dispersions were sealed in quartz cells. Accumulation time per decay was 30 s.

To obtain the donor's lifetime τ_D ($A_2 = 0$, eq. 11), 2γ ($A_2 = 1$, eq. 12) and A_2 values of films homogenized with THF consisting of cross-linked chains (eq. 13), measurements on dry films

were carried out until 10^5 counts were reached at the decay's maximum. τ_D was obtained from films from donor-labeled dispersions with linear chains. 2γ was obtained from films of linear chains prepared from a 1/1 = *m*/*m* blend of donor- and acceptor-labeled dispersions which were homogenized by intermixing dry films with THF first and annealing them overnight at 60 °C ("THF film") afterwards.

Donor fluorescence decay curves were fitted according to the respective model (details provided in Section 2.8) using the Levenberg-Marquardt algorithm.[72] The lamp shift and the background noise were accounted for as well. The weighted residues, χ^2, in case of kinetic measurements were never higher than 3. For measurements up to 10^5 counts at the decay's maximum, they were never higher than 8. All measurements were carried out at least three times, in case of kinetic experiments, one representative curve is shown.

To fit decays from dispersions blended with the tackifying resin ("TR") ($m_{polymer}/m_{tackifier}$ = 3/1), Snowtack FH94G, the two-state model (eq. 13) had to be expanded to account for the tackifier's intrinsic fluorescence (eq. 19).

$$I(t') = I_0 \left[A_2 \cdot \exp\left(\left(-\frac{t'}{\tau_0} \right) - 2\gamma \sqrt{\frac{t'}{\tau_0}} \right) + (1 - A_2) \cdot \exp\left(-\frac{t'}{\tau_0} \right) + A_{TR} \cdot \exp\left(-\frac{t'}{\tau_{TR}} \right) \right] \qquad \text{eq. 19}$$

A_{TR} is an additional fit parameter and τ_{TR} is the lifetime of the TR's fluorescence, as determined from a film of a blend of donor-labeled chains and TR. A_2 and A_{TR} were found to be uncorrelated.

In addition to emitted light, scattered excitation light was detected simultaneously to follow the progress of particle deformation shortly after film casting. Background-subtracted and normalized scattering data, I_{scat}, are provided and were calculated from the raw data, i_{scat}, using eq. 20.

$$I_{scat}(t) = \frac{i_{scat}(t) - i_{scat}(t = \infty)}{i_{scat}(t = 10\ \mathrm{s}) - i_{scat}(t = \infty)} \qquad \text{eq. 20}$$

FRET measurements were carried out on 1/1 (*m*/*m*) mixtures of donor- and acceptor-labeled dispersions ("DA"). Constant fit parameters used in the two-state model (eq. 13) and $A_{2,min}$, the degree of intermixing of labeled chains in the wet dispersion prior to drying (to calculate f_m, eq. 14), are provided in the following. In case of dispersions provided by BASF SE with a serum pH of 2 ("2", Table 7), τ_D was 41 ns and 2γ was 1.93. In case of dispersions with a serum pH of 7 ("7", Table 7), τ_D was 42 ns and 2γ was 2.12. $A_{2,min}$ values are provided in Table 11, discussion on them is done in Section 4.1.

Table 11: $A_{2,min}$ values of dispersions provided by BASF SE.

Dispersion blend	$A_{2,min}$
DA-L-2	0.60
DA-L-2+Al(acac)$_3$	0.55
DA-cov-X-2	0.50
D-L-7	0.60
DA-L-7+Al(acac)$_3$	0.60

For DA-L-2 blended with the tackifier ("DA-L-2+tackifier"), τ_D was 41 ns, τ_{TR} was 6 ns, 2γ was 1.43 ns and $A_{2,min}$ was 0.40.

Constant fit parameters (eq. 13) and $A_{2,min}$ (eq. 14) values for dispersions with different T_g (Table 8) are provided in Table 12.

Table 12: Constant fit parameters and $A_{2,min}$ values of dispersions with different T_g.

Dispersion blend	τ_D [ns]	2γ	$A_{2,min}$
DA-P(BA_{99}-MAA_1)	40	1.57	0.30
DA-P(BA_{78}-MMA_{21}-MAA_1)	41	1.63	0.30
DA-P(BA_{41}-MMA_{58}-MAA_1)	42	1.87	0.33
DA-P(EHA_{99}-MAA_1)	40	1.34	0.25

In case of dispersions prepared by MEP with varying degree of ionic cross-linking by Zn^{2+} (Table 9), τ_D was 40 ns. 2γ was 1.63 and 1.82 for DA-MEP-L-II and DA-MEP-L-V, respectively. $A_{2,min}$ values are provided in Table 13. For blends of DA-MEP-L-II and DA-MEP-L-V with $Zn(acac)_2$ the value of the respective dispersion without the addition of $Zn(acac)_2$ was used.

Table 13: $A_{2,min}$ values of dispersions prepared by MEP to study effects of ionic cross-linking by Zn^{2+}.

Dispersion blend	$A_{2,min}$
DA-MEP-L-II	0.25
DA-MEP-L-V	0.40
DA-MEP-Zn-X-0.5	0.25
DA-MEP-Zn-X-1	0.15
DA-MEP-cov-X	0.25

3.6 Flat-Punch Tack Tests

Flat-punch tack tests were carried out on films from unlabeled dispersions prepared by BASF SE. Details about the properties of the dispersions are given in Ref. [18]. These dispersions have the same composition as those whose interdiffusion was studied, except for the solids content which is 50%. Polymer architectures are linear ("L", 0% gel content), ionically cross-linked (linear + $Al(acac)_3$, ("L+$Al(acac)_3$" in wet dispersion), 85% gel content in final film) and covalently cross-linked ("cov-X", 89% gel content). Two films from each dispersion were applied on glass plates. The wet thickness was 120 μm and controlled using a film applicator, resulting in an estimated dry thickness of h_0 = 60 μm. Dispersions were first dried for 4 days at 23 °C and 50% rH and then in an oven at 50 °C overnight. Five spots of each film were measured. A TA.XT plus Texture Analyzer (Stable Micro Systems) was used for the measurements, a common parameter set was employed.[2] Contact pressure was 1 MPa, contact time was 10 s, compression speed was 30 μm/s and the debonding speed was 10 μm/s. A flat, cylindrical metal stamp with a diameter of d = 2 mm was used as a probe. Measurements were carried out at 23 °C and 50% rH. Overall, the curves had a good reproducibility.

The force F was converted to the stress σ following

$$\sigma = \frac{4F}{\pi d^2} \qquad \text{eq. 21}$$

d is the diameter of the probe. The distance h was converted to the strain ε following

$$\varepsilon = \frac{h - h_0}{h_0} \qquad \text{eq. 22}$$

h_0 is the film thickness. Exemplary stress-strain curves are provided in this thesis, a more sophisticated data interpretation is provided in Ref. [18].

4 Results and Discussion

4.1 Influence of Oligomers on Interdiffusion Studies

Before discussing the film formation kinetics, the value of the first data point in the A_2-curve (eq. 13), A_2 (t = 10 s) = $A_{2,ini}$, is discussed because it is much larger than the expected value of circa zero as shown for DA-L-2 in Figure 27. The time between film casting and the start of recording the first data point was ~5 s.

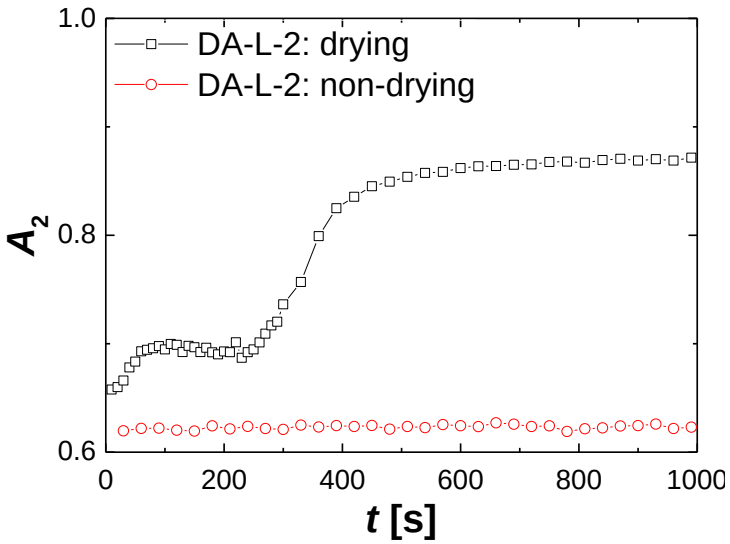

Figure 27: A_2 data for the drying and the wet, non-drying blend of labeled dispersions, DA-L-2.

$A_{2,ini}$ starts a value of circa 0.65, however a value close to zero is expected because no significant interdiffusion, and therefore no FRET between donor- and acceptor-labeled chains, is assumed to take place in the wet dispersion. The A_2 value of the same dispersion which was sealed in a quartz cell in order to prevent drying is also relatively large at 0.6. Subsequent DLS measurements did not reveal an increased particle size, thus aggregation or clustering can be excluded as possible reasons. It is assumed that the large value of $A_{2,ini}$ is caused by labeled, water-soluble oligomers exchanging between the particles immediately after intermixing the

labeled dispersions (sketched in Figure 28). The dispersions were prepared by semi-batch emulsion polymerization and water-soluble oligomers are a known by-product.[70]

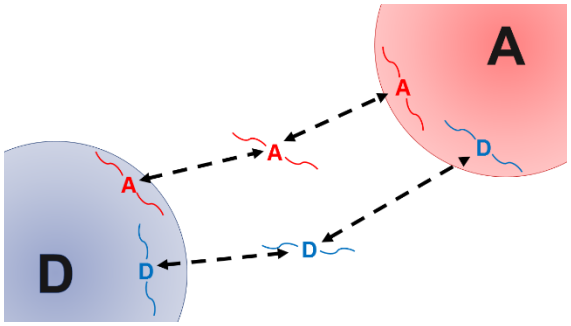

Figure 28: Sketch illustrating the exchange of labeled, water-soluble oligomers between polymer particles in the wet dispersion. D = donor, A = acceptor.

To corroborate the theory that the large $A_{2,ini}$ value can be traced back to water-soluble oligomers, dialysis experiments on diluted dispersions to separate the oligomers were performed by Christopher Hirth within his Bachelor thesis.[73] It was found that dialyzing the dispersions leads to a decrease of $A_{2,ini}$.[73] Further experiments concerning the influence of oligomers on $A_{2,ini}$ were performed within this thesis. The amount of water-soluble oligomers was varied in a series of dispersions prepared by miniemulsion polymerization initiated in the aqueous phase (properties given in Table 8). The water-solubility of the oligomers was controlled employing monomers with different hydrophilicities (based on the extent of hydroplasticization of their corresponding homopolymers following Ref. [55]). Used monomers were methacrylic acid (MAA, hydrophilic), *n*-butyl acrylate (BA, slightly hydrophilic) and 2-ethylhexyl acrylate (EHA, not hydrophilic).[55] In Figure 29, A_2 values obtained on sealed 1/1 = *m*/*m* blends of labeled dispersions (in the following called $A_{2,min}$) are plotted against the composition of the monomer phase (data from Table 12 and Table 13 (DA-MEP-L-V, here called "DA-P(BA_{95}-MAA_5)" to conform to the nomenclature).

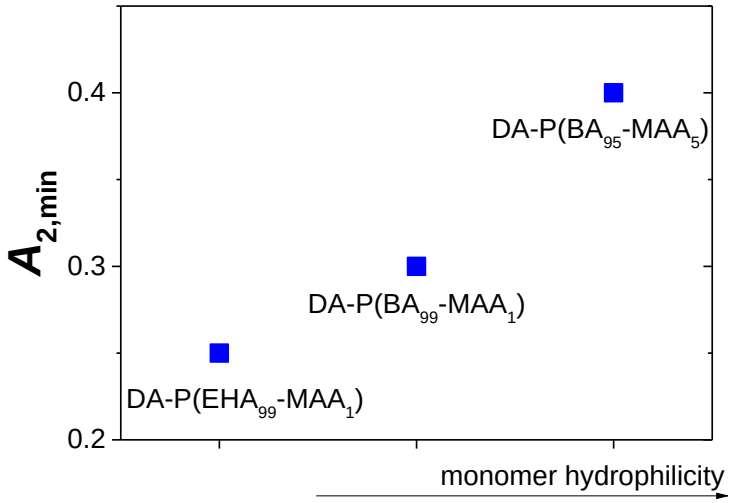

Figure 29: $A_{2,min}$ values of wet, non-drying, 1/1 = *m*/*m* blends of labeled latexes as a function of hydrophilicity of monomers employed during miniemulsion polymerization initiated in the aqueous phase. Number in subscripts are monomer weight percentages.

Clearly, there is a correlation between $A_{2,min}$ and the monomer hydrophilicity. Increasing amount of hydrophilic MAA increases $A_{2,min}$ as more water-soluble are formed, whereas employing EHA instead of BA, the former being more hydrophobic,[55] reduces $A_{2,min}$ because less water-soluble oligomers are formed.

To conform to the literature,[53] the fraction of intermixing, f_m, is used as an indicator for the progress of polymer interdiffusion instead of A_2 in the following. f_m was calculated using the A_2 value obtained on wet, non-drying blends of labeled latexes as $A_{2,min}$ (eq. 14).

4.2 General Film Formation Kinetics of a PSA Dispersion with Linear Chains

First, the overal film formation kinetics of the dispersion with linear chains, DA-L-2, which was provided by BASF SE, is discussed (properties given in Table 7) before focusing on the details of polymer interdiffusion. Most of these results are presented and discussed in Ref. [19].

The fraction of intermixing, f_m (eq. 14) and the intensity of scattered excitation light, I_{scat} (eq. 20), of DA-L-2 are plotted in Figure 30 a) and b), respectively. The dispersion was dried with an air stream (rH ~ 3%).

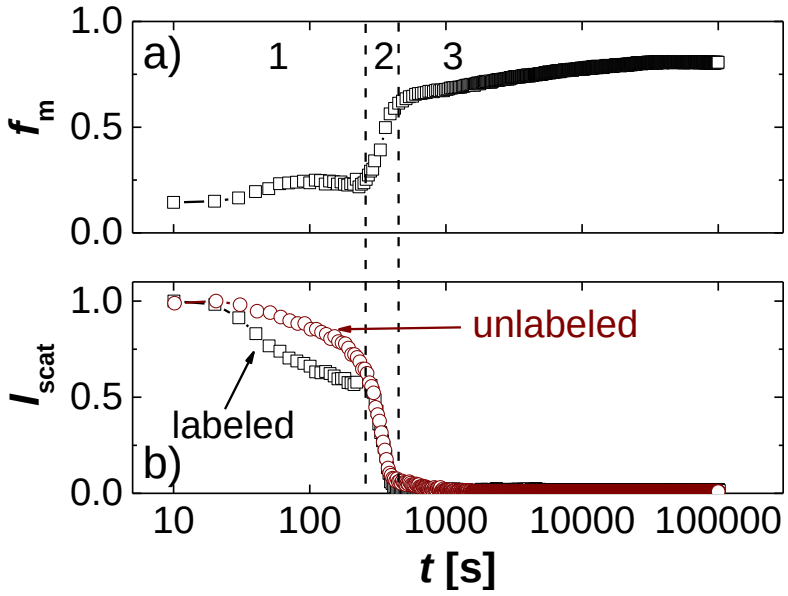

Figure 30: Interdiffusion (a) and scattering (b) kinetics for DA-L-2. Numbers in panel a) refer to the specific phases, the brown curve in b) is obtained from a reference dispersion with no labels. Data already presented in Ref. [19].

Figure 30 reveals that the kinetics of f_m and I_{scat} can be separated into three phases along the logarithmic time axis. Phase 1 and 2 take place when the film is still turbid and scatters light, while phase 3 takes place when the film has turned clear. In phase 1 and 2, the maximum observation depth has not been reached yet and continuously increases as the film dries from top to bottom. For the following interpretations, a sketch is provided in Figure 31.

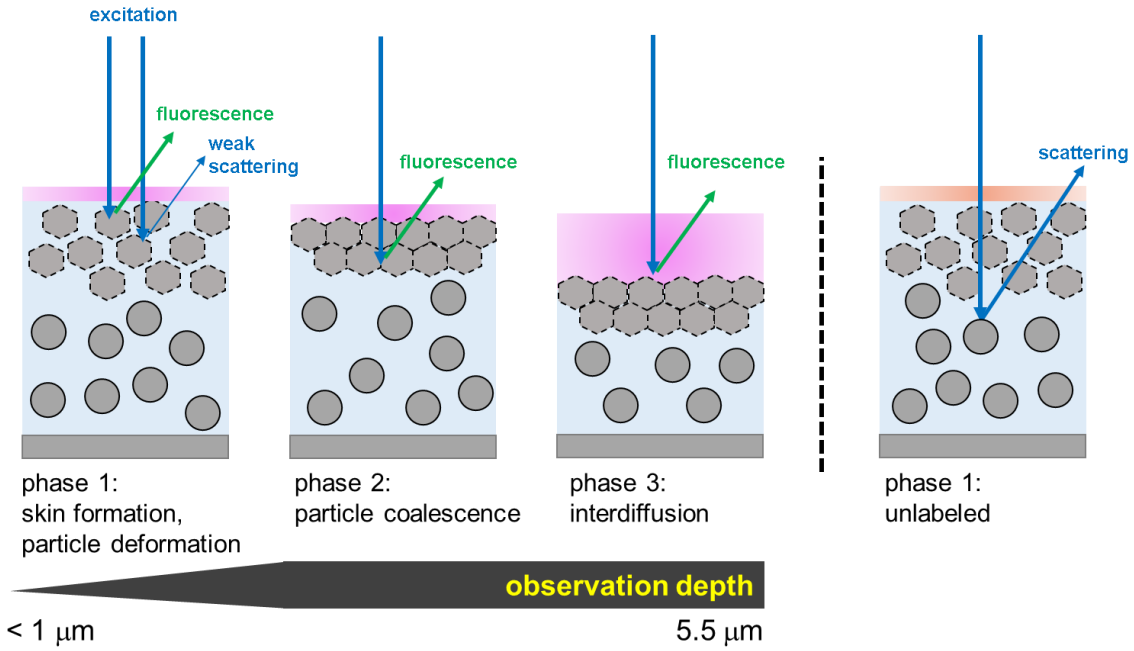

Figure 31: Sketch of the proposed explanation for the three phases of film formation kinetics observed in Figure 30.

Phase 1 is interpreted as the result of skin formation occurring immediately after casting the dispersion. Since the particles are soft, a fast particle deformation at the film–air interface, leading to skin formation, can be expected.[5,39] In this skin layer, interdiffusion already takes place, as indicated by the slight increase of f_m. I_{scat} decreases because the excitation light is absorbed by the donor-dyes in the deformed layers.

For the interpretation of phase 2, it is assumed that the polymer particles beneath the skin have deformed but are still separated by water lamellae. Results indicating particle deformation occurring before drying has finished have been reported in literature as well[74–76] and can be explained either by wet sintering or by a reduced capillary pressure.[5] When the water lamellae separating the particles have dried out, the deformed particles coalesce, causing the film to become transparent. In Figure 30, I_{scat} sharply decreases to zero and f_m strongly increases due to start of interdiffusion between the coalesced particles. Note, that phase 1, is not observed for

a dispersion with unlabeled chains. This is because the excitation light is not attenuated when penetrating through the deformed layer.

In phase 3, only polymer interdiffusion is observed, as indicated by the continuous increase of f_m. The maximum observation depth, which is calculated to be around 5.5 μm, compared to 50 μm final film thickness, is reached and remains constant for the rest of the experiment. Details about the calculations are provided in the Appendix, Section 6.1.

In the following, the interpretations of the phases 1 and 2 are evaluated semi-quantitatively, and the polymer interdiffusion in phase 3 is discussed in more detail.

To evaluate the assumptions made for the explanations of the initial phases 1 and 2, which are assumed to be a consequence of the softness of the polymer particles, a series of labeled model latexes with different polymer T_g were prepared by miniemulsion polymerization (MEP, see Table 8 for properties).

Interdiffusion and scattering kinetics of these dispersions are shown in Figure 32. The dispersions were dried with an air stream.

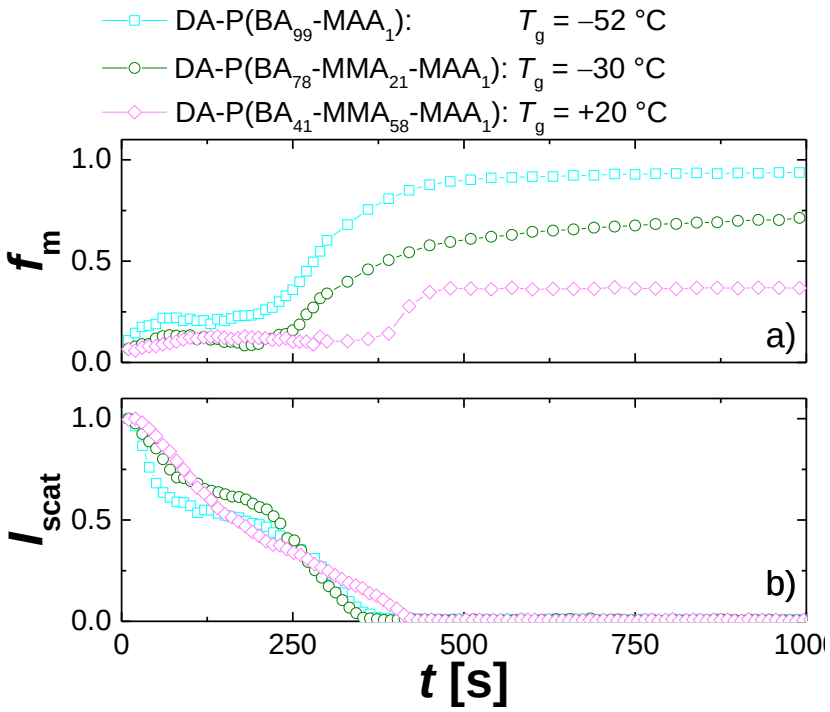

Figure 32: Interdiffusion (a) and scattering data (b) for dispersions with different T_g prepared by miniemulsion polymerization. Dispersions were dried with an air stream.

As expected, polymer interdiffusion (Figure 32 a)) becomes slower with increasing polymer T_g. Regarding the drying kinetics (periods before I_{scat} reaches zero in Figure 32), it is assumed for DA-L-2 (T_g = –33 °C)[18] that drying mainly occurs from top to bottom (top-down drying) due to the softness of the polymer particles. The scattering kinetics (Figure 32 b)) of the soft dispersions with a polymer T_g of –52 °C and –30 °C follow a decrease in three steps along the linear time axis. When plotting I_{scat} data of DA-L-2 from Figure 30 b) against a linear time axis, such a decrease is observed as well (not shown here). The I_{scat}-curve of the hard dispersion with a polymer T_g of +20 °C, however, has a different shape from the other ones and seems to decrease in two steps. This is assumed to be a consequence of edge-in drying. Photographs of the drying dispersions are shown in Figure 33. In case of the soft dispersions with T_g of –52 °C and –30 °C, the turbidity in the center decreases first (top-down drying), causing I_{scat} in Figure 32 b) to decrease. In case of the hard dispersion with T_g of +20 °C, the edge turns clear first

(edge-in drying). Compared to the soft dispersions, the decrease of turbidity in the center is delayed as I_{scat} levels off to zero, once drying from the center to the edge has finished. Combining the results from the photographs with the I_{scat} data, which were always acquired from the center of the film, in Figure 30 b) and Figure 32 b), it can be assumed that the I_{scat} kinetics of the low-T_g dispersions can be qualitatively attributed to top-down drying.

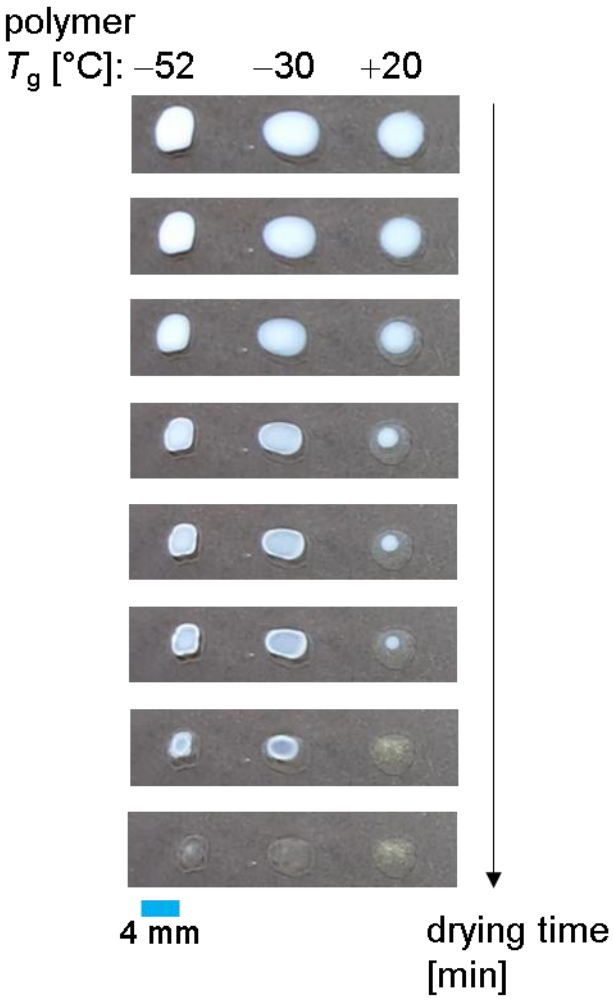

Figure 33: Photographs of drying dispersions with varying T_g. Casting volume: 3 µL, wet thickness: ~190 µm. Dispersions were dried with an air stream at 22 °C.

The focus of this work is the investigation of polymer interdiffusion after particle deformation has finished and the maximum observation depth is reached, i.e. phase 3. For DA-L-2, f_m increases continuously as shown in Figure 30 a). For the sake of estimation of a

diffusion coefficient D, f_m data covering the entire corrected film formation time t'' (eq. 15, with t_0 being the time when phase 3 starts) were fitted to the spherical diffusion model (eq. 16)[65] following (eq. 17) as proposed by the Winnik group.[53] The obtained diffusion coefficient is interpreted as an apparent, cumulative, Fickian diffusion coefficient of all chains that have interdiffused up to a specific film formation time[53] (see Section 2.8 for simplifications made by using this procedure).

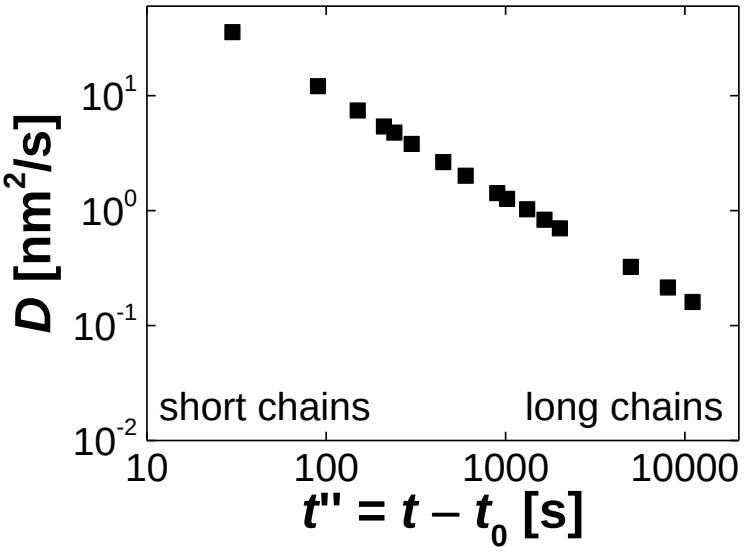

Figure 34: Evolution of polymer diffusion coefficients *D* for DA-L-2 along the corrected film formation time *t''*. t_0 is the time when the film turns clear and only polymer interdiffusion is observed, t_0 ~600 s. Data already presented in Ref. [18].

There is a linear decrease of D against t'' in the log-log plot. Such a linear decrease has been observed in literature as well and is attributed to the broad molecular weight distribution of the polymer.[53,54] At early times, the short, thus fast chains dominate the interdiffusion and contribute to the increase of the fraction of intermixing, f_m, whereas at later times, the longer, slower chains contribute to the increase of f_m as well. Taking the difference between ambient temperature during interdiffusion and polymer T_g into account, which is ~50 °C in the experiments here, the D values are in the range of those obtained on (annealed) coatings, as shown by interdiffusion studies based on FRET,[53] small-angle neutron scattering[51] and

excimer formation.[54] Another plot used in literature is D against f_m. For DA-L-2, it is shown in Figure 35.

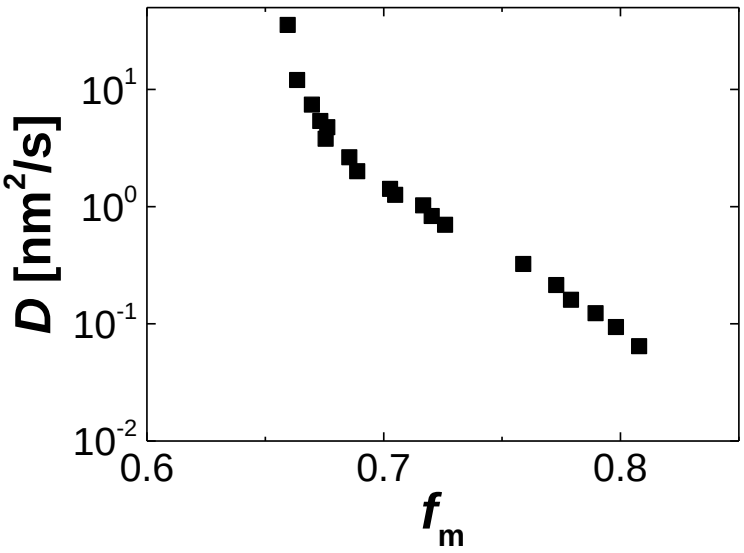

Figure 35: Plot of D vs. f_m for DA-L-2. Data already presented in Ref. [18].

D decreases with increasing f_m because at early times the short, fast chains dominate the interdiffusion and at later times the long chains.[53]

4.3 Influence of Drying Conditions on Interdiffusion

4.3.1 Hydroplasticization

Hydroplasticization describes the plasticizing effect of water on polymers.[55] For coatings, it is known to aid film formation as it accelerates polymer interdiffusion.[56–58] The dispersion DA-L-2 was dried at varying relative humidity, rH, to study the influence of hydroplasticization. rH was controlled using specific drying agents such as silica gel (10% rH), saturated salt solutions (33% rH and 56% rH) and pure water (96% rH). Film formation studies are shown in Figure 36.

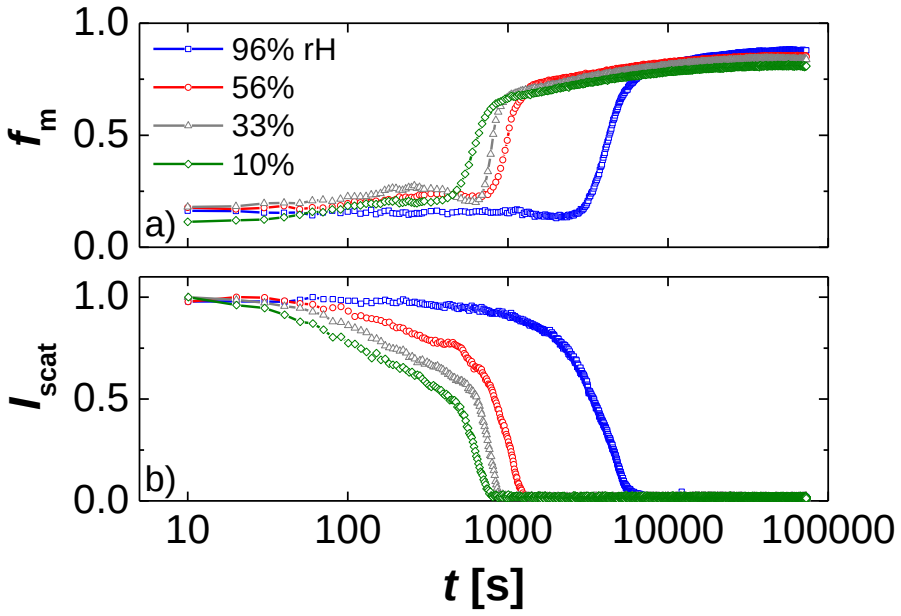

Figure 36: Interdiffusion (a) and scattering kinetics (b) of DA-L-2 at different relative humidity, rH. Data already presented Ref. [19].

It is evident that the start of phase 3 is delayed when rH is increased. This is expected because drying takes longer at higher ambient humidity. For the sake of clarity, plots of f_m data from phase 3 against the corrected film formation time t" are provided in Figure 37. t_0, the time

when I_{scat} reaches zero, are 850 s, 950 s, 1500 s and 7500 s for 10%, 33% 56% and 96% rH, respectively.

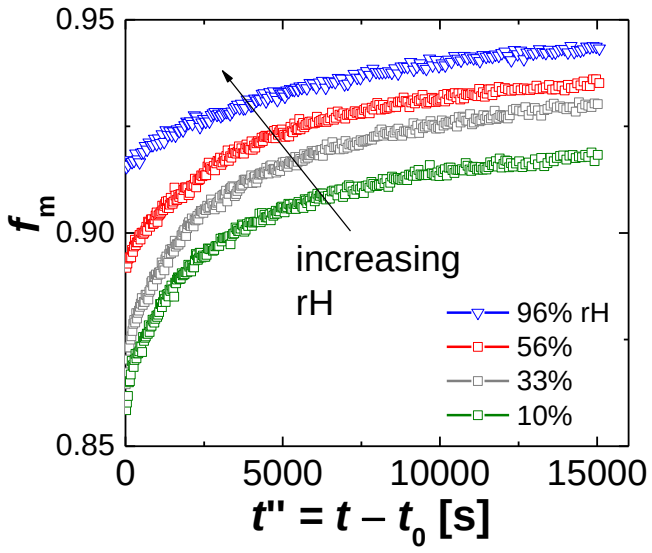

Figure 37: Polymer interdiffusion in DA-L-2 at different rH plotted against the corrected film formation time. Data already presented in Ref. [19].

It is evident that polymer interdiffusion is faster at higher rH, indicating hydroplasticization, as it has been found for polymers in coatings as well.[58]

4.3.2 Interdiffusion at the Film–Air and Film–Substrate Interface

The interdiffusion at the film–air (top) and film–substrate interface (bottom) for DA-L-2 has been studied. This has been possible because the penetration depth of the excitation light is limited and much smaller than the final film thickness (5.5 μm observation depth (details on the calculation given in Section 6.1) compared to 50 μm film thickness). To investigate effects of skin formation, the drying speed was varied. DA-L-2 was dried with an air stream (~ 3% rH), silica gel (10% rH) and pure water (96% rH). Results are shown in Figure 38.

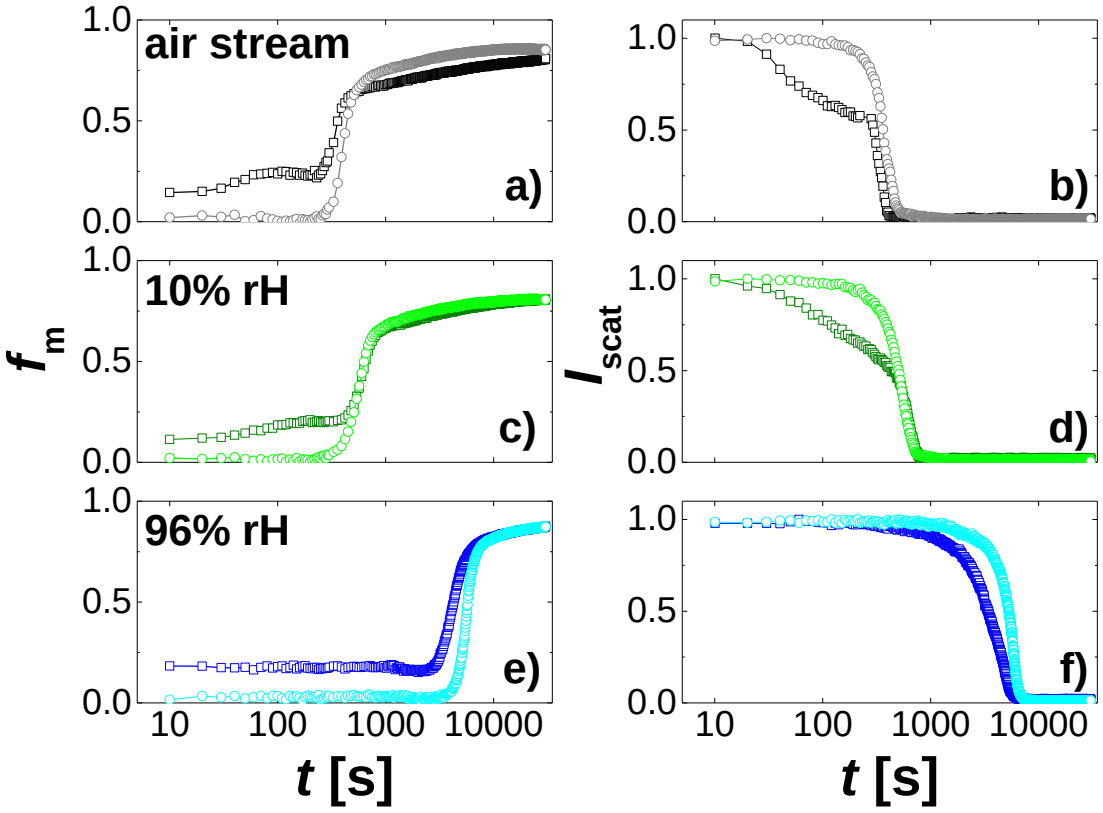

Figure 38: Film formation of DA-L-2 at the film–air (darker colors) and film–substrate interface (lighter colors) at variable drying conditions. Data already presented in Ref. [19].

In all data sets acquired from the bottom of the film, phase 1 is absent. f_m and I_{scat} remain constant for a certain period and then strongly increase and decrease, respectively. Also, f_m always starts higher at the top than it does at the bottom, indicating skin formation immediately after film casting. In case of drying of DA-L-2 with an air stream (Figure 38 a)), interdiffusion at the bottom is faster than at the top. This is the consequence of a more pronounced skin formation ($Pe >> 1$) due to fast drying.[5] The skin keeps water within the film, thereby leading to hydroplasticization of polymer chains at the bottom. For slower drying at 10% rH and 96% rH, interdiffusion is almost equally fast at both interfaces after I_{scat} has leveled off to zero.

4.4 Influence of a Tackifying Resin on Interdiffusion

Tackifiers are frequently blended with PSAs to increase their tackiness.[1] The effect of the tackifying resin Snowtack FH94G, a tackifier for acrylic PSAs, on interdiffusion has been studied (see Section 3.1 and the data sheet for properties). The tackifier was added as a separate aqueous emulsion to DA-L-2 such that the weight ratio was $m_{tackifier}/m_{polymer} = 1/3$ ("DA-L-2+tackifier"). To fit decays from DA-L-2+tackifier, eq. 19 had to be used to account for the tackifier's intrinsic fluorescence (~6 ns). Long-time interdiffusion data in which f_m is plotted against t" are shown in Figure 37. Film formation kinetics including the scattering kinetics, which are unaffected by the presence of a tackifier, are provided Ref. [19].

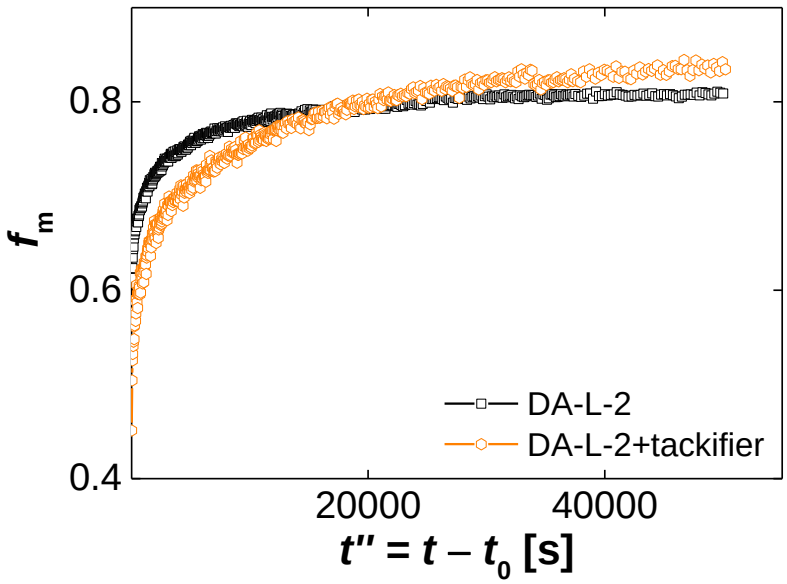

Figure 39: Influence of a tackifying resin on the interdiffusion of DA-L-2. t_0 ~400 – 450 s.

At early times, interdiffusion in the latex blended with the tackifier is slower. This can be attributed to the fact the tackifier is initially not mixed with the polymer dispersion. It dilutes the polymer particles and might form barriers against interdiffusion. However, at later times (after circa 20000 s), interdiffusion in the film containing the tackifier becomes faster than in the film with linear chains only. The tackifier has dissolved in the polymer phase, loosens the

entanglements of the polymer chains and thus increases their mobility (despite increasing the polymer T_g from −33 °C (DA-L-2) to −20 °C (DA-L-2+tackifier)).[19] The interdiffusion studies are in accord with literature results, in which an increased polymer mobility in acrylic PSA films blended with tackifiers was deduced from studies based on dynamical mechanical analysis and atomic force microscopy images.[59,60]

4.5 Influence of $Al(acac)_3$ on Interdiffusion

The influence of the ionic cross-linker, aluminum acetylacetonate, $Al(acac)_3$, on interdiffusion was studied to investigate whether it is possible to prepare homogeneous PSA films with ionically cross-linked chains from dispersions. A series of dispersions with different polymer architectures was investigated. Labeled dispersions with linear chains (DA-L-2), linear chains blended with 1 pphm $Al(acac)_3$ (DA-L-2+$Al(acac)_3$, 75% gel content of final film, ionic cross-linking) and covalently cross-linked chains (DA-cov-X-2, 87% gel content of final film) were studied (serum pH of these dispersions are 2, more properties are given in Table 7). Interdiffusion (f_m) and light scattering data (I_{scat}) are shown in Figure 36. Most of the following results have been presented and discussed in Ref. [18].

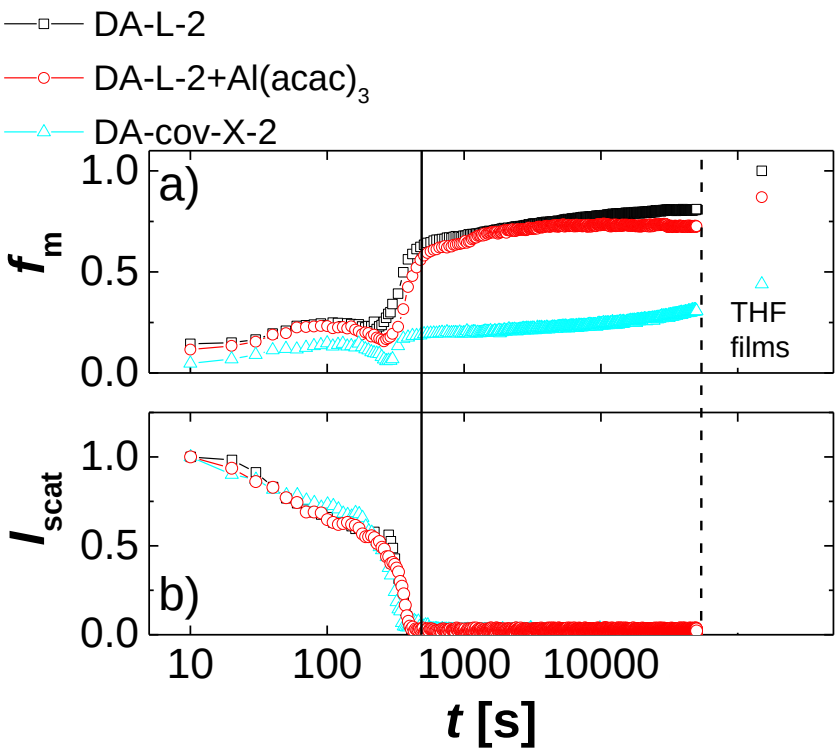

Figure 40: Interdiffusion (a) and scattering kinetics (b) for dispersions DA-L-2, DA-L-2+$Al(acac)_3$ and DA-cov-X-2. Dispersions were dried with an air stream. Data already presented in Ref. [18]. THF films: f_m values of final films homogenized with THF.

Only interdiffusion data after I_{scat} has reached zero (solid line in Figure 40) are discussed in the following because the processes occurring during earlier times, which have already been discussed in Section 4.2, are not affected by the polymer architecture. However, one aspect to mention is that for model dispersions prepared by MEP, it was found that the addition of metal acetylacetonates in *large* amounts (9 pphm, compared to 1 pphm in Figure 40) affects the kinetics of I_{scat}. This is because acetylacetone formed after cross-linking reaction (see Ref. [15] and Reaction (I, page 19)) absorbs the excitation light, thereby decreasing I_{scat}. More on this issue is discussed in Section 4.6 and in the Appendix, Section 6.3. Nevertheless, for the dispersions provided by BASF SE, absorption of excitation light by acetylacetone is negligible due to its low concentration. In the following, the long-time interdiffusion, after the solid black line in Figure 36 is discussed.

In case of DA-L-2+$Al(acac)_3$, interdiffusion kinetics is similar to that of DA-L-2 until around 5000 s at f_m ~0.7, where the curve flattens. As suggested in Ref. [15] and Reaction (I, page 19), it can be assumed that a certain degree of ionic cross-linking in the wet dispersion before film casting is present. The gels of films from DA-L-2+$Al(acac)_3$, while being insoluble in MEK, are completely soluble in acetylacetone, implying that an equilibrium is present in the wet dispersion. The similarity between interdiffusion data of DA-L-2 and DA-L-2+$Al(acac)_3$, suggests that the degree of cross-linking prior to film casting is rather small. Polymer cross-linking mainly takes place after film casting when acetylacetone, the by-product of the cross-linking reaction, can evaporate. The cross-linking reaction is slow to the extent that it does not retard interdiffusion and allows for a large degree of intermixing of chains from neighboring particles. In case of the reference dispersion with covalently cross-linked chains, DA-cov-X-2, almost no interdiffusion has occurred, as expected. The f_m values of the films after homogenization with THF ("THF films" in Figure 40) are 1, 0.87 and 0.44 for DA-L-2, DA-

L-2+Al(acac)$_3$ and DA-cov-X-2, respectively. Results of flat-punch tack tests on final films from dispersions with similar polymer architectures are provided in Section 4.7.

To evaluate the mechanical strength in the final films that has developed during interdiffusion, tensile tests were performed at BASF SE. Films were prepared from dispersions having the same polymer architecture as those whose interdiffusion kinetics are presented in Figure 40. Properties of the dispersions and the stress-strain curves obtained on their final films are provided in Ref. [18]. Here, the results of the tensile tests are shortly summarized. It was found that the film from the dispersion with linear chains does not break but flows until the end of the experiment. The film from a dispersion with linear chains blended with Al(acac)$_3$ shows strong strain-hardening, proving ionic cross-linking. For covalent cross-linking, weaker strain-hardening was observed. The films consisting of ionically and covalently cross-linked chains, which both nearly have the same gel content (~87 %), fracture at the same strain. However, the stress at fracture was much larger in case of ionic cross-linking by Al(acac)$_3$. This can be explained by the interdiffusion studies in Figure 40 a). In case of DA-L-2+Al(acac)$_3$, interdiffusion is possible and chains from adjacent particles can entangle with each other whereas in case of DA-cov-X-2, chains are fixed within their particles and no interdiffusion occurs, leading to the formation of a fragile film.[18] Thus, it can be concluded that the combination of interdiffusion studies by FRET (Figure 40 a)) and tensile tests (Ref. [18]) have proven that it is possible to prepare homogeneous films with a high degree of ionic cross-linking from dispersions blended with Al(acac)$_3$.

Next, a more detailed discussion about the long-time interdiffusion in Figure 40 is done. In Figure 41, estimated diffusion coefficients D for DA-L-2 and DA-L-2+Al(acac)$_3$ are plotted against f_m.

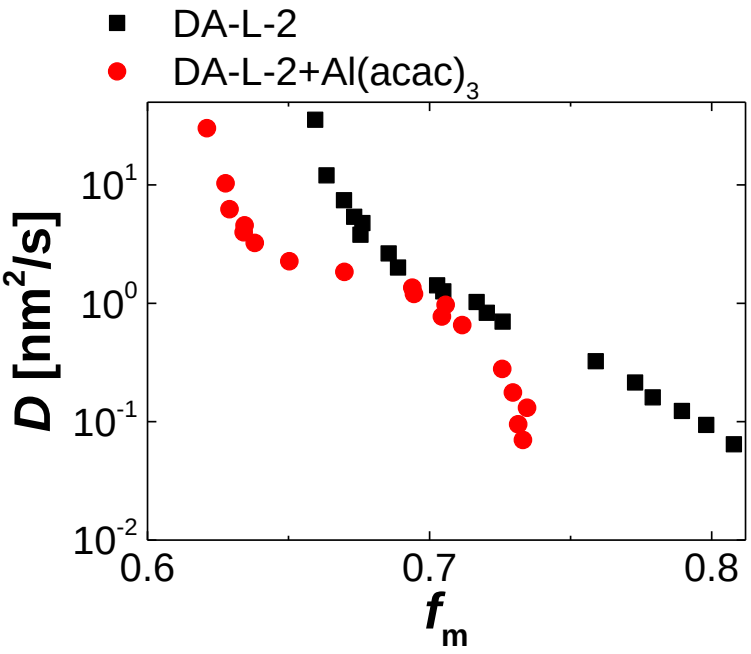

Figure 41: Plot of polymer diffusion coefficients against the fraction of intermixing for DA-L-2 and DA-L-2+Al(acac)$_3$. t_0 was ~600 s. Data already presented in Ref. [18].

Interdiffusion kinetics for DA-L-2 and DA-L-2+Al(acac)$_3$ are similar, as indicated by the same range of D and f_m values. For DA-L-2+Al(acac)$_3$, interdiffusion becomes slower at f_m values slightly above 0.7 because polymer cross-linking by Al(acac)$_3$ starts to retard interdiffusion. For DA-cov-X-2, data are not shown because f_m stays constant at ~0.2 as no interdiffusion takes place.

The effect of the pH of the dispersion's serum on interdiffusion and cross-linking reaction was investigated as well. After an emulsion polymerization has finished, the serum pH is usually acidic due to decomposition reactions of the persulfate initiator[68] (for the dispersions whose film formation studies are presented in Figure 40, serum pH is 2). In order to improve the colloidal stability,[5] the serum is usually neutralized to 7 after polymerization has finished

(here, aqueous ammonia solution was used). Interdiffusion data for DA-L-2 and DA-L-7 with and without $Al(acac)_3$ are shown in Figure 42. I_{scat} data are not affected by the serum pH, and thus not shown here, but in Ref. [18].

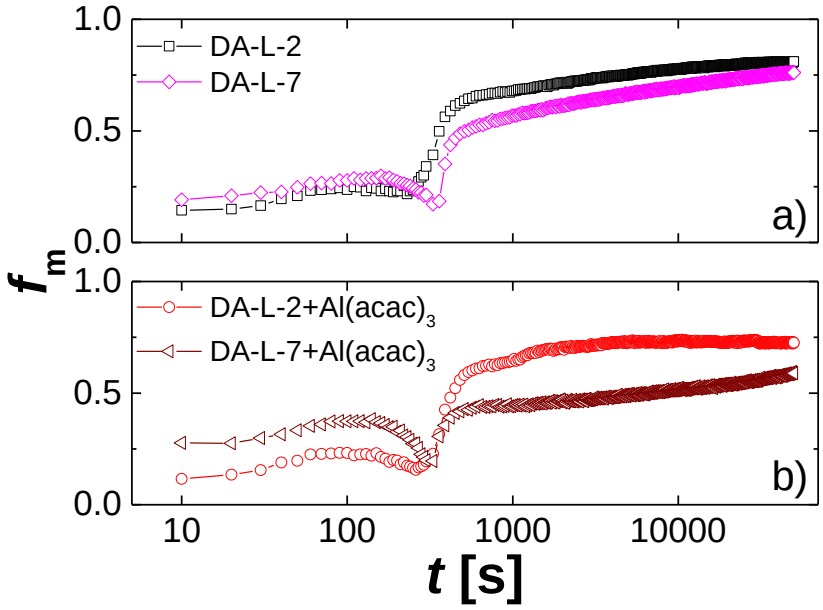

Figure 42: Impact of serum pH on the progress of polymer interdiffusion in dispersions with linear chains (a) and linear chains blended with $Al(acac)_3$ (b). Data already presented in Ref. [18].

First, the influence of the serum pH on interdiffusion of linear chains (Figure 42 a)) is discussed. Interdiffusion in case of DA-L-7 is delayed compared to DA-L-2. This is traced back to the conversion of methacrylic acid units located at the particle surface into their more hydrophilic ammonia salts. It is known that methacrylic acid used as a co-monomer during emulsion polymerization can partially accumulate at the particle boundaries (probably in form of oligomers) in the final dispersion.[77] These oligomers form a barrier against interdiffusion.[78] When the carboxylic acid groups in these oligomers are converted into their more hydrophilic carboxylate salts, this barrier effect is more pronounced for the interdiffusion of the hydrophobic polymer chains in case of DA-L-7.[78] Eventually, however, the f_m data of DA-L-2 and DA-L-7 become similar.

Next, the influence of the serum pH on interdiffusion and cross-linking reaction is discussed (Figure 42 b)). The interdiffusion of DA-L-7+$Al(acac)_3$ is much slower than that of DA-L-2+$Al(acac)_3$, which cannot only be attributed to the aforementioned stronger barrier effect for interdiffusion at higher pH. It is assumed that the polymer cross-linking reaction is faster in case of DA-L-7+$Al(acac)_3$ than in case of DA-L-2+$Al(acac)_3$. According the mechanism of Reaction (I) (Ref. [15] and Figure 9), the *carboxylate* group, COO^- reacts with $Al(acac)_3$, and in DA-L-7+$Al(acac)_3$ more of these are present due to the neutralization.

One aspect that is qualitatively discussed is the reversibility (i.e. the transient nature) of the ionic bond between carboxylate groups in the polymer chains and Al^{3+} cations. In principle, a reversibility of the bond can be expected. Ionic cross-links between carboxylate groups in soft polymers and metal cations such as Na^{+}[29] or Zn^{2+}[12] were found to be reversible. Upon exposing these ionically cross-linked polymer films to elevated temperatures, carboxylate groups attached to the polymer chains can reversibly detach from metal cations.[12,29–34] The interdiffusion data provided here (Figure 40 and Figure 42), however, do not unambiguously prove the transient nature of the ionic bond between Al^{3+} and carboxylate groups, making further research necessary. This can include the examination of interdiffusion in a film forming latex in which chains are cross-linked by Al^{3+} prior to film casting. Employing the aluminum salt of methacrylic acid, i.e. aluminum trimethacrylate, as a co-monomer instead of methacrylic acid to achieve ionic cross-linking during emulsion polymerization is not possible due to the insolubility of aluminum trimethacrylate in water and organic solvents. Alternatively, ionic cross-linking of chains in the polymer particles can be achieved by eliminating acetylacetone from a blend of a dispersion of linear chains and $Al(acac)_3$ before film casting.

4.6 Influence of the Reversibility of the Ionic Bond between Carboxylate Groups and Zn^{2+} on Interdiffusion

In this section, the influence of the reversibility of the ionic bond between carboxylate groups and Zn^{2+} on polymer interdiffusion is investigated. Rheological measurements by Bose *et al*. in Ref. [12] have proven that this bond is reversible. Ionic cross-linking of chains in dispersions prior to film formation can be achieved by employing the zinc salt of methacrylic acid, zinc dimethacrylate, ZnDMA, as a co-monomer during the synthesis. According to interdiffusion studies of dispersions provided by BASF SE (data shown in Ref. [18]), it seems that the ionic bond between carboxylate groups and Zn^{2+} does not hinder interdiffusion. To corroborate the findings from Ref. [18], interdiffusion in films from model dispersions with ionically cross-linked chains prepared by miniemulsion polymerization (MEP, see Table 8 and Table 9) was investigated.

Dispersions with linear chains (DA-MEP-L-II, 0% gel content), chains ionically cross-linked by Zn^{2+} (DA-MEP-Zn-X-0.5 ($n_{COOH}/n_{Zn(II)}$ = 4/1, 40% gel content) and DA-MEP-Zn-X-1 ($n_{COOH}/n_{Zn(II)}$ = 2/1, 80% gel content), and a reference dispersion with covalently cross-linked chains (DA-MEP-cov-X (75% gel content)) were investigated. f_m data plotted against the corrected film formation time t" are shown in Figure 43. Note, that the polymer's T_g is not affected by cross-linking through Zn^{2+},[18] a value of T_g ~ –50 °C can be expected for all latexes investigated here (see Section 3.4). f_m and I_{scat} data of DA-MEP-Zn-X-1 in the initial times shortly after film casting (not shown here) do not differ from those of the dispersions prepared by BASF SE, whose data are provided in Ref. [18].

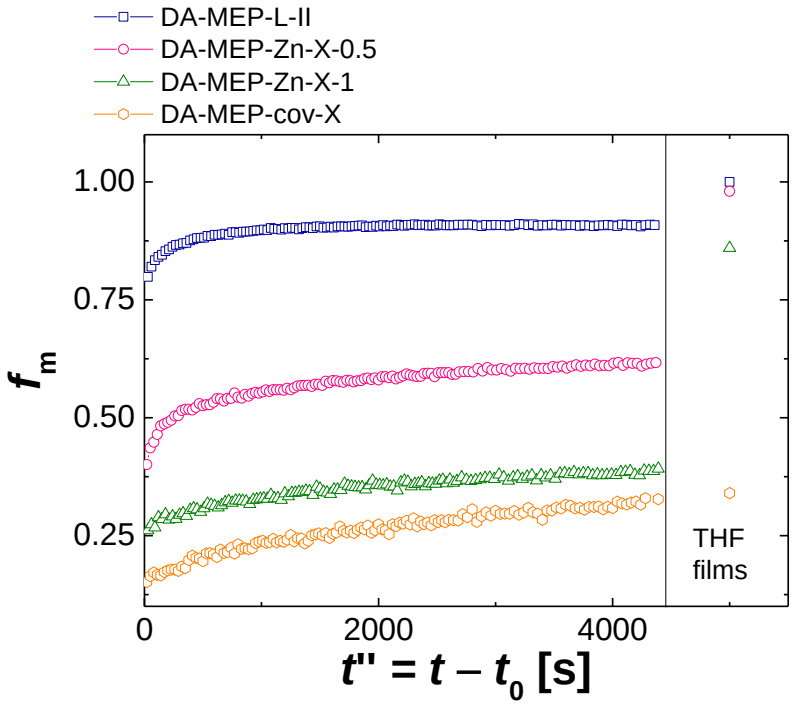

Figure 43: Influence of ionic cross-linking by Zn^{2+} on interdiffusion. t_0 ~500 – 600 s.

It is evident that interdiffusion is slowed down with increasing ZnDMA content. Annealing (also prior to THF homogenization, data not shown here) further increases f_m in case of both, DA-MEP-Zn-X-0.5 and DA-MEP-Zn-X-1. As expected, an increase of f_m for DA-MEP-cov-X was not observed upon annealing. Considering that DA-MEP-Zn-X-1 and DA-MEP-cov-X-1 have large and nearly similar gel contents (~ 70–80%), an increase of f_m in the former case is only plausible if bonds between Zn^{2+} and carboxylate groups in the chains open and close in a dynamic equilibrium. The results here further support the findings in Ref. [18]. Therefore, ionic cross-linking by Zn^{2+} prior to film formation might be an approach to prepare homogeneous films consisting of cross-linked chains from aqueous dispersions. f_m values of THF films are 1, 0.98, 0.87 and 0.34 for DA-MEP-L, DA-MEP-Zn-X-0.5, DA-MEP-Zn-X-1 and DA-MEP-cov-X, respectively.

To estimate polymer diffusion coefficients, f_m data at corrected film formation times t'' = 400 s, 1000 s, 2500 s, were fitted to the spherical diffusion model and plotted against f_m

in Figure 43. For comparison, D values for the latex DA-P(BA_{41}-MMA_{58}-MAA_1) with a calculated T_g of 20 °C (Table 8) and (f_m data from Figure 32 a)) are provided as well.

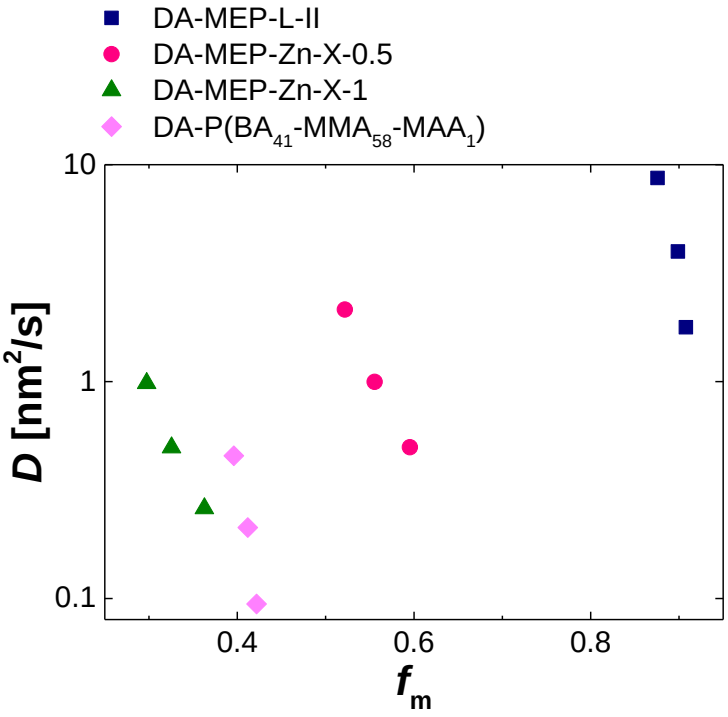

Figure 44: Polymer diffusion coefficients against the fraction of intermixing for dispersions with ionically cross-linked chains by Zn^{2+} (T_g ~ –50 °C) and a reference dispersion with T_g ~ +20 °C.

Polymer interdiffusion is significantly slowed down with increasing degree of cross-linking by Zn^{2+}. In case of DA-MEP-Zn-X-1, the film with the highest cross-linking degree, long-time interdiffusion is comparable to that in a film of linear chains having a T_g of 20 °C. Therefore, ionic polymer cross-linking by Zn^{2+}, albeit being reversible, can reduce chain mobility significantly.

Next, results of interdiffusion studies on dispersions with linear chains intermixed with $Zn(acac)_2$ are presented. Investigated dispersions are DA-MEP-L-II (w_{BA}/w_{MAA} = 98/2) and DA-MEP-L-V (w_{BA}/w_{MAA} = 95/5) (Table 9) blended with different amounts of $Zn(acac)_2$ (3.7 – 9.2 pphm, see Table 10), with the aim to cross-link chains after interdiffusion. Cross-linking of linear chains by $Zn(acac)_2$ might be advantageous in terms of the formation of

homogeneous films if the cross-linking reaction is slower than polymer interdiffusion and if the degree of cross-linking before drying is small (see Reaction (I)). Addition of $Zn(acac)_2$ occurred such that a molar ratio of $n_{COOH}/n_{Zn(II)} = 4/1$ ("0.5") or $n_{COOH}/n_{Zn(II)} = 2/1$ ("1") was present. Gel contents of final films from DA-MEP-L-V+$Zn(acac)_2$-0.5 and DA-MEP-L-V+$Zn(acac)_2$-1 are 43% and 78%, respectively. In case of DA-MEP-L-II+$Zn(acac)_2$-1, the gel content is 30%.[III]

f_m data against the corrected film formation time t" are provided in Figure 45. I_{scat} data are not shown because acetylacetone, formed as a result of polymer cross-linking reaction (Reaction (I)), was found to absorb excitation light at 290 nm at high concentrations. More on this issue is discussed in the Appendix, Section 6.3. The following discussions concern the long-time interdiffusion.

[III]Provided gel contents are average values of films from donor- and acceptor-labeled latexes. In case of DA-MEP-V+$Zn(acac)_2$, they did not differ with respect to the label. However, in case of D-MEP-L-II+$Zn(acac)_2$-1 and A-MEP-L-II+$Zn(acac)_2$-1, gel contents were 45% and 15%, respectively (see Table 10). This difference has been discussed in Section 3.4. It is assumed that the actual gel contents of D-MEP-L-II+$Zn(acac)_2$-1 and A-MEP-L-II+$Zn(acac)_2$-1 are rather similar because results of interdiffusion studies of a blend of D-MEP-L-II+$Zn(acac)_2$-1 and A-MEP-L-II (data not shown here) are identical to those of DA-MEP-L-II which are presented in Figure 44.

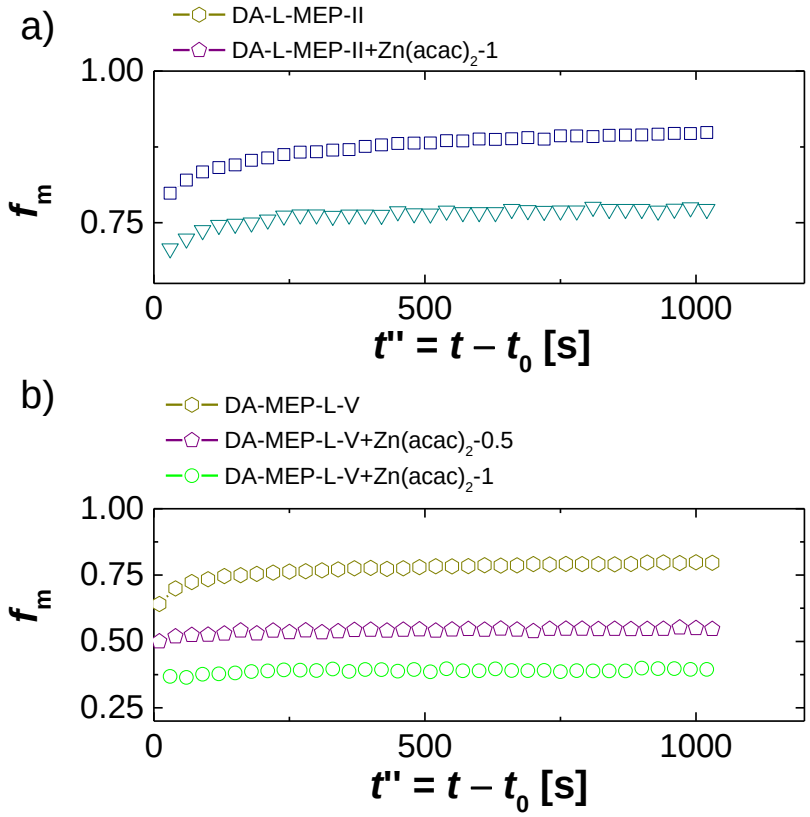

Figure 45: Interdiffusion in film forming dispersions with linear chains blended with varying amounts of Zn(acac)$_2$. t_0 = 500 – 600 s. a): w_{BA}/w_{MAA} = 98/2, b): w_{BA}/w_{MAA} = 95/5.

In all dispersions blended with Zn(acac)$_2$ interdiffusion is slowed down compared to the respective latex with linear chains only. This implies that significant polymer cross-linking has already occurred in the wet latex. When the vials containing the respective latex were opened, evaporating acetylacetone, resulting from the cross-linking reaction, could be smelled. f_m values of THF films of the dispersions investigated in Figure 45 are 1 in all cases, except for DA-MEP-L-V+Zn(acac)$_2$, where it is 0.87.

In the following, the findings of Figure 45 are qualitatively discussed with respect to results of interdiffusion studies of dispersions provided by BASF SE. In case of dispersions provided by BASF SE (Table 2, Figure 40 and Figure 42) which were blended with 1 pphm Al(acac)$_3$, the interdiffusion data suggest that the degree of cross-linking prior to film casting is small and

that polymer cross-linking mainly takes place after film casting. In these dispersions, no acetylacetone could be smelled upon opening the vial containing the latex. However, in case of DA-MEP-L-II and DA-MEP-L-V, evaporating acetylacetone could be smelled from the latexes upon blending with 1 pphm of either $Zn(acac)_2$ or $Al(acac)_3$ (interdiffusion data of the latter not shown here).[IV] Since the composition of the dispersions prepared by MEP and the dispersions provided by BASF SE are different from each other (amounts of MAA employed, surfactants, solids content, etc., see Table 7 and Table 10) a comparative interpretation of these findings regarding cannot be done.

Regarding the preparation of films with ionically cross-linked chains from latexes, blending dispersions prepared by MEP following the recipe in Section 3.3 (Table 5) with metal acetylacetonates is not suitable because the degree of cross-linking in the wet dispersion appears to be relatively large. The fact that aggregation of polymer particles takes place after stirring (as discussed in Section 3.4 (Table 10)) makes it necessary to improve the recipe. Alternatively, semi-batch emulsion polymerization can be employed to prepare dispersions having properties close to the dispersions provided by BASF SE (see Table 7 and Ref. [19]). The dispersions by BASF SE have a better colloidal stability because polymer particles in dispersions blended with metal acetylacetonates were found not to aggregate to a polymer film while stirring.

[IV] Regarding interdiffusion kinetics, the differences between DA-MEP-L-V and DA-MEP-L-V+$Al(acac)_3$ (data not shown here), are smaller than in case of blending with $Zn(acac)_2$. Further research regarding this issue is necessary to obtain information about the kinetics of the cross-linking reaction and the degree of cross-linking before drying.

4.7 Tack Measurements

Flat-punch tack tests were carried out on final films from unlabeled dispersions provided by BASF SE. The properties of these latexes are almost similar to those whose interdiffusion was studied (Section 4.5), with the exception of the solids content which is 50% (see Ref. [18] for properties). Exemplary stress-strain curves for dispersions with linear chains ("L", 0% gel content), linear chains blended with $Al(acac)_3$ ("L+$Al(acac)_3$", 85% gel content, ionic cross-linking) and covalently cross-linked chains ("cov-X", 89% gel content) are provided in Figure 46. A more sophisticated discussion on these data is provided in Ref. [18].

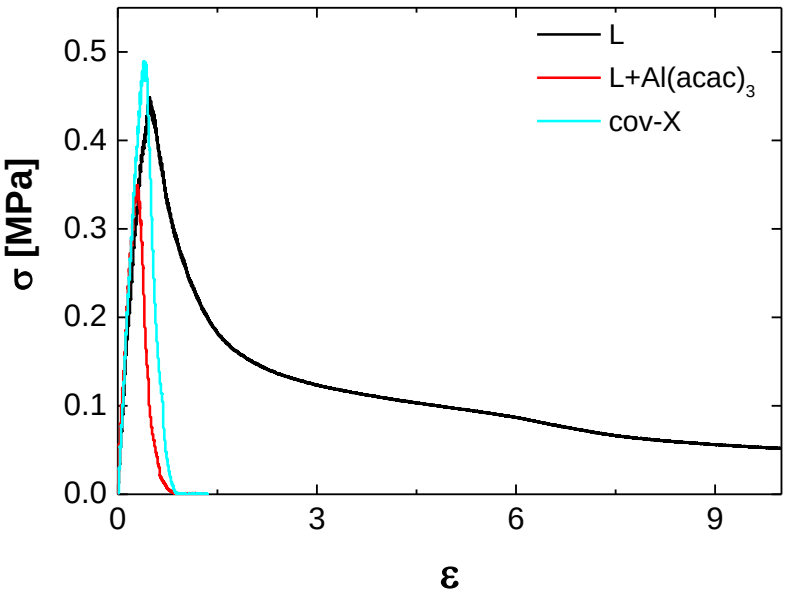

Figure 46: Exemplary stress-strain curves for dispersions with linear chains (L), ionically cross-linked chains (L+$Al(acac)_3$) and covalently cross-linked (cov-X) chains. Data have been presented in Ref. [18].

The peak stresses are similar, while the maximum strain, ε_{max}, which is when σ levels off to zero, is significantly reduced for the cross-linked polymer films, which is characteristic for such high degrees of cross-linking.[22] The cohesion is increased significantly while the adhesion to the probe is decreased. The stress-strain curves of L+$Al(acac)_3$ and cov-X are very similar to each other. However, as suggested by interdiffusion studies (see Figure 40) and

tensile tests (see Ref. [18]), the final film from L+$Al(acac)_3$ is more homogeneous and mechanically stable than the film from cov-X due to a more pronounced polymer interdiffusion in the former case.

5 Conclusion and Outlook

5.1 Conclusion

The combination of FRET and light scattering has been proven to be a powerful tool to study film formation of industrially relevant PSA dispersions.

In the first part of this thesis, the film formation of a dispersion with linear chains in terms of the softness of the polymer particles has been investigated. It was found that particle deformation along the depth profile of the film occurs in two steps. A skin is formed immediately after casting the dispersion. The particles under the skin deform but are separated by water lamellae. The particles come into contact once the lamellae dry out. As a result of skin formation, polymer interdiffusion at the bottom of the film can be faster than at the top. Hydroplasticization and the acceleration of polymer interdiffusion in a latex blended with a tackifying resin were observed.

In the second part, the influence of $Al(acac)_3$ on interdiffusion in film forming dispersions provided by BASF SE was studied. Interdiffusion in a latex of linear chains blended with $Al(acac)_3$ is nearly identical to that of the same latex with linear chains only. Therefore, it can be concluded that homogeneous films consisting of ionically cross-linked chains with a large gel content could be prepared from the dispersions. The interdiffusion data suggest that the degree of ionic cross-linking in the dispersion prior to drying is rather small and that cross-linking mainly occurs after film casting. Neutralizing the serum pH from 2 to 7 leads to a faster cross-linking reaction and slower interdiffusion.

In the third part, interdiffusion of latexes in which chains were cross-linked by Zn^{2+} before drying were studied with respect to the reversibility of the ionic bond between Zn^{2+} and carboxylate groups in the chains. These studies were carried out on model dispersions prepared by miniemulsion polymerization in which chains were cross-linked by using ZnDMA as a co-

monomer during the synthesis. The findings from Ref. [18] were further corroborated as it could be shown that reversible polymer cross-linking by Zn^{2+}does not hinder interdiffusion but slows it down. Blending model dispersions prepared by miniemulsion polymerization with metal acetylacetonates decreases their colloidal stability as particle aggregation occurs while stirring. Compared to the dispersions by BASF SE, the degree of cross-linking prior to film casting is much higher in case of the model dispersions.

5.2 Outlook

Further studies should concern the reversibility of the ionic bond between aluminum cations and carboxylate groups in the polymer chains. Rheological studies on films cross-linked by Al^{3+} can be carried out to investigate the bond lifetime. To evaluate the influence of the reversibility of the Al^{3+}-carboxylate bond, interdiffusion studies on dispersions blended with $Al(acac)_3$ from which acetylacetone has been removed prior to film formation can be performed. The reversibility of the bond can also be investigated with respect to self-healing in polymer films.

Miniaturization of semi-batch emulsion polymerization is necessary in order to synthesize dispersions having properties close to industrially relevant dispersions. For future experiments, this is of crucial relevance because dispersions prepared by miniemulsion polymerization have a decreased colloidal stability upon intermixing with metal chelates.

6 Appendix

6.1 Estimation of Observation Depth for FRET/Light Scattering Measurements

The observation depth is calculated semi-quantitatively for the initial wet state and the final dry state. The arguments are shortly outlined, a more critical and sophisticated discussion about the calculations is provided in Ref. [19]. Calculations were done for DA-L-2, but the results are valid for all other systems as well because concentrations of donor- and acceptor were always kept constant. In general, both scattering and absorption can contribute to the attenuation of the intensity of detected light.

In the initial wet state, attenuation originates from scattering. The attenuation coefficient for excitation light (λ = 290 nm), α_{scat} is calculated following eq. 23.[79]

$$\alpha_{scat} = \frac{N}{V}\sigma = \frac{N}{V}\frac{8}{3}\left(\frac{2\pi n_{liq} a}{\lambda}\right)^4 \left(\frac{{n_P}^2 - 1}{{n_P}^2 + 2} - \frac{{n_{liq}}^2 - 1}{{n_{liq}}^2 + 2}\right)^2 \pi a^2 \qquad \text{eq. 23}$$

N/V is the number density of particles ($\approx$ 0.3), n_{liq} the refractive index of water ($\approx$ 1.35), n_P the refractive index of the polymer particles ($\approx$ 1.5) and a the particle radius ($\approx$ 60 nm). α_{scat} is calculated to be $\approx$ 0.588 μm.

The attenuation due to absorption is calculated from Lambert-Beer's law. For the excitation light (λ = 290 nm), the principal source of absorption is the donor (Phen-MMA), and for emitted light, it is the acceptor (NPP-A). The attenuation coefficient for the excitation light, $\alpha_{abs,290}$ is calculated as

$$\alpha_{abs,290} = \varepsilon_D c_D \ln(10) \qquad \text{eq. 24}$$

ε_D is the molar extinction coefficient of the donor, and c_D its concentration.

The spectrum of attenuation of emitted light by the acceptor, $\alpha_{abs}(\lambda)$, can be calculated following eq. 25.

$$\alpha_{abs}(\lambda) = \ln(10)\, c_A \varepsilon_A(\lambda) \qquad \text{eq. 25}$$

c_A is the molar concentration of the acceptor and $\varepsilon_A(\lambda) = \varepsilon_{NPP\text{-}A}(\lambda)$ its molar extinction coefficient. The donor does not absorb light at $\lambda > 300$ nm, and thus its contribution to attenuation can be neglected.

In order to estimate a depth of observation, the probabilities for excitation and detection need to be combined. For the following calculations, the factor $2^{1/2}$ has entered the respective equations because light is detected at an angle of 45° relative to the excitation beam. For scattering in the *initial wet state*, the depth of observation is given as

$$z_{obs,scat} = \frac{\int z \cdot \exp(\alpha_{scat}(z+\sqrt{2}z))dz}{\int \exp(\alpha_{scat}(z+\sqrt{2}z))dz} = \frac{1}{\alpha_{scat}(1+\sqrt{2})} \qquad \text{eq. 26}$$

A value of $z_{obs,scat} \approx 0.7$ µm is calculated. The depth of observation for fluorescence in the *dry state* (with no scattering occurring) is

$$z_{obs,abs} = \int g(\lambda) \left[\frac{\int_0^\infty z \cdot \exp(-(\alpha_{abs,290} \cdot z + \alpha_{abs}(\lambda) \cdot z(1+\sqrt{2})))dz}{\int_0^\infty \exp(-(\alpha_{abs,290} \cdot z + \alpha_{abs}(\lambda) \cdot z(1+\sqrt{2})))dz} \right] d\lambda \qquad \text{eq. 27}$$

$g(\lambda)$ is a normalized weight function. It is calculated by

$$g(\lambda) = \frac{I_D(\lambda) T(\lambda) \int_0^\infty \exp(-(\alpha_{abs,290} \cdot z + \alpha_{abs}(\lambda) \cdot z(1+\sqrt{2})))dz}{\int_0^\infty (I_D(\lambda) T(\lambda) \int_0^\infty \exp(-(\alpha_{abs,290} \cdot z + \alpha_{abs}(\lambda) \cdot z(1+\sqrt{2})))dz) d\lambda} \qquad \text{eq. 28}$$

$I_D(\lambda)$ is the normalized intensity of emitted light by the donor and $T(\lambda)$ the transmittance of the longpass filter inside the TCSPC setup. $z_{obs,abs}$ is calculated to be 5.5 µm, spectra used for the calculations are shown in Figure 47.

Spectra of monomeric dyes were recorded in solvents in which they match those of the corresponding dry films (D-L-2 and A-L-2). For the donor, the solvent was dimethyl sulfoxide and for the acceptor, it was *n*-butyl acrylate. In the solutions and in the final films, c_D was 29 mmol/L and c_A was 18.1 mmol/L. The extinction coefficient of the donor at 290 nm, ε_D, in dimethyl sulfoxide was measured to be 1.114 L/(mol·µm). The fluorescence spectrum of the donor was recorded with a Jasco spectrophotometer FP-8500 and absorption spectra were recorded with a Jasco spectrophotometer V670.

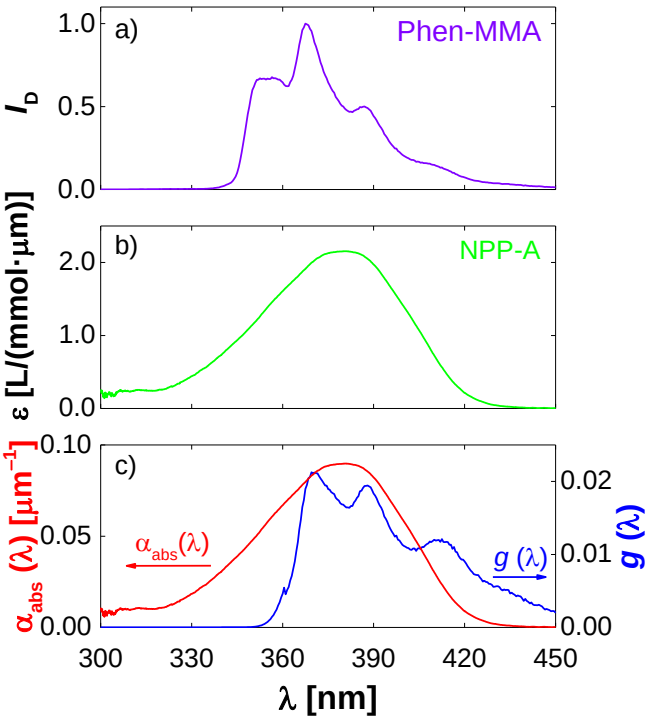

Figure 47: a) Normalized emission spectrum of Phen-MMA in dimethyl sulfoxide excited at 290 nm, b) molar extinction coefficient of NPP-A in *n*-butyl acrylate, c) g(λ) and α_{abs} (λ). Data already presented in Ref. [19].

6.2 Dye-Sensitive GPC Measurements

GPC measurements in which UV detectors sensitive to the dye were employed in addition to DRI detection were carried out on films from D-MEP-L-II and A-MEP-L-II (Table 9) at BASF SE (see Ref. [19] for experimental details). In case of donor-labeling achieved by employing Phen-MMA as a co-monomer, detection wavelength was 290 nm, in case of acceptor-labeling, achieved by employing NPP-A, detection wavelength was 380 nm. Elution curves for are given in Figure 48.

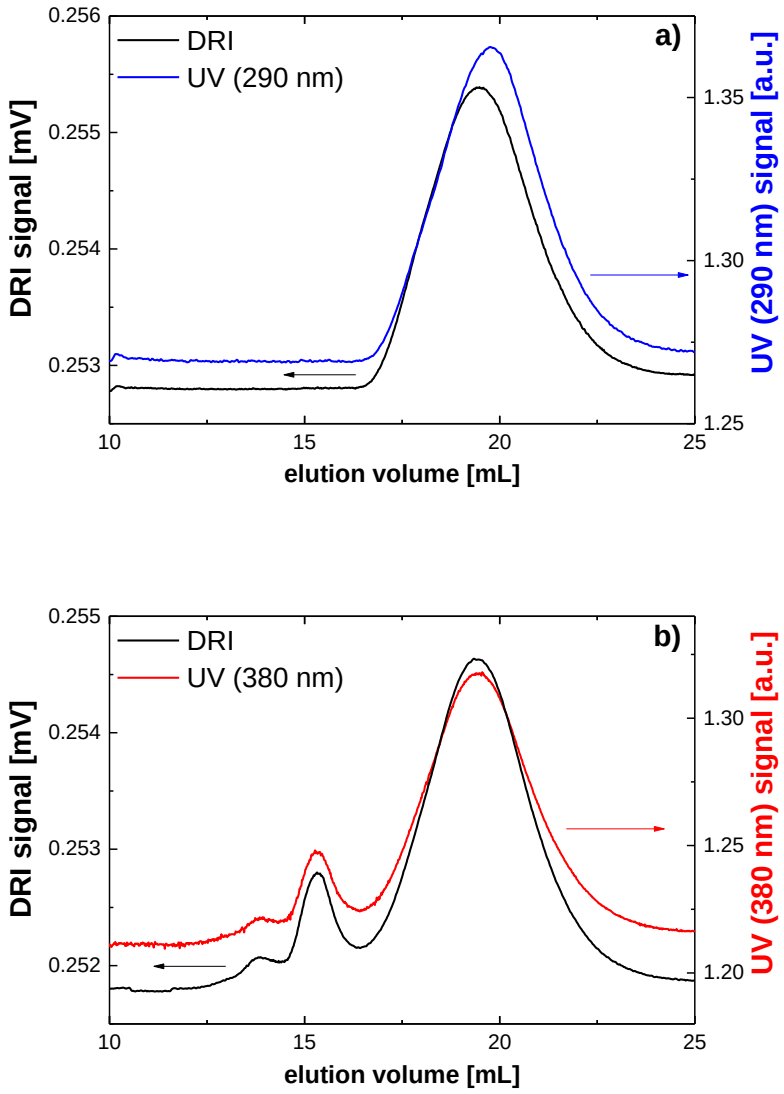

Figure 48: GPC measurements with DRI and UV-detection sensitive to the respective dye. a) Donor (Phen-MMA): 290 nm, b) Acceptor (NPP-A): 380 nm.

Cleary, the elution curves acquired with DRI and UV detection almost overlap, proving incorporation of labels along the chains independent of molecular weight.

6.3 UV Absorption Spectra of Acetylacetone and Metal Acetylacetonates

UV absorption spectra of solutions of acetylacetone, $Al(acac)_3$ and $Zn(acac)_2$ in cyclohexane (spectroscopic grade) were recorded (Jasco spectrophotometer V670). Cyclohexane has been chosen as a solvent because it is not expected to react with the metal acetylacetonates. Normalized spectra are shown in Figure 49. The solubility of $Al(acac)_3$ and $Zn(acac)_2$ in cyclohexane was found to be poor (less than 5 mg salt in 3 mL solvent). In both cases, undissolved salt has sedimented.

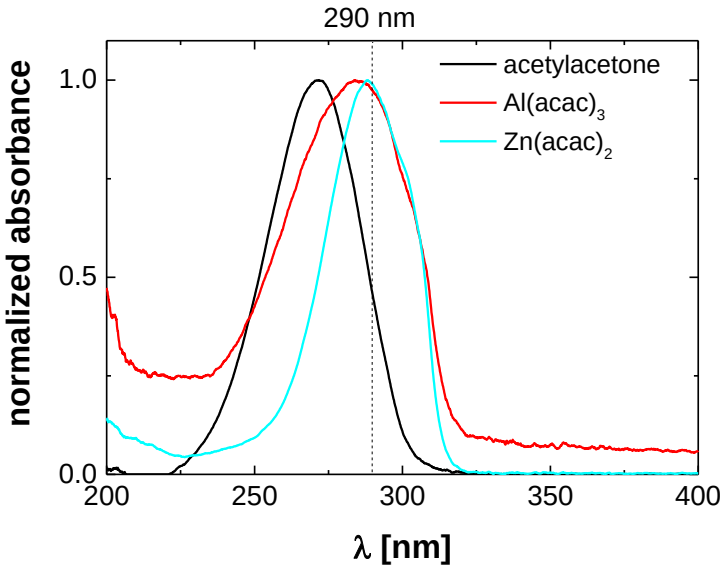

Figure 49: Normalized absorption spectra of acetylacetone, $Al(acac)_3$ and $Zn(acac)_2$ in cyclohexane.

Clearly, acetylacetone, $Al(acac)_3$ and $Zn(acac)_2$ absorb light at 290 nm. For low concentrations (1 pphm), the absorption of scattered excitation light, I_{scat} at 290 nm in case of both $Al(acac)_3$ and $Zn(acac)_2$ is negligible (Figure 40), however, for high concentrations (9 pphm), it does affect the I_{scat} kinetics (data not shown here). Still, in terms of interdiffusion quantified with FRET measurements, the presence of metal acetylacetonates does not seem to

interfere because there is no spectral overlap between the absorption spectrum of acetylacetone and the donor's emission spectrum (see Figure 47).

7 References

1 A. V. Pocius, *Adhesion and adhesives technology. An introduction*, Second Edition, Hanser, **2002**.

2 C. Creton, M. Ciccotti, Fracture and adhesion of soft materials: A Review, *Rep. Prog. Phys.* **2016**, *79*, 046601.

3 C. Creton, Pressure-Sensitive Adhesives: An introductory course, *MRS Bull.* **2003**, *28*, 434–439.

4 R. Jovanović, M. A. Dubé, Emulsion-based pressure-sensitive adhesives: A review. *J. Macromol. Sci. Polymer Rev.* **2004**, *44*, 1–51.

5 J. L. Keddie, A. F. Routh, Fundamentals of latex film formation, Springer, First Edition, **2010**.

6 A. Zosel, B. Schuler, The Influence of Surfactants on the Peel Strength of Water-based Pressure Sensitive Adhesives, *J. Adhes.* **1999**, *70*, 179–195.

7 J. Feng, H. Pham, V. Stoeva, M. A. Winnik, Polymer diffusion at ambient temperature. *J. Polym. Sci. Part B: Polym. Phys.* **1998**, *36*, 1129–1136.

8 A. Zosel, G. Ley, Influence of cross-linking on structure, mechanical properties, and strength of latex films. *Macromolecules* **1993**, *26*, 2222–2227.

9 P. Pinenq, M. A. Winnik, B. Ernst, D. Juhué, Polymer diffusion and mechanical properties of films prepared from cross-linked latex particles. *J. Coat. Technol.* **2000**, *72*, 45–61.

10 T. Tamai, P. Pinenq, M. A. Winnik, Effect of cross-linking on polymer diffusion in poly(butylmethacrylate-*co*-butyl acrylate) latex films. *Macromolecules* **1999**, *32*, 6102–6110.

11 J. W. Taylor, M. A. Winnik, Functional Latex and Thermoset Latex Films, *JCT Research* **2004**, *1*, 163–190.

12 R. K. Bose, N. Hohlbein, S. J. Garcia, A. M. Schmidt, S. van der Zwaag, Connecting supramolecular bond lifetime and network mobility for scratch healing in poly(butyl acrylate) ionomers containing sodium, zinc and cobalt, *Phys. Chem. Chem. Phys.* **2015**, *17*, 1697–1704.

13 Z. Czech, Crosslinking of pressure sensitive adhesive based on water-borne acrylate, *Polym. Int.* **2003**, *52*, 347–357.

14 S. D. Tobing, A. Klein, Molecular parameters and their relation to the adhesive performance of acrylic pressure-sensitive adhesives, *J. Appl. Polym. Sci.* **2001**, *79*, 2230–2244.

15 Z. Czech, M. Wojciechowicz, The crosslinking reaction of acrylic PSA using chelate metal acetylacetonates, *Eur. Polym. J.* **2006**, *42*, 2153–2160.

16 J. R. Lakowicz, *Principles of fluorescence spectroscopy*, Third Edition, Springer Science+Business Media LLC, **2006**.

17 Y. Wang, M. A. Winnik, Polymer diffusion across interfaces in latex films. *J. Chem. Phys.* **1993**, *97*, 2507–2515.

18 H. Wahdat, M. Gerst, M. Rückel, S. Möbius, J. Adams, Influence of Delayed, Ionic Polymer Cross-linking on Film Formation Kinetics of Waterborne Adhesives, *Macromolecules* **2019**, *52*, 271–280.

19 H. Wahdat, C. Hirth, D. Johannsmann, M. Gerst, M. Rückel, J. Adams, Film Formation of Pressure-Sensitive Adhesives (PSAs) Studied with Förster Resonance Energy Transfer (FRET) and Scattering Intensity, *Macromolecules* **2018**, *51*, 4718–4726.

20 Online article about Pressure Sensitive Adhesives, **2015**. Link: https://polymerdatabase.com/Adhesives/PSAs.html, last visit: 29.10.2018.

21 H. Lakrout, P. Sergot, C. Creton, Direct observation of cavitation and fibrillation in a probe tack experiments on model acrylic pressure-sensitive adhesives, *J. Adhes.* **1999**, *69*, 307–359.

22 F. Deplace, C. Carelli, S. Mariot, H. Retsos, A. Chateauminois, K. Ouzineb, C. Creton, Fine tuning the adhesive properties of a soft nanostructured adhesive with rheological measurements, *J. Adhes.* **2009**, *85*, 18–54.

23 J. Brandrup, E. H. Immergut, *Polymer handbook*, Third Edition, John Wiley & Sons, **1989**.

24 Y. Osada, J. Ping Gong, Y. Tanaka, Polymer gels, *J. Macromol. Sci. Polymer Rev.* **2004**, *44*, 87–112.

25 P. Du, X. Wang, Reversible cross-linking polymer-based self-healing materials, *Recent Advances in Smart Self-Healing Polymers and Composites*, First Edition, Elsevier, **2015**.

26 S. Seiffert, J. Sprakel, Physical chemistry of supramolecular polymer networks, *Chem. Soc. Rev.* **2012**, *41*, 909–930.

27 Z. Czech, Synthesis and cross-linking of acrylic PSA systems, *J. Adhes. Sci. Technol.* **2007**, *21*, 625–635.

28 W. Mächtle, J. Rieger, Ion exchange in carboxylated latices – AUC studies using sedimentation and density gradient techniques, *Colloid Polym. Sci.* **1995**, *273*, 708–716.

29 Y. Lu, L. Liu, M. Tian, H. Geng, L. Zhang, Study on mechanical properties of elastomers reinforced by zinc dimethacrylate, *Eur. Polym. J.* **2005**, *41*, 589 – 598.

30 Y. Miwa, J. Kurachi, Y. Kohbara, S. Kutsumizu, Dynamic ionic crosslinks enable high shear strength and ultrastrechability in a single elastomer, *Commun. Chem.* **2018**, *1*, 1–8.

31 Y. Cai, Y. Lapitski, Formation and dissolution of chitosan/pyrophosphate nanoparticles: Is the ionic cross-linking reaction of chitosan reversible?, *Colloids Surf. B.* **2014**, *115*, 100–108.

32 S. J. Jr. Kalista, J. R. Pflug, R. J. Varley, Effect of ionic content on ballistic self-healing in EMAA copolymers and ionomers, *Polym. Chem.* **2013**, *4*, 4190–4926.

33 N. Hohlbein, A. Shaaban, A. R. Bras, W. Pyckhout-Hintzen, A. M. Schmidt, Self-healing dynamic bond-based rubbers: Understanding the mechanisms in ionomeric elastomer model systems, *Phys. Chem. Chem. Phys.* **2015**, *17*, 21005–21017.

34 C. Xu, L. Cao, B. Lin, X. Liang, Y. Chen., Design of self-healing supramolecular rubbers by introducing ionic cross-links into natural rubber via a controlled vulcanization, *ACS Appl. Mater. Interfaces* **2016**, *8*, 17728–17737.

35 M. Sievers, J. C. Namyslo, F. Lederle, E. G. Hübner, Proof of concept for molecular velcro based on the attractive interaction between porphyrin and pyridine containing copolymers, *Express Polym. Lett.* **2018**, *12*, 556–568.

36 T. Christ, M. Gerst, H. Harrer, M. Rückel, D. Wulff, *Advanced Polymer Design for Adhesive Tapes*, Online Presentation **2016**. Link: https://www.pstc.org/files/Wulff_Dick.pdf

37 W. Clegg, I. R. Little, B. P. Straughan, Zinc carboxylate complexes: structural characterization of the mixed-metal linear trinuclear complexes MZn2(crot)6(base)2, *Inorg. Chem.* **1988**, *27*, 1916–1923.

38 S. S. Voyutski, Amendment to the papers by Bradford, Brown and co-workers: "Concerning mechanism of film formation from high polymer dispersions". *J. Polym. Sci.* **1958**, *32*, 528–530.

39 F. T. Carter, R. M. Kowalczyk, I. Millichamp, M. Chainey, J. L. Keddie, Correlating particle deformation with water concentration profiles during latex film formation: Reasons that softer latex films take longer to dry. *Langmuir* **2014**, *30*, 9672–9681.

40 A. F. Routh, W. B. Russel, A Process Model for Latex Film Formation: Limiting Regimes for Individual Driving Forces, *Langmuir* **1999**, *15*, 7762–7773.

41 M. Rubinstein, R. H. Colby, *Polymer Physics*, Oxford University Press, First Edition, **2003**.

42 M. Doi, S. F. Edwards, Dynamics of concentrated polymer systems. Part 1. – Brownian motion in the equilibrium state. *J. Chem. Soc. Faraday Trans.* **1978**, *2*, 1789–1801.

43 A. Karim, A. Mansour, G. P. Felcher, Short-time relaxation at polymeric interfaces. *Phys. Rev. B. Condensed Matter*, **1990**, *42*, 6846–6849.

44 T. P. Lodge, Reconciliation of the molecular weight dependence of diffusion and viscosity in entangled polymers. *Phys. Rev. Lett.* **1999**, *83*, 3218–3221.

45 J. W. Vanderhoff, Mechanism of film formation of latices. *Br. Polym. J.* **1970**, *2*, 161–173.

46 S. Prager, M. Tirrel, The healing at polymer-polymer interfaces. *J. Chem. Phys.* **1981**, *75*, 5194–5198.

47 Y. H. Kim, R. P. Wool, A theory of healing at a polymer-polymer interface. *Macromolecules* **1983**, *16*, 1115–1120.

48 J. L. Keddie, P. Meredith, R. A. Jones, A. M. Donald, Kinetics of film formation in acrylic latices studied with multiple-angle-of-incidence ellipsometry and environmental SEM. *Macromolecules* **1995**, *28*, 2673–2682.

49 K. D. Kim, L. H. Sperling, A. Klein, B. Hammouda, Reptation Time, temperature, and cosurfactant effects on the molecular interdiffusion rate during polystyrene latex film formation. *Macromolecules* **1994**, *27*, 6841–6850.

50 A. Zosel, Mechanical properties of films from polymer latices. *Polym. Adv. Technol.* **1995**, *6*, 263–269.

51 K. Hahn, G. Ley, H. Schuller, R. Oberthür, On particle coalescence in latex films. *Colloid Polym. Sci.* **1986**, *264*, 1092–1096.

52 K. Hahn, G. Ley, R. Oberthür, On particle coalescence in latex films (II). *Colloid Polym. Sci.* **1988**, *266*, 631–639.

53 Y. Wang, C.-L. Zhao, M. A. Winnik, Molecular diffusion and latex film formation: An analysis of direct nonradiative energy transfer experiments. *J. Chem. Phys.* **1991**, *95*, 2143–2153.

54 R. Casier, M. Gauthier, J. Duhamel, Using pyrene excimer fluorescence to probe polymer diffusion in latex films. *Macromolecules* **2017**, *50*, 1635–1644.

55 J. G. Tsavalas, D. C. Sundberg, Hydroplasticization of polymers: model prediction and application to emulsion polymers. *Langmuir* **2010**, *26*, 6960–6966.

56 J. Feng, M. A. Winnik, Effect of water on polymer diffusion in latex films. *Macromolecules* **1997**, *30*, 4324–4331.

57 J. C. Haley, Y. Liu, M. A. Winnik, W. Lau, The onset of polymer diffusion in a drying acrylate: how water initially retards coalescence but ultimately enhances interdiffusion. *J. Coat. Technol. Res.* **2008**, *5*, 157–168.

58 M. Soleimani, J. C. Haley, W. Lau, M. A. Winnik, Effect of hydroplasticization on polymer diffusion in poly(butyl acrylate-*co*-methyl methacrylate) and poly (2-ethylhexyl-*co*-tert-butyl methacrylate) latex films. *Macromolecules* **2010**, *43*, 975–985.

59 T. G. Wood, The Effects of tackification on waterborne acrylic pressure sensitive adhesive, *Adhes. Age* **1987**, *40*, 19–23.

60 J. Mallégol, G. Bennett, P. J. McDonald, J. L. Keddie, O. Dupont, Skin development during the film formation of acrylic pressure sensitive adhesives containing tackifying resin, *J. Adhes.* **2006**, *82*, 217–328.

61 A. Aradian, E. Raphaël, P.-G. de Gennes, Strengthening of a Polymer Interface: Interdiffusion and Crosslinking, *Macromolecules* **2000**, *33*, 9444–9451.

62 A. Aradian, E. Raphaël, P.-G. de Gennes, A Scaling Theory of the Competition between Interdiffusion and Cross-linking at Polymer Interfaces, *Macromolecules* **2002**, *35*, 4036–4043.

63 T. Förster, Zwischenmolekulare Energiewanderung und Fluoreszenz, *Ann. Phys.* **1948**, *6*, 55–75.

64 J. P. S. Farinha, J. M. G. Martinho, S. Kawaguchi, A. Yekta, M. A. Winnik, Direct Nonradiative Energy Trasnfer in Polymer Interfaces: Fluorescence Decay Functions from Concentration Profiles Generated by Fickian Diffusion. *Macromolecules* **1995**, *28*, 6084–6088.

65 J. Crank, *The Mathematics of Diffusion*, Second Edition, Oxford University Press, **1975**, p 30.

66 A. Turshatov, J. Adams, New monomeric FRET-acceptor for polymer interdiffusion experiments on polymer dispersions, *Polymer* **2007**, *48*, 7444–7448.

67 Q. Wang, S. Fu, T. Yu, Emulsion Polymerization, *Prog. Polym. Sci.* **1994**, *19*, 703–753.

68 I. M. Kolthoff, I. K. Miller, The Chemistry of Persulfate. I. The Kinetics and Mechanism of the Decomposition of the Persulfate Ion in Aqueous Medium, *J. Am. Chem. Soc.* **1951**, *73*, 3055–3059.

69 K. Landfester, Miniemulsions for Nanoparticle Synthesis, *Top. Curr. Chem.* **2003**, *227*, 75–123.

70 Z. Wang, A. J. Paine, A. Rudin, Control of surfactant level in starve-fed emulsion polymerization. I. Sulfate-containing oligomers: Preparation and appliation as surfactant in emulsion polymerization, *J. Polym. Sci. Part A: Polym. Chem.* **1995**, *33*, 1597–1606.

71 T. G. Fox, Influence of Diluent and of Copolymer Composition on the Glass Temperature of a Polymer System, *Bull. Am. Phys. Soc.* **1956**, *1*, 123.

72 D. W. Marquardt, An Algorithm for Least-Squares Estimation of Nonlinear Parameters, *J. Soc. Indust. Appl. Math.* **1963**, *11*, 413–414.

73 C. Hirth, Beitrag von kurzkettigen Polymeren zur Filmbildung von Polymerdispersionen, *Bachelor Thesis*, Clausthal University of Technology, **2016**.

74 J. Mallégol, J. P. Gorce, O. Dupont, C. Jeynes, P. J. McDonald, J. L. Keddie, Origins and effects of a surfactant excess near the surface of waterborne acrylic pressure-sensitive adhesives, *Langmuir* **2002**, *18*, 4478–4487.

75 J. A. Kimber, M. Gerst, S. G. Kazarian, Fast drying and film formation of latex dispersions studied with FTIR spectroscopic imaging, *Langmuir* **2014**, *30*, 13588–13595.

76 T. L. Crowley, A. R. Sanderson, J. D. Morrison, M. D. Barry, A. J. Mortonjones, A. R. Rennie, Formation of bilayers and plateau borders during the drying of film-forming latices as investigated by small-angle neutron scattering, *Langmuir* **1992**, *8*, 2110–2123.

77 T. Ding, E. S. Daniels, M. S. El-Aasser, A. Klein, Synthesis and Characterization of Functionalized Polymer Latex Particles Through a Designed Semicontinous Emulsion Polymerization, *J. Appl. Polym. Sci.* **2005**, *97*, 248–256.

78 H. B. Kim, M. A. Winnik, Factors Affecting Interdiffusion Rates in Films Prepared from Latex Particles with a Surface Rich in Acid Groups and Their Salts, *Macromolecules* **1995**, *28*, 2033–2041.

79 H. C. van de Hulst, *Light Scattering by Small Particles*, Second Edition, Dover: New York, **1981**, 70.

8 Glossary of Important Symbols and Abbreviations

2γ	Parameter quantifying number of acceptors surrounding a donor in a sphere with a radius R_F
A	Acceptor
A_2	Fit-parameter in the two-state model, amount of donor intermixed with acceptors
$A_{2,min}$	A_2 value of a wet, non-drying mixture of donor- and acceptor-labeled dispersions
acac	Acetylacetonate
acac–H	Acetylacetone
$Al(acac)_3$	Aluminum acetylacetonate
A_{TR}	Additional fit-parameter accounting for the intensity of the tackifier's intrinsic fluorescence
BA	*n*-Butyl acrylate
BASF SE	Badische Anilin und Soda Fabrik Societas Europaea
Calc.	Calculated
cov-X	Covalent cross-linking
D	Diffusion coefficient
D	Donor
DDM	1-dodecyl mercaptane
d_h	Hydrodynamic diameter

DLS	Dynamic light scattering
DSC	Differential scanning calorimetry
EGDMA	Ethylene glycol dimethacrylate
EHA	2-Ethylhexyl acrylate
f_m	Fraction of intermixing
FRET	Förster resonance energy transfer
GPC	Gel permeation chromatography
HD	Hexadecane
I	Fluorescence intensity
I_0	Intensity immediately after the UV flash
I_{scat}	Background-corrected and normalized scattering intensity
L	Linear
MAA	Methacrylic acid
MEK	Methyl ethyl ketone
MEP	Miniemulsion polymerization
MMA	Methyl methacrylate
M_w	Mass weighted molecular weight
NaPS	Sodium persulfate
NPP-A	1-(4-Nitrophenyl)-2-pyrrolidinemethyl acrylate
PDI	Polydispersity index

Phen-MMA	(9-Phenanthryl)methyl methacrylate
PSA	Pressure-sensitive adhesive
r	Distance
Ref.	Reference
R_F	Förster radius
rH	Relative humidity
SDS	Sodium dodecyl sulfate
t	Film formation time
t'	Decay time
t''	Corrected film formation time
t_0	Time when I_{scat} reaches zero
TCSPC	Time-correlated single-photon counting
T_g	Glass transition temperature
THF	Tetrahydrofuran
THF film	Films consisting of donor- and acceptor-labeled chains homogenized by intermixing with THF
UV	Ultraviolet
$Zn(acac)_2$	Zinc acetylacetonate
ZnDMA	Zinc dimethacrylate
Zn-X	Ionic cross-linking by Zn^{2+}

$z_{obs,abs}$	Observation depth for the final dry state (< 5.5 μm)
$z_{obs,scat}$	Observation depth for the initial wet state (< 1 μm)
α_{abs}	Attenuation coefficient connected to absorption
α_{scat}	Attenuation coefficient connected to scattering
ε	Strain
ε_{max}	Maximum Strain
λ	Wavelength in nanometers
σ	Stress
σ_{max}	Peak Stress
τ_D	Donor's fluorescence lifetime
τ_{TR}	Lifetime of the intrinsic fluorescence of the tackifier

9 List of Publications

Publications in Peer-Reviewed Journals

- M. Mocan, H. Wahdat, H. M. van der Kooij, W. M. de Vos, M. Kamperman, *J. Membr. Sci.* **2018**, *548*, 502–509. **DOI:** 10.1016/j.memsci.2017.11.047
  „Systematic Variation of Membrane Casting Parameters to Control the Structure of Thermo-Responsive Isoporous Membranes"
- H. Wahdat, C. Hirth, D. Johannsmann, M. Gerst, M. Rückel, M. Gerst, J. Adams *Macromolecules* **2018**, *51*, 4718–4726.* **DOI:** 10.1021/acs.macromol.8b00423
  „Film Formation of Pressure-Sensitive Adhesives (PSAs) Studied with Förster Resonance Energy Transfer (FRET) and Scattering Intensity"
- H. Wahdat, M. Gerst, M. Rückel, S. Möbius, J. Adams, *Macromolecules* **2019**, *52*, 271–280.* **DOI:** 10.1021/acs.macromol.8b01870
  „Influence of Delayed, Ionic Polymer Cross-Linking on Film Formation Kinetics of Waterborne Adhesives"
- H. Wahdat, M. Gerst, J. Adams, in preparation.*
  „Influence of the reversibility of ionic cross-linking between carboxylate groups in polymer chains and Zn^{2+} on the stage of interdiffusion during film formation of soft acrylic polymer dispersions"

  * Data from this thesis.

Talks and Poster Presentations

- Talk: „Drittes Niedersächsisches Symposium Materialtechnik", Clausthal-Zellerfeld, Germany, 02/2019.
- Poster Presentation: 5th International Conference on Physical and Theoretical Chemistry, Edinburgh, United Kingdom, 10/2018.

- Talk: “Gesellschaft Deutscher Chemiker (GdCh) Kolloqium”, Clausthal-Zellerfeld, 07/2018.
- Talk: “Oberflächentechnik und –funktionalisierung” Graduate Colloquium, Clausthal-Zellerfeld, Germany, 01/2018.

10 Curriculum Vitae

Personal

Name (First, Last)	Hares Wahdat
Date of Birth:	19.03.1992
Place of Birth:	Goslar, Germany
Nationality:	German
E-Mail:	hares.wahdat@web.de

Education

12/2016 – 02/2019	*PhD Student in Chemistry*, Institute of Physical Chemistry, Clausthal University of Technology, under Supervision of PD Dr. Jörg Adams Grade: >1,0 ("summa cum laude") - *Thesis:* Film Formation of Ionically Cross-Linked Pressure-Sensitive Adhesives Dispersions Studied with Förster Resonance Energy Transfer
10/2014 – 11/2016	*M. Sc. in Chemistry*, Clausthal University of Technology Grade: 1,0 - Compulsory Modules: Modern Inorganic Chemistry, Spezielle Physikalische Chemie (eng. Special Physical Chemistry) - Master Thesis under Supervision of PD Dr. Jörg Adams: Investigation of Interdiffusion in Polymer Adhesives Using FRET (Grade: 1,0)
01/2016 – 04/2016	*Research Internship*, Institute of Physical Chemistry and Soft Matter, Wageningen, Netherlands, under Supervision of Dr. Marleen Kamperman - *Subject of Research*: Thermoresponsive Nanoporous Membranes from Block Copolymers
10/2011 – 10/2014	*B. Sc. in Chemistry*, Clausthal University of Technology Grade: 1,1 - Bachelor Thesis under Supervision of Prof. Dr. Eike G. Hübner at Institute of Organic Chemistry: Molekulare Klettverschlüsse (eng. Molecular Velcros) (Grade: 1,0)
08/2004 – 06/2011	*Abitur*, Christian-von-Dohm Gymnasium, Goslar, Germany (Grade: 2,6)

Work Experience

12/2016 – to date	*Scientific Assistant*, Institute of Physical Chemistry, Clausthal University od Technology - Supervision of Students - Tutor for Physical Chemistry - Optimization of Tutorials of Physical Chemistry
10/2013 – 11/2016	*Tutor for Physical Chemistry*, Institute of Physical Chemistry, Clausthal University of Technology
04/2014 – 12/2015	*Tutor for Pupils*, Schülerhilfe, Goslar